Spring 2014

# Thermal properties of zirconium diboride - transition metal boride solid solutions

Devon Lee McClane



Department:

# THERMAL PROPERTIES OF ZIRCONIUM DIBORIDE – TRANSITION METAL BORIDE SOLID SOLUTIONS

by

DEVON LEE MCCLANE

A THESIS

Presented to the Faculty of the Graduate School of the

MISSOURI UNIVERSITY OF SCIENCE AND TECHNOLOGY

In Partial Fulfillment of the Requirements for the Degree

MASTER OF SCIENCE

IN

MATERIALS SCIENCE AND ENGINERING

2014

Approved by

William G. Fahrenholtz, Advisor
Greg E. Hilmas, Co-Advisor
Wayne Huebner

## PUBLICATION THESIS OPTION

The thesis has been prepared in the style utilized by the Journal of the American Ceramic Society. Pages 1-28 contain an Introduction and Literature Review for background purposes. Pages 29-59 entitled "Thermal Properties of (Zr,TM)$B_2$ Solid Solutions with TM = Hf, Nb, W, Ti, and Y" was accepted for publication in the Journal of the American Ceramic Society in February of 2014. Pages 60-92 entitled "Thermal Properties of (Zr,TM)$B_2$ Solid Solutions with TM = Ta, Mo, Re, V, and Cr" was submitted to the Journal of the American Ceramic Society in March of 2014. Conclusions and Future Work sections are also included in pages 93-97. An Appendix is included for the purpose of presenting work that was performed, but not presented in either journal paper.

## ABSTRACT

This research focuses on the thermal properties of zirconium diboride ($ZrB_2$) based ceramics. The overall goal was to improve the understanding of how different transition metal (TM) additives influence thermal transport in $ZrB_2$. To achieve this, $ZrB_2$ with 0.5 wt% carbon, and 3 mol% of individual transition metal borides, was densified by hot-press sintering. The transition metals that were investigated were: Y, Ti, Hf, V, Nb, Ta, Cr, Mo, W, and Re. The room temperature thermal diffusivities of the compositions ranged from 0.331 $cm^2/s$ for nominally pure $ZrB_2$ to 0.105 $cm^2/s$ for $(Zr,Cr)B_2$ and converged around 0.155$cm^2/s$ at higher temperatures for all compositions. Thermal conductivities were calculated from the diffusivities, using temperature-dependent values for density and heat capacity. The electron contribution to thermal conductivity was calculated from measured electrical resistivity according to the Wiedemann-Franz law. The phonon contribution to thermal conductivity was calculated by subtracting the electron contribution from the total thermal conductivity. Rietveld refinement of x-ray diffraction data was used to determine the lattice parameters of the compositions. The decrease in thermal conductivity for individual additives correlated directly to the metallic radius of the additive. Additional strain appeared to exist for additives when the stable TM boride for that metal had different crystal symmetries than $ZrB_2$. This research provided insight into how additives and impurities affect thermal transport in $ZrB_2$. The research potentially offers a basis for future modeling of thermal conductivity in ultra-high temperature ceramics based on the correlation between metallic radius and the decrease in thermal conductivity.

# ACKNOWLEDGEMENTS

First, I would like to thank my advisors Dr. William Fahrenholtz and Dr. Gregory Hilmas for their support and guidance over the past two years. Their assistance in writing and reviewing papers for publication has been crucial. I would also like to thank them for encouraging me to travel to conferences and present my research, allowing me to become more comfortable standing in front of a crowd, and grow as a public speaker. Finally, I would like to thank them for taking an interest in helping me find a job.

I would like to thank Dr. Wayne Huebner for residing on my committee, as well as volunteering his time for discussion. Additionally, I would like to acknowledge the Air Force Office of Scientific Research under the direction of Dr. Ali Sayir for funding my research through contract number FA9550-09-1-0168.

Next, I would like to thank my colleagues in the Missouri S&T UHTC research group. They taught me how to operate the equipment that I needed to complete my research, as well as provided insightful conversation that assisted in my understanding of ceramic processing. Just as importantly, they provided entertainment, making my time in Rolla more enjoyable.

Finally, I would like to thank my friends and family for their constant support and belief in me. Without them I would not have been able to make it to where I am today.

# TABLE OF CONTENTS

Page

PAPER



SECTION

# LIST OF ILLUSTRATIONS

PAPER 2

# LIST OF TABLES

# 1. INTRODUCTION

Development of structural materials capable of withstanding temperatures in excess of 2000°C is critical for development of hypersonic vehicles. In addition to being able to withstand these high temperatures, the material should have high strength, good oxidation resistance, high thermal conductivity, and a low density.[1] These idealized properties have made investigation of a few select transition metal borides desirable, one of which is zirconium diboride.

Zirconium diboride ($ZrB_2$) is a transition metal boride (TMB) that belongs to the class of ultra-high temperature ceramics.[1] Like several other transition metal diborides, $ZrB_2$ has a P6/mmm hexagonal crystal structure.[2] These structures are comprised of B-B covalent bonds, TM-TM metallic bonds, and TM-B ionic and covalent bonds. This combination of bonding provides $ZrB_2$ with some unique properties, including a melting temperature in excess of 3000°C, high strength (>275 MPa), good chemical inertness, as well as high thermal and electrical conductivities.[1, 3, 4, 5] Due to these desirable properties, $ZrB_2$ has been proposed for use in high temperature electrodes, refractory linings, cutting tools, and leading edges on hypersonic vehicles.[6, 7, 8, 9, 10] In many of these applications, such as leading edges, it is desirable to have fully dense parts, as well as having a high thermal conductivity.[1] However, $ZrB_2$ is often difficult to sinter to full density without using high temperatures and pressures or incorporating sintering aids.[11]

The reported room temperature thermal conductivities for nominally pure $ZrB_2$ range from as low as 56 W/m•K up to 133 W/m•K,[12,13] without a definitive study to describe the reasons for the differences. One possible explanation for these discrepancies is the presence of impurities. However, the effects of these impurities on the thermal

properties of $ZrB_2$ have not been investigated. The purpose of this research was to systematically investigate the effect of different transition metal additions on the thermal properties of $ZrB_2$. All of the additives formed solid solutions with $ZrB_2$. The research addresses several questions including:

1. What transition metal impurities have the greatest influence on the thermal conductivity of $ZrB_2$?
2. How does the presence of an impurity in solid solution affect electron and phonon conduction?
3. What factors contribute to reducing thermal transport in $(Zr,TM)B_2$ ceramics?

Taken as a whole, the research described in this thesis has the potential to improve the understanding of factors that control the thermal conductivity in $(Zr,TM)B_2$ ceramics as well as provide a basis for future modeling of the thermal conductivity in ultra-high temperature ceramics.

# 2. LITERATURE REVIEW

## 2.1 CRYSTALLOGRAPHY AND BONDING

Transition metal (TM) diborides typically exhibit hexagonal symmetry.[14] Additionally, the majority of these diborides, such as $YB_2$, $TiB_2$, $ZrB_2$, $HfB_2$, $VB_2$, $NbB_2$, $TaB_2$, and $CrB_2$, all have the same P6/mmm symmetry[2], shown in Figure 2.1[7]. These structures are comprised of alternating boron and TM planes. The boron plane is arranged in a six member ring ($sp^2$ hybridized) and the TM plane is arranged in a hexagonal close packed structure. Each boron atom is surrounded by 3 other in plane boron atoms as well as 6 out of plane TM atoms. Each TM atom is surrounded by 6 in plane TM atoms and 12 out of plane boron atoms.[15, 16] The unit cell contains one formula unit. This structure is unusual in the sense that it is comprised of B-B covalent bonds, TM-TM metallic bonds, and TM-B covalent and ionic bonds.[17] Depending on the size of the transition metal, the *a*-lattice parameter is either controlled by the TM-TM contacts, B-B contacts, or a balance between the B-B attractive forces and TM-TM repulsive forces.[7] The *c*-lattice parameter is related to the TM-B bond strength. This axis increases more significantly with increasing TM size than the *a*-lattice parameter axis.[2, 7]

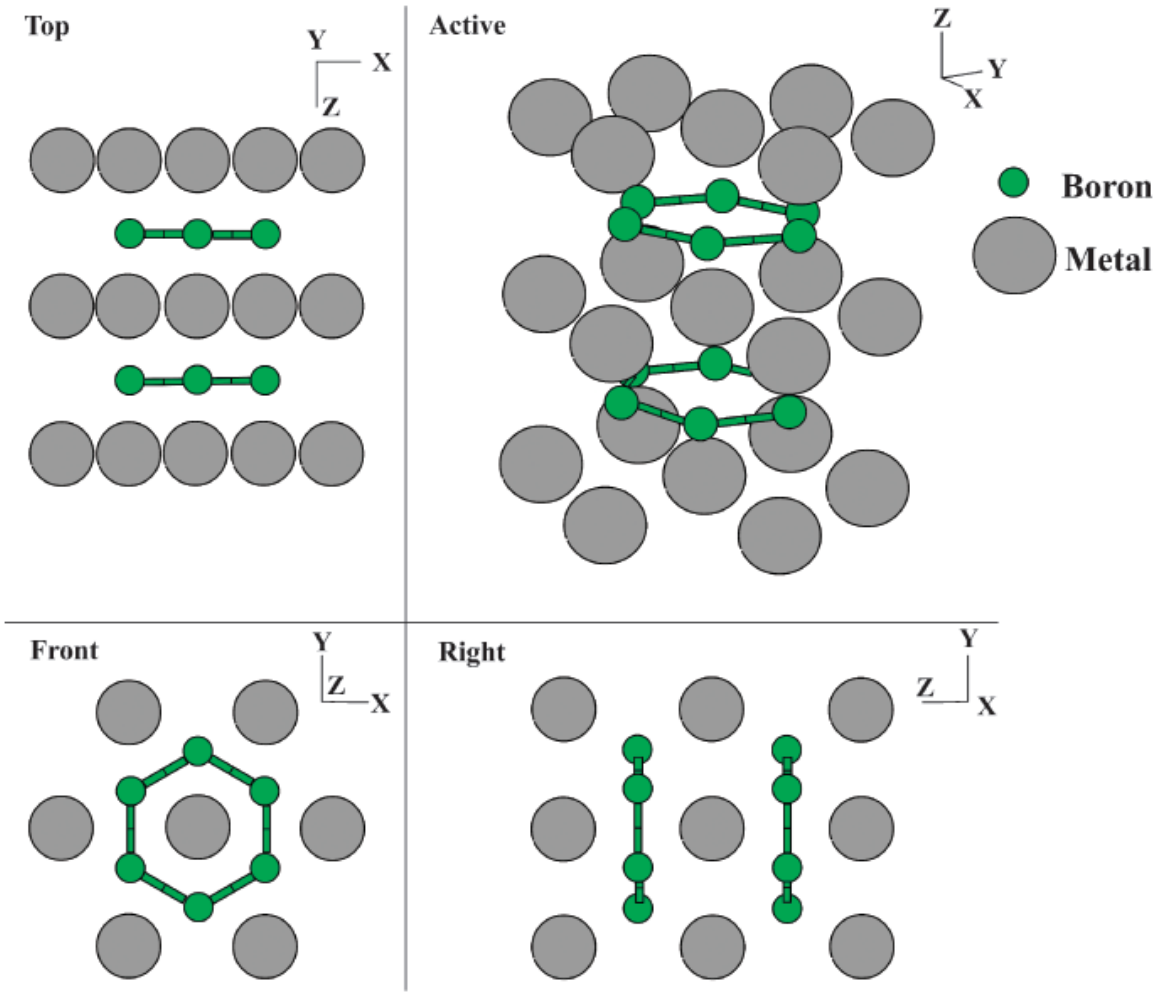


**Figure 2.1:** $AlB_2$ crystal structure that shows the P6/mmm symmetry.[7]

The B-B bond strength in the $TMB_2$ contributes to the stiffness of the crystal lattice as well as the hardness, strength, and chemical stability of the ceramic.[7] In the TM-B bonds of $TMB_2$ ceramics, the TM donates 2 electrons and each B atom in the unit cell accepts one.[15, 18] The TM-B bond strength contributes to the melting temperature.[7] Additionally, the remaining free valence electrons allow for the high thermal and electrical conductivities in the TM-TM planes.

Although the majority of transition metals form the stoichiometric diborides with the P6/mmm symmetry discussed above, there are a few exceptions. For example, $ReB_2$ forms the $P6_3/mmc$ crystal structure shown in Figure 2.2.[19] While this is still a hexagonal structure, the boron planes are buckled, resulting in a larger *c*-lattice parameter than the P6/mmm transition metal diborides.

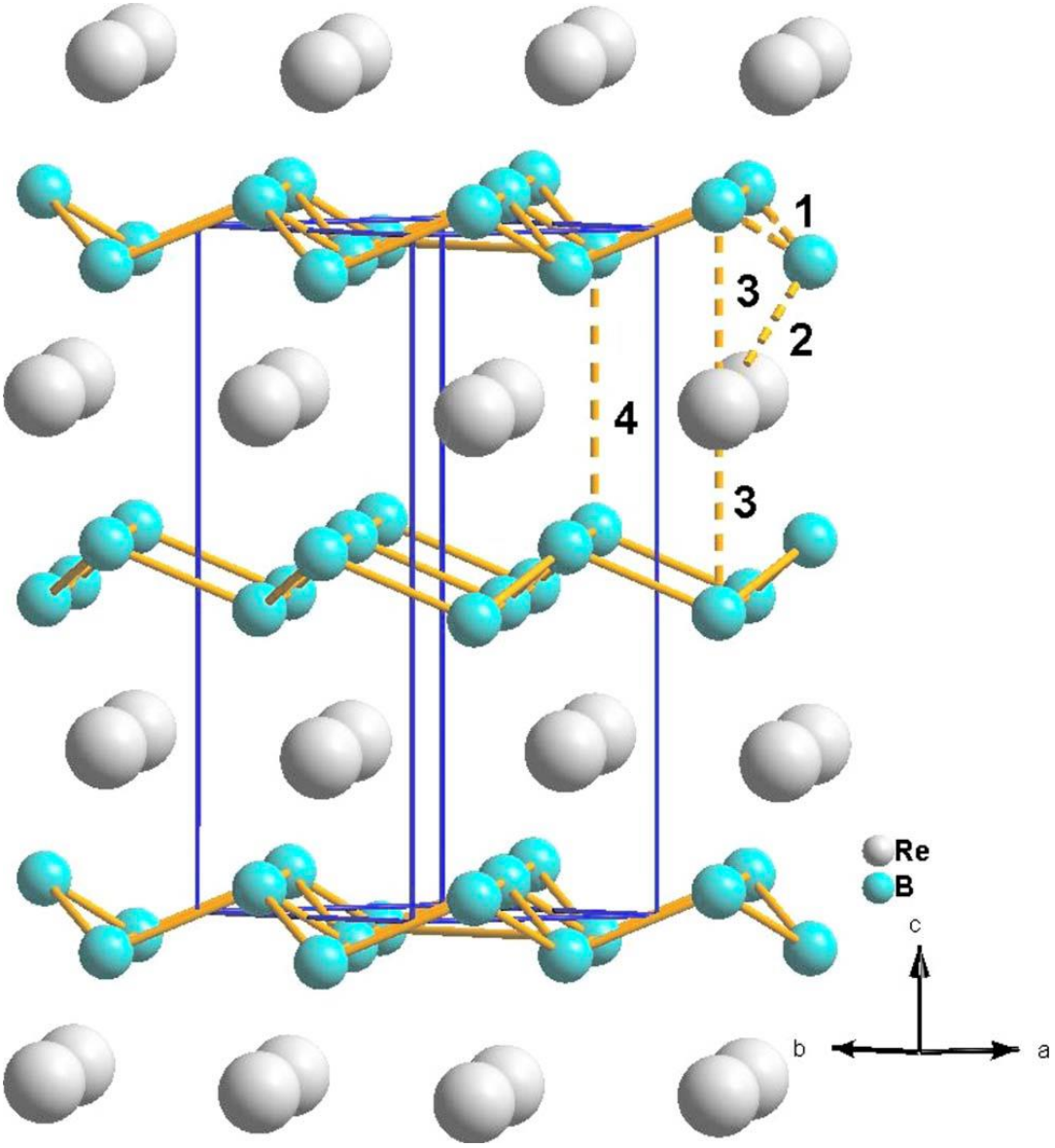


**Figure 2.2:** $ReB_2$ crystal structure that shows the $P6_3/mmc$ symmetry.[19]

Tungsten has been reported to favor forming $W_2B_5$ and $W_2B_4$ instead of $WB_2$ and molybdenum has been reported to favor forming $Mo_2B_5$ and $Mo_2B_4$ instead of $MoB_2$.[20, 21, 22] The major difference between the $TM_2B_5$ and $TM_2B_4$ structures is the addition of an extra boron atom that sits in the center of the buckled boron rings. All three of the W compounds have the same symmetry, $P6_3/mmc$, shown in Figure 2.2 and Figure 2.3b, although the unit cell is different. In comparison, both $Mo_2B_5$ and $Mo_2B_4$ have the $R\bar{3}m$ symmetry, shown in Figure 2.3a.[20, 23] Although $MoB_2$ and $Mo_2B_4$ are chemically the same, they are classified differently to not confuse the compounds and structures.

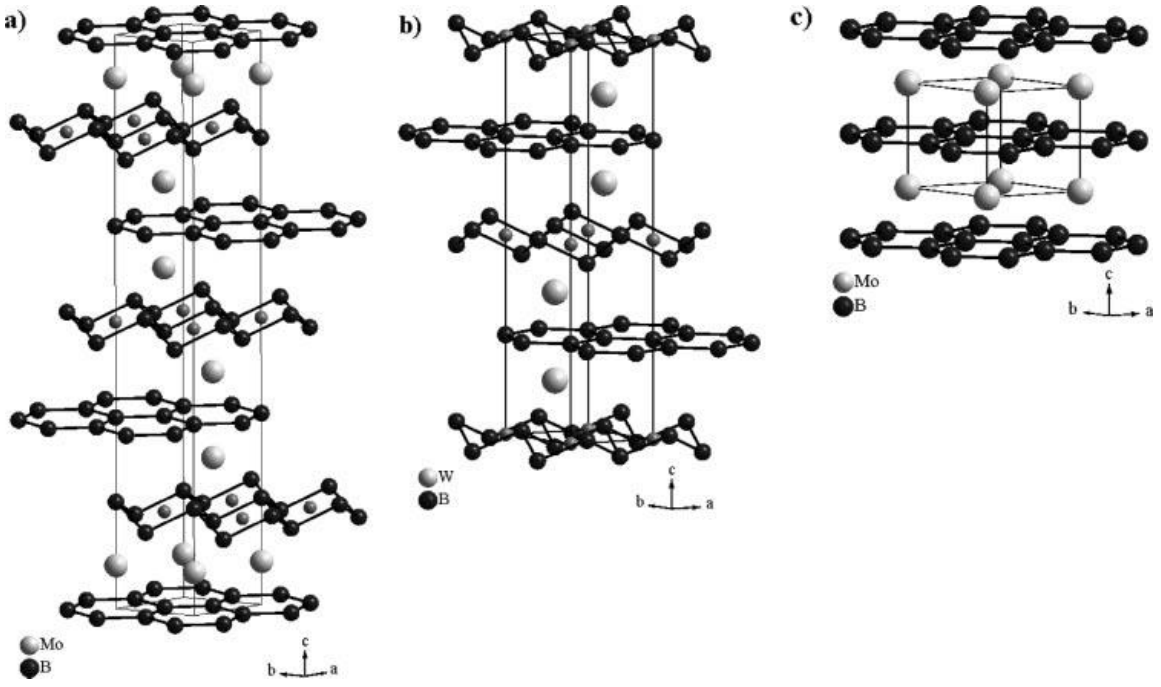


**Figure 2.3:** Crystal structure of a) $Mo_2B_5$, showing $R\bar{3}m$ symmetry b) $W_2B_5$ showing $P6_3/mmc$ symmetry and c) $MoB_2$ showing P6/mmm symmetry.[20]

## 2.2 THERMAL PROPERTIES

**2.2.1 Thermal Conductivity.** Thermal energy can be transferred by three different mechanisms, conduction, convection, and radiation.[24] Thermal conductivity is the physical property that quantifies the ability of a material to transfer heat, and is a function of the heat flux through a material and the temperature gradient, shown in Equation 1, where k is the thermal conductivity (W/m•K), $\vec{q}$ is the heat flux (J/s•m$^2$), and $\vec{\nabla}$T is the temperature gradient (K/m).[25, 26]

$$k = \frac{-\vec{q}}{\vec{\nabla}T} \tag{1}$$

Thermal conductivity can be further broken down into the mechanisms that allow for the transfer of thermal energy, Equation 2. These include phonon conduction ($k_p$), electron conduction ($k_e$), and photon conduction ($k_{pt}$). Photon conduction allows for heat to be transferred through electromagnetic radiation.[24] Because of this, photon conduction is not present in fully dense opaque materials. Phonon and electron conduction are discussed in more detail in Sections 2.3.1.2 and 2.3.1.3

$$k = k_p + k_e + k_{pt} \tag{2}$$

Thermal conductivity can be measured using the hot plate method, hot-wire method, or comparative heat flow method.[27, 28, 29] In these test methods, a temperature gradient is created in a specimen, and assuming steady-state heat flow, the conductivity is determined from the slope of the temperature profile. However, it is often difficult to maintain a set temperature gradient. Because of this, thermal diffusivity, heat capacity, and density are often measured and used to calculate the thermal conductivity according to Equation 3, where k is thermal conductivity (W/m•K), $p$ is density (g/cm$^3$), $C_p$ is heat capacity (J/g•K), and α is thermal diffusivity (cm$^2$/s).[26, 30] Thermal diffusivity and heat capacity are discussed in more detail in Sections 2.3.2 and 2.3.3.

$$k = pC_p\alpha \tag{3}$$

**2.2.1.1 Phonon conduction.** Phonon conduction refers to the energy that is transferred due to lattice vibrations. Using a classical gas model, the conductivity can be related to $l$, the mean free path (m), $v$, the average velocity (m/s), and ($C_v$), the constant volume heat capacity of the material (J/m$^3$•K), as shown in Equation 4.[25, 26]

$$k \cong \frac{1}{3}C_v l v \tag{4}$$

The amount of energy that can be transferred is a balance between constructive and destructive lattice vibrations. The conductivity is a function of temperature, and can be split into four regimes, as shown in Figure 2.4.[31] In the first regime, phonons become excited and the resulting lattice vibrations help to transfer heat, proportional to the temperature cubed ($\sim T^3$). Once a high enough temperature is reached, phonon interactions, also called Umklapp scattering[32], occur and result in a decrease of thermal conductivity. Equation 5 shows the behavior of conduction as a function of temperature for this regime, where k is the thermal conductivity, $\theta_D$ is the Debye temperature (K), and T is the temperature (K).

$$k \sim e^{-\theta_D/T} \tag{5}$$

The Debye temperature is the temperature where a crystal's highest normal mode of vibration is reached, i.e. where maximum lattice vibration occurs. Above the Debye temperature, the conductivity decreases proportional to the inverse of the temperature, 1/T. At even higher temperatures, regime 4, the thermal conductivity becomes temperature independent.[31]

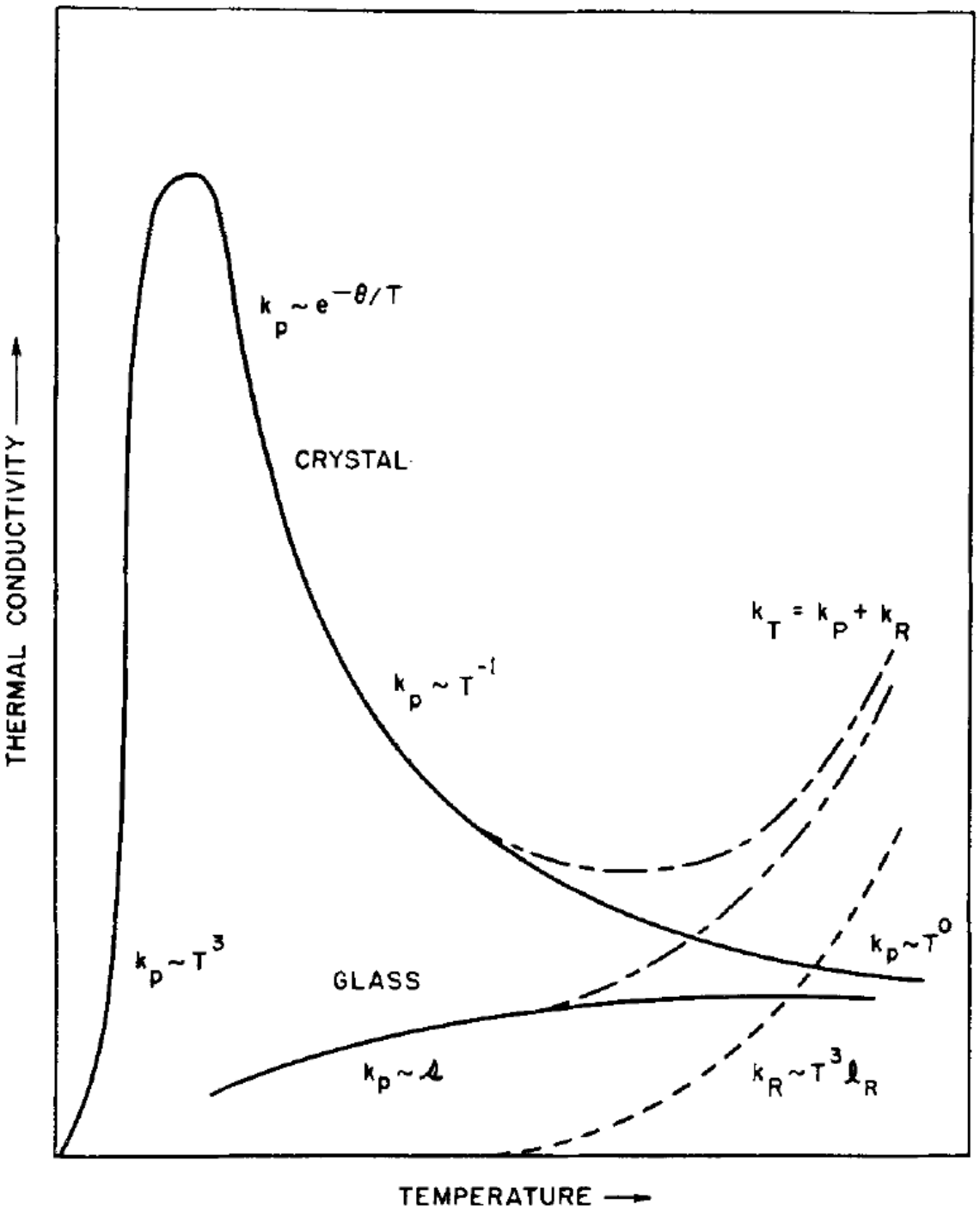


**Figure 2.4:** Phonon contribution to thermal conductivity as a function of temperature.[31]

**2.2.1.2 Electron conduction.** Electron conduction refers to the energy that is transferred due to free electron motion. The electron contribution to thermal conductivity is related to the electrical conductivity of the material according to the Wiedemann-Franz law shown in Equation 6, where $k_e$ is the electron contribution to thermal conductivity (W/m•K), L is the Lorenz number ($W\Omega/K^2$), T is temperature (K), and σ is the electrical conductivity (S/m).

$$k_e = LT\sigma \tag{6}$$

**2.2.1.3 Lorenz number.** Originally, Wiedemann and Franz observed that the relationship between the thermal and electrical conductivities were a constant value for several different metals at room temperature. Later, Lorenz confirmed this constant for various temperatures, giving rise to Equation 6. The Lorenz number was solved for using Fermi-Dirac statistics by Sommerfeld in 1927. He was able to get the value shown in Equation 7, where $k_B$ is Boltzmann's constant (J/K), and e is electron charge (C).[33]

$$L_o = \frac{\pi^2(k_B)^2}{3e^2} = 2.44 \times 10^{-8} W\Omega K^{-2} \tag{7}$$

However, this is an ideal value that assumes that the electron gas is highly degenerate and that scattering is elastic in nature.[33, 34] The actual Lorenz number of a material is temperature dependent and can be related to the theoretical value according to Equation 8, where $l_T$ is the mean free path for thermal conduction and $l_e$ is the mean free path for electrical conduction.[33]

$$L = L_o \frac{l_T}{l_e} \tag{8}$$

Several methods for measuring the Lorenz number have been proposed. These include measuring the thermal and electrical conductivities under high magnetic fields or at liquid helium temperatures in an attempt to separate the contributions to thermal conduction by stopping either electron or phonon transport.[35, 36, 37] One paper, by Sharma[38], proposed a method of determining the Lorenz number graphically. By using Equations 2 and 6, as well as assuming that phonon conduction is proportional to $T^{-1}$, regime 3, Equation 9 can be used to determine the Lorenz number. This is done by graphing kT as a function of $T^2\sigma$. The slope of the linear trend line that is fit to this data is the Lorenz number of the material. Additionally, the added constant term is related to the phonon contribution, and therefore, should be positive.

$$kT = LT^2\sigma + constant \tag{9}$$

**2.2.1.4 Thermal conductivity of transition metal boride ceramics.** The thermal conductivity of several transition metal boride ceramic compositions has been tested. Figure 2.5 shows the behavior of the conductivity as a function of temperature for some of these ceramics. It is evident that these materials are highly conductive, with values comparable to several metals.[39] Additionally, it has been found that the electron contribution accounts for over 2/3 of the thermal conductivity for $ZrB_2$.[40, 41, 42]

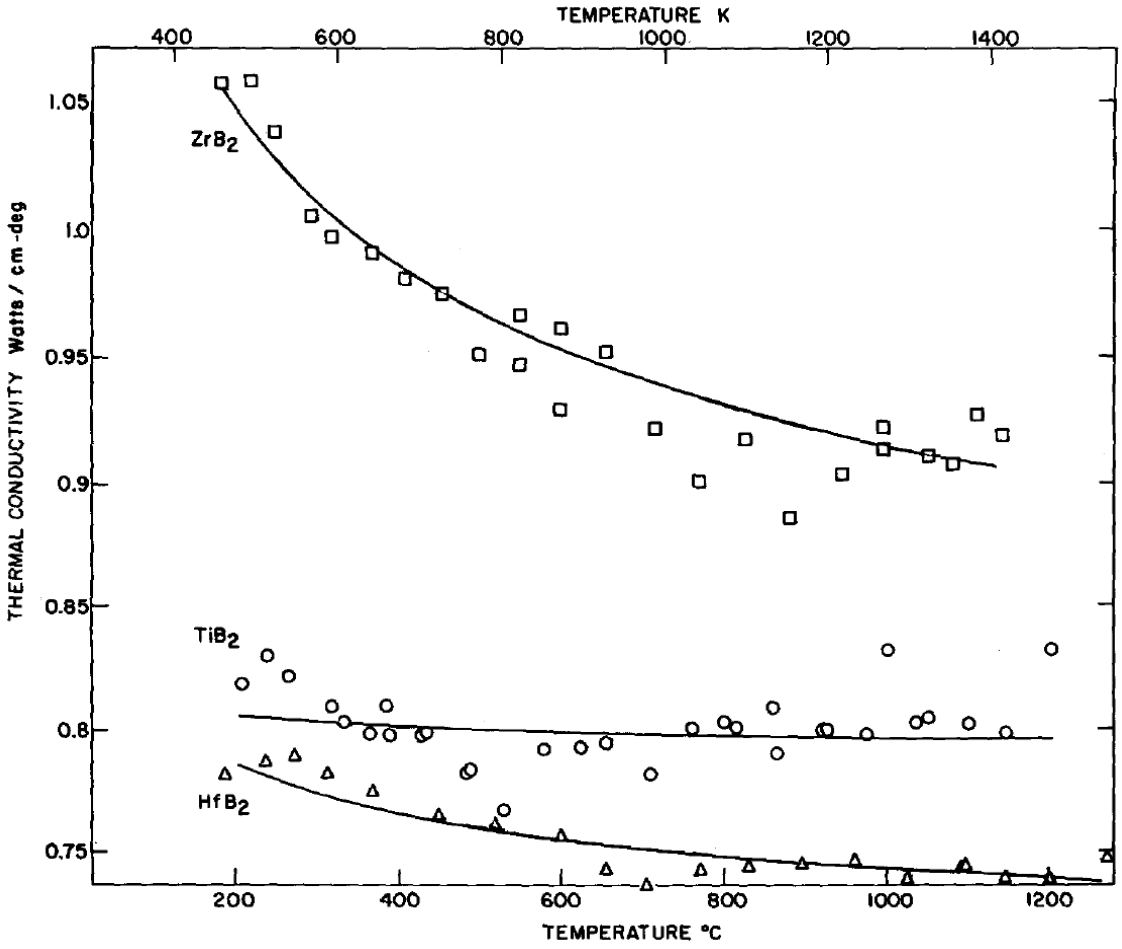


**Figure 2.5:** Thermal conductivity of $ZrB_2$, $TiB_2$, and $HfB_2$ from 200°C to 1200°C.[43]

Further evaluation has been conducted on $ZrB_2$ at room temperature, with values ranging widely. Some examples of these room temperature thermal conductivities, as well as how the powders were processed and densified, from several different studies are shown in Table 2.1.

**Table 2.1:** Room temperature thermal conductivity of nominally pure $ZrB_2$ ceramics.

| Author | Processing/Densification Technique | Thermal Conductivity @ 25°C (W/m•K) |
|---|---|---|
| Guo[13] | Reaction Spark-Plasma Sintering of $ZrH_2$ and B powders that were ball-milled with SiC media | 133.01 |
| Zhang[41] | Spark-Plasma Sintering of commercially available $ZrB_2$ | 108 |
| Thompson[44] | Hot-Press Sintering of commercially available $ZrB_2$ that was ball-milled with $ZrB_2$ media | 92 |
| Thompson[45] | Hot-Press Sintering of commercially available $ZrB_2$ that was attrition-milled with WC media | 58.7 |
| Zimmermann[12] | Hot-Press Sintering of commercially available $ZrB_2$ that was attrition-milled with WC media | 56 |

**2.2.2 Thermal Diffusivity.** Thermal diffusivity is the ratio between a materials' ability to conduct and to store thermal energy. In other words, thermal diffusivity is the measurement of thermal inertia through a solid.[46] Since thermal conductivity can be difficult to measure directly, thermal diffusivity is often measured and then used to calculate the thermal conductivity according to Equation 3.

Thermal diffusivity is commonly measured by the laser flash method, shown in Figure 2.6. In this test setup, a thin sample, typically 10 to 12.5mm in diameter, is hit by a high intensity, radiant energy pulse. The thickness of the sample should be such that the half rise time, discussed later, is between 10 and 1000 ms. Additionally, the pulse should not have a duration longer than 2% of the half rise time. This pulse of energy is absorbed on the front face and the temperature rise of the back face is recorded.[30]

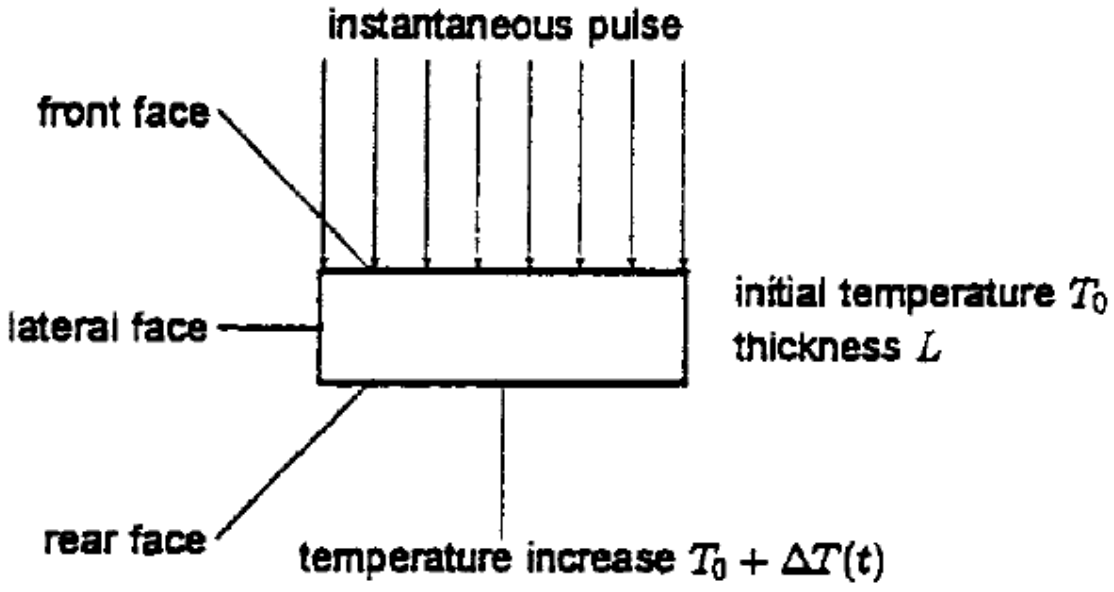


**Figure 2.6:** Schematic showing laser flash method for determining thermal diffusivity.[30]

The thermal diffusivity is then calculated from the thickness of the sample and the time that it took for the rear face to reach a percentage of the maximum value, according to Equation 10, where α is the diffusivity ($cm^2/s$), L is the sample thickness (cm), and $t_{0.50}$ is the half rise time (s).[30] The constant value in the equation was derived by Parker using the equation for temperature distribution in a thermally insulated solid of uniform thickness that was derived by Carslaw and Jeager.[47]

$$\alpha = 0.13879 \frac{L^2}{t_{0.50}} \tag{10}$$

This test method makes the assumption that the initial energy pulse is uniform and has a negligible time compared to the measured rise time. It also neglects radial heat loss and assumes that the specimen is homogeneous and isotropic.[48] An ideal thermograph, which shows how $t_{0.50}$ is determined, is pictured in Figure 2.7.

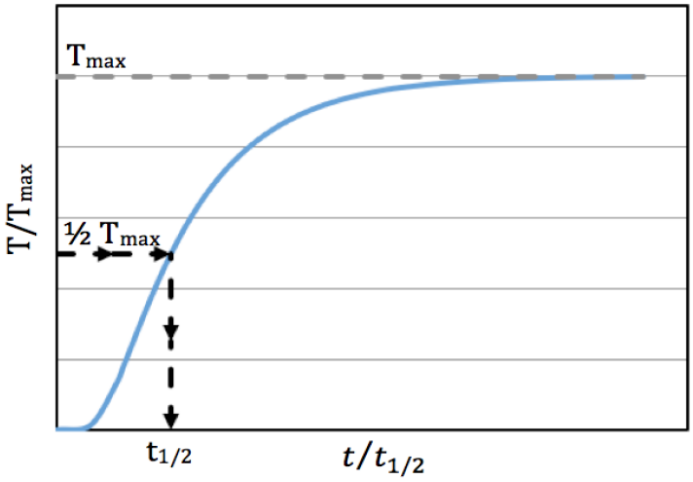


**Figure 2.7** Ideal laser flash thermograph.[47]

Several other methods have been used to correct the measured thermal diffusivity for radiant heat loss, and pulse time.[30, 49, 50] One of these methods is the Clark and Taylor method, shown in Equations 11 and 12, where α is the thermal diffusivity, $K_R$ is the correction factor and $t_n$ is the time it takes for the temperature to rise to the $n^{th}$ fraction of the $T_{max}$.

$$\alpha_{corrected} = \frac{\alpha K_R}{0.13885} \tag{11}$$

$$K_R = -0.3461467 + 0.361578\left(\frac{t_{0.75}}{t_{0.25}}\right) - 0.06520543\left(\frac{t_{0.75}}{t_{0.25}}\right)^2 \tag{12}$$

The thermal diffusivities of several $ZrB_2$ and $HfB_2$ ceramics with SiC and $Si_3N_4$ additions are shown in Figure 2.8. All of the values decrease with increasing temperature through the tested temperature range.

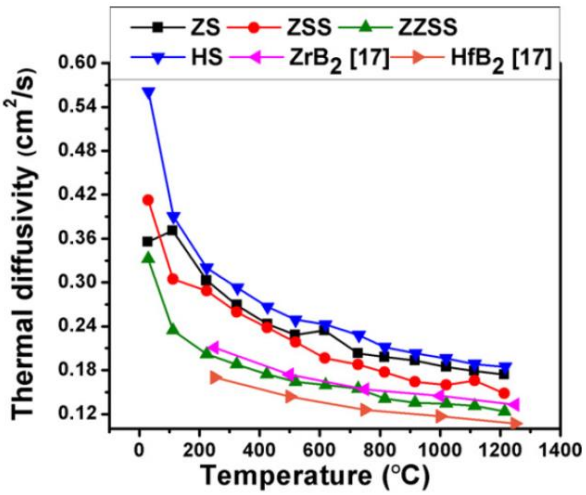


**Figure 2.8:** Thermal diffusivity of $ZrB_2$ and $HfB_2$ ceramics.[51, 52]

**2.2.3 Heat Capacity.** Heat capacity is the physical property that quantifies the amount of energy required to raise the temperature of a material (J/mol•K). This material property can be defined at constant volume ($C_v$) or constant pressure ($C_p$), shown in Equations 13 and 14 respectively, where $\frac{d\bar{U}}{dT}$ is the change in internal energy as a function of temperature and $\frac{d\bar{H}}{dT}$ is the change in enthalpy as a function of temperature.[53]

$$C_v = (\frac{d\bar{U}}{dT})_V \quad (13)$$

$$C_p = (\frac{d\bar{H}}{dT})_P \quad (14)$$

The relationship between these two values is shown in Equations 15 and 16, where β is the volume expansion coefficient ($K^{-1}$), γ is the Grüneisen parameter, T is the temperature (K), K is the bulk modulus (Pa), and $\bar{V}$ is the molar volume ($m^3$/mol).[25]

$$C_p = C_v(1 + \beta\gamma T) \quad (15)$$

$$\gamma = \frac{\beta K \bar{V}}{C_v} \quad (16)$$

Heat capacity is often measured by differential scanning calorimetry (DSC), adiabatic calorimetry, and the laser flash method.[48, 54, 55] In these test methods, the amount of energy required to change the temperature of a material is measured and

compared to a standard reference material. The differences between the measured and reference material can then be used to determine the heat capacity of the material.

Similar to thermal conduction, the heat capacity of a material can also be split into phonon and electron contributions. The phonon contribution depends on the number of vibrational modes that are available for transferring heat.[26] The low temperature constant volume heat capacity of a material (J/mol•K) has been modeled by Einstein ($C_E$) and Debye ($C_D$), shown in Equations 17 and 18 respectively, where $N_A$ is Avogadro's number ($mol^{-1}$), $k_B$ is Boltzmann's constant (J/K), h is Planck's constant (J•s), $f$ is the vibration frequency ($s^{-1}$), T is the temperature (K), and $\theta_D$ is the Debye temperature (K).

$$C_E = 3N_A k_B \left(\frac{hf}{k_B T}\right) \frac{e^{hf/k_B T}}{(e^{hf/k_B T}-1)^2} \tag{17}$$

$$C_D = 9N_A k_B \left(\frac{T}{\theta_D}\right)^3 \int_0^{\theta_D/T} \frac{x^4 e^{-x}}{(1-e^{-x})^2}\, dx \tag{18}$$

The Debye temperature, the temperature where maximum lattice vibration occurs (K), is shown in Equation 19, where h is Planck's constant (J•s), $f$ is the maximum vibrational frequency in a material ($s^{-1}$), and $k_B$ is Boltzmann's constant (J/K).[25, 53]

$$\theta_D = \frac{hf}{k_B} \tag{19}$$

The maximum wave velocity, *v*, (m/s) is the velocity of vibration in a material that is associated with the maximum wave frequency, according to Equation 20, where λ is the minimum wavelength (m).[53]

$$v = f\ \lambda \tag{20}$$

This velocity can be solved for according to Equations 21-23, where $v_t$ is the transverse wave velocity (m/s), $v_l$ is the longitudinal wave velocity (m/s), K is the bulk modulus (Pa), G is the shear modulus (Pa), and *p* is the density (kg/m$^3$).[56, 57]

$$v = \left[\frac{1}{3}\left(\frac{2}{v_t^3} + \frac{1}{v_l^3}\right)\right]^{-1/3} \tag{21}$$

$$v_t = \sqrt{\frac{G}{p}} \tag{22}$$

$$v_l = \sqrt{\frac{(B+\frac{4}{3}G)}{p}} \tag{23}$$

At high temperatures the constant volume heat capacity of a material approaches a maximum value of ~3R, shown in Figure 2.9. This value was originally derived by Dulong and Pettit and is dependent on the number of modes for transferring heat within a material.[26]

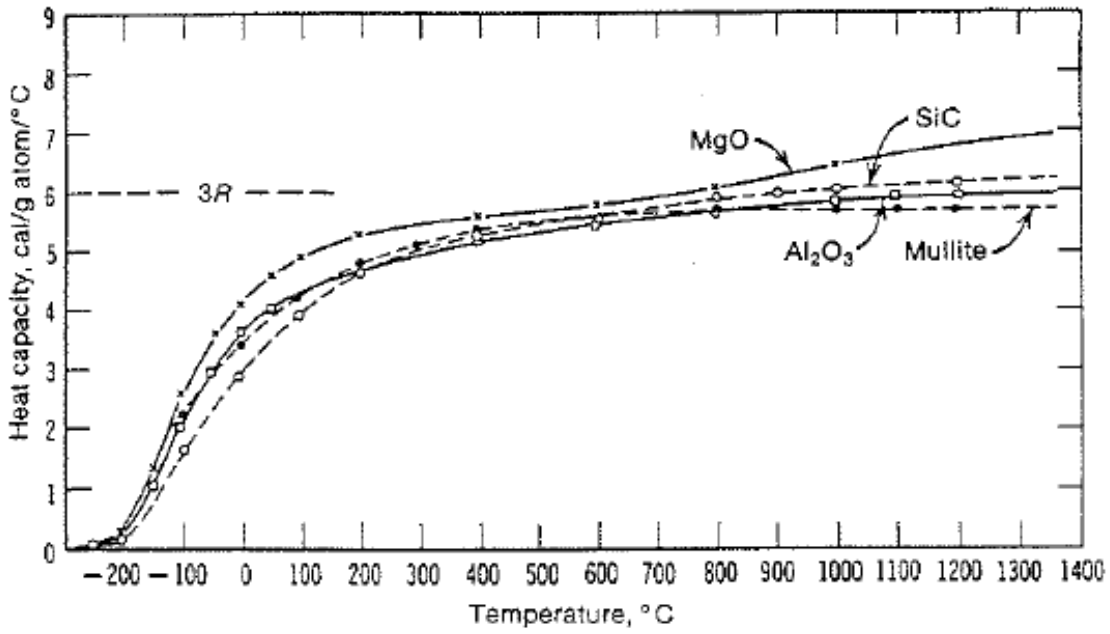


**Figure 2.9:** Heat capacity of common oxide ceramics.[58]

The electron contribution to heat capacity ($C_{el}$) is shown in Equation 24, where $N(E_F)$ is the electron density of states at the Fermi level, $k_B$ is Boltzmann's constant (J/K), and T is temperature (K).[25]

$$C_{el} = \frac{2\pi^2}{3} N(E_F) k_B^2 T \tag{24}$$

While this equation predicts the behavior at high temperatures, it does not agree with experimental values below the Debye temperature. This has been attributed to electron-phonon interactions that change the value of $N(E_F)$.[25]

The heat capacity of several transition metal borides as a function of temperature can be seen in Figure 2.10. Although there are some relatively large differences at temperatures just above 0K, the heavier transition metal diborides have higher constant pressure molar heat capacities, and the values converge at higher temperatures.

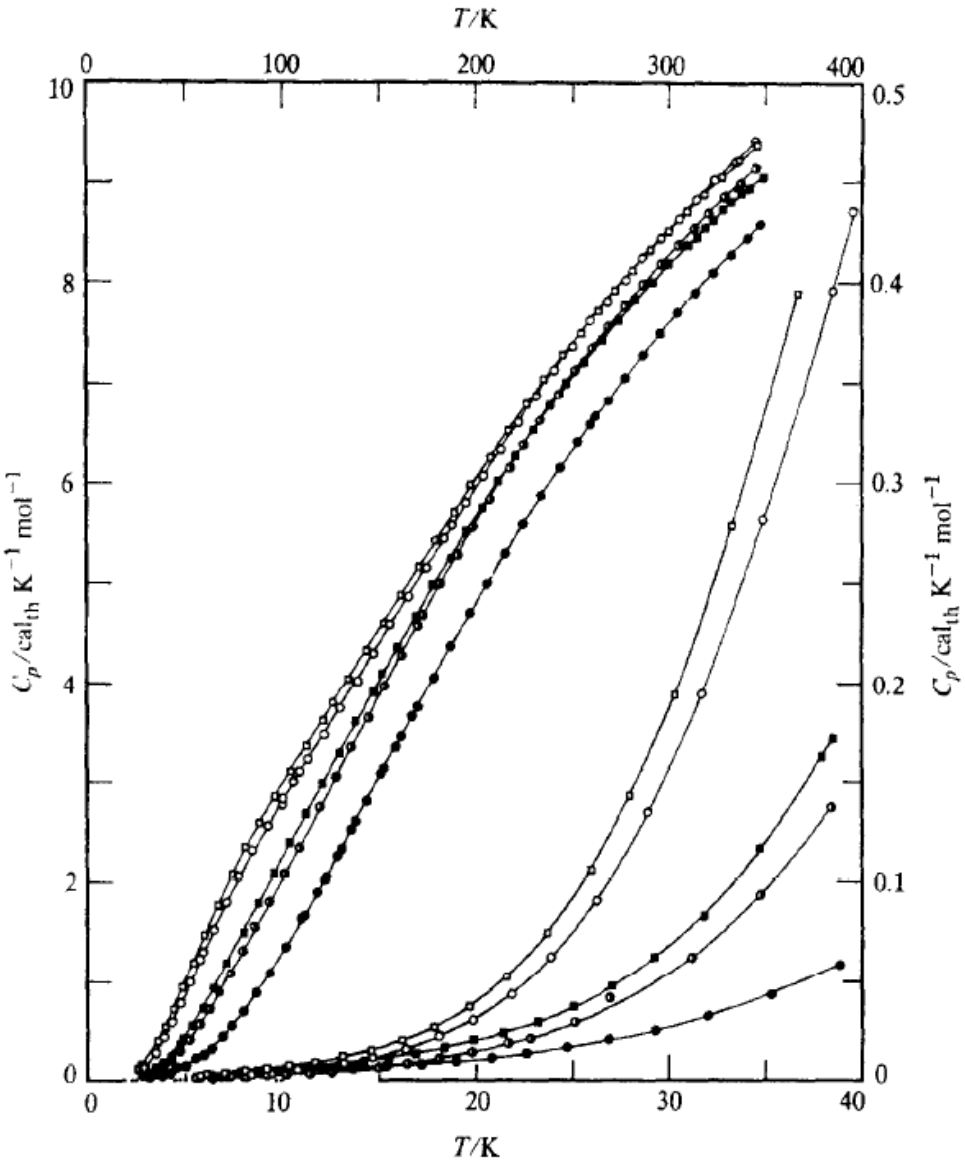


FIGURE 1. Heat capacities of transition element diborides: ●, $TiB_2$; □, $TaB_{2.11}$; ◑, $ZrB_2$;[1] ■, $NbB_{1.963}$;[2] and ○, $HfB_2$[3].

**Figure 2.10:** Heat capacity of various transition metal diborides.[59, 60]

**2.2.4 Thermal Expansion.** Thermal expansion is the physical property that quantifies the change in the dimensions of a material as a function of temperature. Thermal expansion for bulk materials can be measured using a push-rod dilatometer.[61] The linear expansion data for $ZrB_2$ in the *a* and *c* directions, as well as for the polycrystalline material, are shown in Figure 2.11.

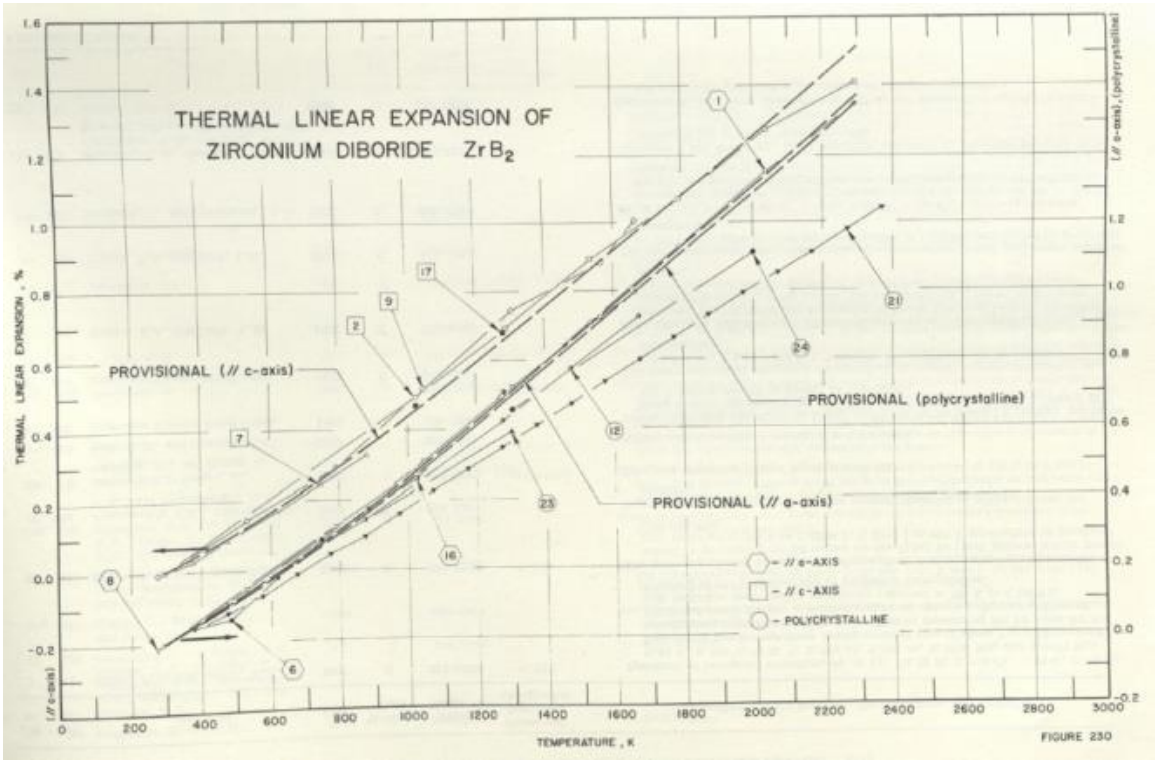


**Figure 2.11:** Linear thermal expansion data $ZrB_2$.[62]

For transition metal diborides, the thermal expansion coefficient in the *a* direction does not change much with changing transition metal. However, the thermal expansion coefficient in the *c* direction decreases with increasing radius of the metal atom.[15]

## 2.3 ELECTRICAL PROPERTIES

Electrical resistivity (ρ) is the inverse of the electrical conductivity (σ), and is the physical property that quantifies the opposition to the flow of electric current through a material. In metallic conductors, the electrical conductivity depends on *n*, the number of charge carriers ($m^{-3}$) and μ, their mobility ($m^2$/V-s), shown in Equation 25, where *e* is the charge of an electron (C). The mobility term, is a function of τ, the mean scattering time (s), and $m_e$, the mass of an electron (kg), Equation 26.[63]

$$\sigma = ne\mu \tag{25}$$

$$\mu = \frac{e\tau}{m_e} \tag{26}$$

Electrical resistivity is often measured by the van der Pauw method.[64] In this method, a known current is applied through a material and the resulting change in voltage is measured. The input current, output current, and measured voltage points are switched between four different locations on the perimeter of the specimen to find the average resistivity across the material, according to Equations 27 – 29, where ρ is the resistivity (Ω-m), f is a function of the resistance ratio, t is the thickness (m), I is the current (A), and V is the voltage (V). The subscripts to the voltage correspond to the current input, output and the voltage measurement locations.[64]

$$\rho_{average} = \frac{\rho_a + \rho_b}{2} \tag{27}$$

$$\rho_a = \frac{\pi f_a t}{4I\ln(2)}[V_{21,34} + V_{12,34} - V_{32,41} + V_{23,41}] \quad (28)$$

$$\rho_b = \frac{\pi f_b t}{4I\ln(2)}[V_{43,12} + V_{34,12} - V_{14,23} + V_{41,23}] \quad (29)$$

The electrical resistivity of most materials changes with temperature. In metals, the electrical resistivity increases linearly with increasing temperature at high temperatures and follows a power law function, called the Bloch-Grüneisen formula, at low temperatures.[65, 66] These same trends have been observed in transition metal diborides, shown in Figure 2.12 and Figure 2.13. Additionally, some of the transition metal diborides have been reported to exhibit superconductivity at temperatures near 0K.[67, 68]

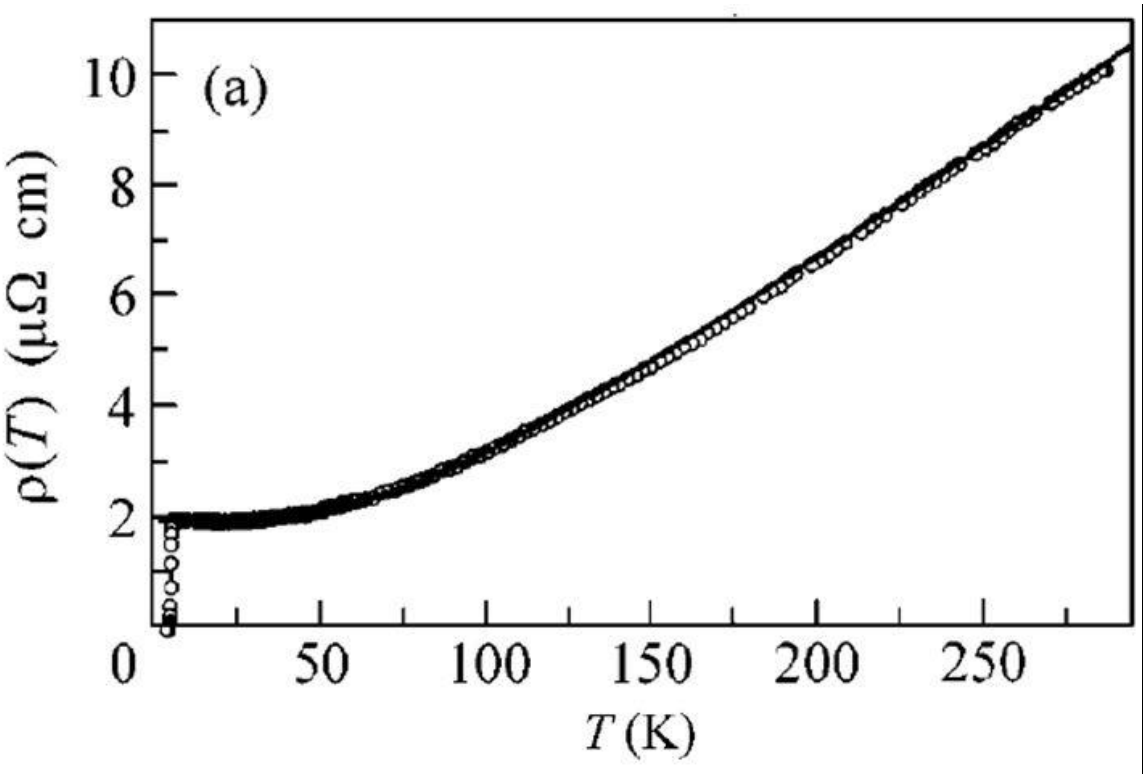


**Figure 2.12:** Electrical resistivity of $ZrB_2$, as a function of temperature (K).[67]

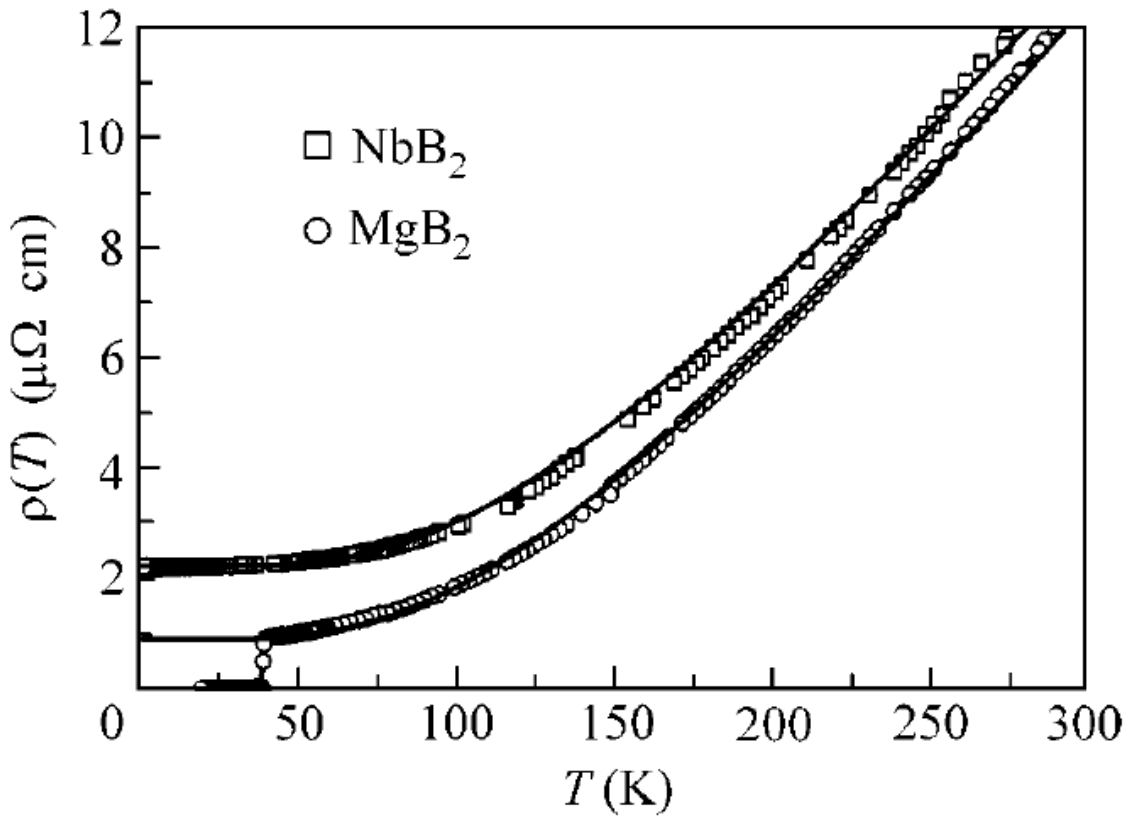


**Figure 2.13:** Electrical resistivity of $NbB_2$ and $MgB_2$, as a function of temperature (K).[67]

For materials with a second phase present, a number of equations exist for modeling the electrical resistivity. For example, Equation 30 shows a simple volumetric mixing model, where ρ is the resistivity and *x* is the volume fraction of the continuous and dispersed phases. This works well for materials that have similar electrical properties, and do not interact with each other.[69, 70]

$$\rho = x_c\rho_c + x_d\rho_d \tag{30}$$

If the materials form a solid solution the resulting electrical resistivity can be higher than either of the constituents, due to electron scattering. This behavior is described by Nordheim's rule for solid solutions, shown in Equation 31, where ρ is the resistivity, x is the volume fraction of the solid solution additive, and c is the Nordheim coefficient.[63]

$$\rho = x_a\rho_a + (1 - x_a)\rho_b + cx_a(1 - x_a) \tag{31}$$

This relationship has been seen for some transition metal boride solid solutions, shown if Figure 2.14.[4] Since the maximum resistivity does not occur at the 50 mol% concentration, it indicates that the constituents are contributing to the electrical conductivity differently.

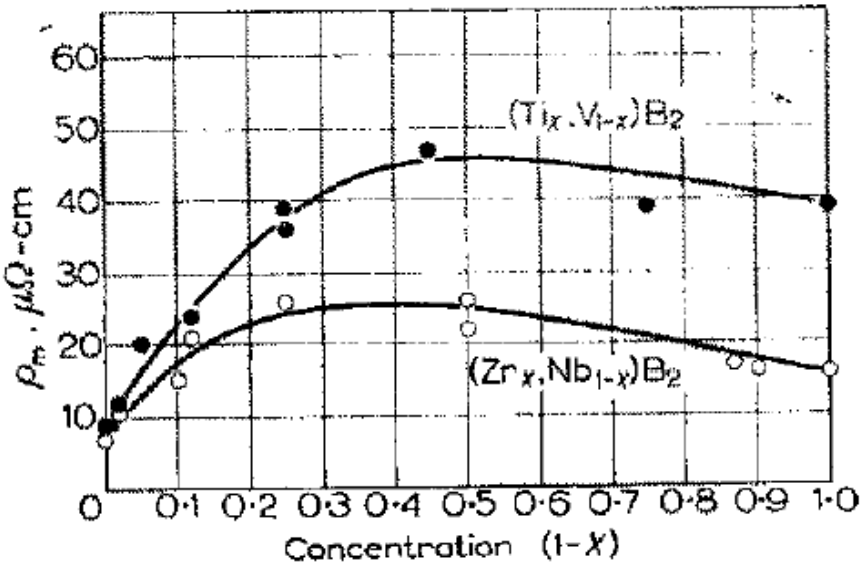


**Figure 2.14:** Electrical resistivity for (Ti,V)$B_2$ and (Zr,Nb)$B_2$ ceramics.[4]

## 2.4 USE OF ADDITIVES IN $ZrB_2$

Several additives have been shown to help densify and improve certain properties of $ZrB_2$. For example C and $B_4C$ have been shown to remove oxygen impurities from $ZrB_2$ powders, aiding in densification.[71, 72, 73, 74] Additionally, SiC and $MoSi_2$ have been shown to help with oxidation resistance by forming a $SiO_2$ passivation layer on the surface.[75, 76, 77] Refractory metals and metal diborides form solid solutions with $ZrB_2$ and decrease the diffusion rate of oxygen through the material.[78, 79] Despite the benefits described above, the addition of a second material to $ZrB_2$ has been shown to influence its thermal properties.[12, 44, 45, 80] Papers 1 and 2 systematically investigated the influence of transition metal additions on the thermal properties of $ZrB_2$.

# PAPER

## 1. THERMAL PROPERTIES OF (Zr,TM)$B_2$ SOLID SOLUTIONS WITH TM = Hf, Nb, W, Ti, AND Y

Devon L. McClane*, William G. Fahrenholtz, and Gregory E. Hilmas

Materials Science and Engineering Department, Missouri University of Science and Technology, Rolla, Missouri 65409

**Abstract**

The thermal properties were investigated for hot pressed zirconium diboride – transition metal boride solid solutions. The transition metal additives included hafnium, niobium, tungsten, titanium, and yttrium. The nominal additions were equivalent to 3 at% of each metal with respect to zirconium. Powders were hot pressed to nearly full density at 2150°C using 0.5 wt% carbon as a sintering aid. Thermal diffusivity was measured using the laser flash method. Thermal conductivity was calculated from the thermal diffusivity results using temperature-dependent values for density and heat capacity. At 25°C the thermal conductivity ranged from 88 to 34 W/m•K for specimens with various additives. Electrical resistivity measurements and the Wiedemann-Franz law were used to calculate the electron contribution of the thermal conductivity and revealed that thermal conductivity was dominated by the electron contribution. The decrease in thermal conductivity correlated to a decrease in unit cell volume, indicating that lattice strain may affect both phonon and electron transport in $ZrB_2$.

## I. Introduction

Zirconium diboride ($ZrB_2$) is a transition metal boride with a hexagonal crystal structure and P6/mmm symmetry.[1] $ZrB_2$ has a combination of metallic, ionic, and covalent bonds.[2] Due to its strong covalent bonds, $ZrB_2$ has a high melting temperature of 3250°C.[3] This melting temperature classifies $ZrB_2$ as an ultra-high temperature ceramic (UHTC).[4] UHTCs have been proposed for use in many different applications due to their high melting temperatures (>3000°C), as well as their high strength and chemical inertness.[5] Some of these applications include, but are not limited to, use as leading edges on hypersonic vehicles, refractory linings, high temperature electrodes, and cutting tools.[6] In applications such as hypersonic vehicles, it is desirable for the material to have a high thermal conductivity, allowing for the heat to be transported away from the leading edges.[4]

Because of a low coefficient of self-diffusion, high temperatures and pressures are often required for densifying $ZrB_2$.[7] To help the densification process, sintering aids such as boron carbide ($B_4C$), tungsten carbide (WC), silicon carbide (SiC), and molybdenum disilicide ($MoSi_2$) have been used to remove oxygen from the surface of the $ZrB_2$ powders and decrease grain coarsening.[8] These additives are effective sintering aids that can improve mechanical properties and the oxidation resistance of $ZrB_2$.[9,10,11] However, they can have a negative impact on the thermal conductivity. For example, the thermal conductivity at room temperature varies widely with values ranging from 108 W/m•K for nominally pure $ZrB_2$ prepared by reactive spark plasma sintering (SPS) of elemental powders[12], to less than 60 W/m•K for $ZrB_2$ prepared from powders attrition milled with WC media.[13] While no definitive study has been reported, one possible reason for this difference is the presence of impurities from the milling process.

Several other transition metal borides also exhibit properties that are similar to $ZrB_2$. For example, hafnium diboride, niobium diboride, titanium diboride and yttrium diboride all have the same P6/mmm crystal symmetry.[1] Metal diborides also exhibit significant mutual solubility.[1] Additionally, several metal borides have been reported to have high thermal and electrical conductivities.[14] However, no definitive study has been reported. One possible reason for this difference is the presence of impurities from the milling process. The purpose of this investigation was to analyze the effect that various transition metal borides (TMBs) have on the thermal properties of $ZrB_2$.

**II. Experimental Procedure**

Zirconium diboride and phenolic resin were batched with either a transition metal boride or with elemental transition metal and boron powders to produce the compositions shown in Table I. The starting powders were: $ZrB_2$ (Grade B, H.C. Starck), $HfB_2$ (Grade A, H.C. Starck), niobium (-325 mesh, 99.8%, Johnson Matthey), tungsten (<0.5um, 99.9%, Johnson Matthey), $TiB_2$ (Grade HCT-F, Momentive), yttrium (-40 mesh, 99.9%, Alfa Aesar), and amorphous boron (SB99, SB Boron Corporation, Bellwood, IL). Phenolic resin (Georgia Pacific) was added as a carbon source, which acted as a densification aid.

With the exception of $(Zr,Y)B_2$, the $ZrB_2$, TMB or transition metal, and boron powders were mixed by ball milling, with $ZrB_2$ media, in acetone at 60 rpm for 24 hrs. Next, phenolic resin was added followed by ball milling at 30 rpm for one hour. Hexane was used as the solvent for $(Zr,Y)B_2$ in an attempt to minimize contact between the

yttrium powder and oxygen. The powders were dried by rotary evaporation at a temperature of 70 °C, vacuum of 68 kPa, and a rotation speed of 60 rpm.

Dried powders were sieved through a 60 mesh screen and loaded into a 44.5 mm diameter circular graphite die (Graphite Products Corp, Madison Heights, MI) that was lined with graphite paper and sprayed with boron nitride (Cerac, SP-108, Milwaukee, WI). Densification was accomplished in a graphite element hot press (Thermal Technology Inc., Model HP20-3060-20, Santa Rosa, CA). Below 1600°C, the hot press was heated at a rate of 25°C/min under mild vacuum, (23 Pa). Reaction holds of one hour were utilized at 1250°C, 1450°C, and 1600°C to facilitate removal of surface oxides from the $ZrB_2$ particles. After the hold at 1600°C, the furnace was filled with flowing helium at a pressure of ~$10^5$ Pa. In addition, a uniaxial pressure of 32 MPa was applied and the powder was heated at 40°C/min to 2150°C. Specimens were held until ram travel had stopped for 10 minutes. At that point, the furnace power was turned off and it was allowed to cool naturally to room temperature. The pressure was removed after the temperature dropped below 1250°C.

The resulting billets were ground to produce parallel faces and cut into specimens that were either 12.7 mm by 12.7 mm by 2.5 mm rectangular prisms or 25.4 mm diameter by 1 mm tall cylinders. Archimedes method (ASTM standard C830-00)[15] was used to determine the bulk density and apparent porosity of the specimens using vacuum infiltration with distilled water as the immersing medium. The bulk and crystallographic densities were then used to determine the relative density. Crystallographic densities were estimated from nominal compositions and lattice parameters determined using x-ray diffraction (XRD) analysis. The temperature-dependent density values were determined

from measured Archimedes bulk density and the linear expansion data for polycrystalline $ZrB_2$ from Touloukian[16], according to Equations 1 and 2, where ρ is the density ($g/cm^3$), $\Delta L/L_o$ is the equation for percent linear expansion (%) from Touloukian[16], shown in Equation 2, and T is temperature (K).

$$\rho = \rho_o\left(1 + \frac{\frac{\Delta L}{L_o}}{100}\right)^3 \quad (1)$$

$$\frac{\Delta L}{L_o} = -0.135 + 3.940 \times 10^{-4}T + 2.390 \times 10^{-7}T^2 - 3.976 \times 10^{-11}T^3 \quad (2)$$

For microstructure analysis, specimens were polished with diamond abrasive slurry (South Bay Technologies, San Clemente, CA) to 0.25 μm and etched with potassium hydroxide (Fisher Scientific, Fair Lawn, NJ) at 210°C. The microstructure was investigated by imaging with scanning electron microscopy (SEM; S570 or S4700, Hitachi, Japan) and the grain size was determined by examining at least 150 grains per composition with image analysis software (ImageJ, National Institutes of Health, Bethesda, MD). The rectangular prisms were coated with graphite spray (Sprayon, Cleveland, OH) and used for measuring the thermal diffusivity, using the laser flash technique (Flashline 5000, Anter Corp, Pittsburg, PA) following ASTM standard E1461-11.[17] The Clark and Taylor method was used to calculate the thermal diffusivity from the measured temperature rise times according to Equations 3-5, where α is the thermal diffusivity ($cm^2/s$), $K_R$ is the Clark and Taylor correction factor, L is the thickness of the specimen (cm), and $t_n$ is the time required for the temperature to increase by the designated fraction(s).[17]

$$\alpha_{corrected} = \frac{\alpha K_R}{0.13885} \quad (3)$$

$$\alpha = 0.1388\frac{L^2}{t_{0.50}} \quad (4)$$

$$K_R = -0.3461467 + 0.361578\left(\frac{t_{0.75}}{t_{0.25}}\right) - 0.06520543\left(\frac{t_{0.75}}{t_{0.25}}\right)^2 \quad (5)$$

An exponential fit was applied to the thermal diffusivity data, shown in Equation 6, where α is the diffusivity ($cm^2/s$) and T is temperature in Kelvin.

$$\alpha = ae^{b/T} \quad (6)$$

The resulting trend line for thermal diffusivity, from Equation 6, was combined with the temperature-dependent bulk density, from Equation 1, and the heat capacity values for $ZrB_2$ from NIST-JANAF[18], shown in Equation 7, to calculate the thermal conductivity using Equation 8,[13] where $k_t$ is the thermal conductivity (W/m•K), α is the thermal diffusivity ($cm^2/s$), $\rho$ is the density ($g/cm^3$), *Cp* is the heat capacity (J/mol•K), *M* is the molar mass (g/mol), and T is the temperature in Kelvin. The conductivity was then corrected for porosity using the Maxwell equation[19] shown in Equation 9, where k is the total intrinsic thermal conductivity (W/m•K), and P is the volume fraction of porosity.

$$C_p = 66.96241 + 5.665010\left(\frac{T}{1000}\right) + 1.433879\left(\frac{T}{1000}\right)^2 - 0.151665\left(\frac{T}{1000}\right)^3 - 1.835999\left(\frac{T}{1000}\right)^{-2} \quad (7)$$

$$k_t = \frac{\left(\frac{100cm}{m}\right)\alpha\rho C_p}{M} \quad (8)$$

$$k = k_t \frac{(1+0.5\,P)}{(1-P)} \quad (9)$$

The electrical resistivity was measured using the cylindrical specimens and the van der Pauw method described in ASTM standard F76-08.[20] A linear trend line was fit to the measured values, shown in Equation 10.

$$\rho = aT + b \quad (10)$$

The electron contribution to the thermal conductivity was estimated using the calculated resistivity relation and the Wiedemann-Franz law, shown in Equation 11, where $k_e$ is the electron contribution to the thermal conductivity (W/m•K), $L_o$ is the theoretical Lorenz number ($2.44 \times 10^{-8}$ W•Ω/K$^2$), T is the temperature (K), and σ is the electrical conductivity (S/m).[13]

$$k_e = L_o T \sigma \quad (11)$$

The phonon contribution to thermal conductivity, $k_{p,}$ was determined by subtracting the electron portion from the total thermal conductivity, shown in Equation 12.

$$k_p = k - k_e \tag{12}$$

X-ray diffraction analysis was used to identify crystalline phases. Part of a billet of each composition was crushed, ground in an alumina mortar, and sieved through a 200 mesh screen. Rietveld refinement of XRD data was used to determine the lattice parameters.

**III. Results and Discussion**

Table II summarizes the microstructural characteristics of the materials examined in this study including measured bulk density, porosity, and average grain size. In addition, the crystallographic density was calculated from the nominal compositions. All of the ceramics reached >98.5% relative density. Archimedes measurements indicated that the specimens had negligible open porosity.

The transition metal additives appear to dissolve into the $ZrB_2$ matrix. Figure 1 shows the SEM micrographs of thermally etched cross sections. The molten salt etch used to highlight the grain structure exaggerated the size of the pores, but the micrographs still allow grain size measurement along with identification of pore locations. The amount of porosity was minimal, the pores were primarily round in shape,

and intragranular. The range of porosity values among the compositions was small, ranging from 0 to 1.5 vol%. The black phase, which was primarily located on the grain boundaries, was residual carbon that was not removed by reaction with oxides or did not go into solution. The amount of carbon present is approximately the same in all specimens, ~1 vol%, and is not expected to influence comparisons between the measured thermal properties. The measured average grain size ranged from 8 to 29 um. Based on previous analysis by Zimmermann[13], the grain sizes were large enough that they were not expected to have a significant effect on the measured thermal properties. In addition, XRD analysis (not shown) indicated that all of the hot pressed ceramics contained a single crystalline phase consistent with the $ZrB_2$ structure. Overall, the materials that were produced appear to be suitable to study the influence of the transition metal additives without significant effects from differences in porosity or grain size.

Figure 2 shows the measured thermal diffusivity values for all of the compositions. The standard deviation was found to be less than 1.5% of the average diffusivity, of three shots, at each temperature for all compositions. The diffusivity data were fit with an exponential trend line (Equation 6). The values for *a* and *b* as well as the regression of the fits are shown in Table III. The measured thermal diffusivity ranged from 0.331 $cm^2/s$ for $(Zr,Y)B_2$, to 0.128 $cm^2/s$ for $(Zr,W)B_2$ at 25°C and 0.253 $cm^2/s$ for $(Zr,Y)B_2$, to 0.115 $cm^2/s$ for $(Zr,W)B_2$ at 200°C. The diffusivity for all of the compositions decreased with temperature, although at different rates. These values indicate that small amounts of transition metals can have a large impact on thermal transport in $ZrB_2$, affecting both the magnitude of the values and the degree at which thermal diffusivity changes with temperature.

Figure 3 shows thermal conductivities calculated using Equation 9 for all of the compositions. Nominally pure $ZrB_2$ had the highest thermal conductivity with a value of 88 W/m•K at 25°C that decreased to 86 W/m•K at 200°C. The room temperature value is lower than the thermal conductivity of 108 W/m•K reported by Zhang[12] for $ZrB_2$ produced by reactive spark plasma sintering of elemental powders. However, Zhang's is one of the highest values reported for $ZrB_2$ to date and may be due to the higher purity that resulted from the in-situ synthesis and densification process. The thermal conductivity of nominally pure $ZrB_2$ measured in the present study is similar to the value of 92 W/m•K reported by Thompson[21] for $ZrB_2$ produced by hot pressing of commercially available powders. Both of these values are significantly higher than 56 W/m•K, which was reported by Zimmermann[13] for powders that had been attrition milled with WC media. Hence, the room temperature thermal conductivity of nominally pure $ZrB_2$ produced in the present study is consistent with values reported for fully dense phase-pure $ZrB_2$ produced from commercial powder.

The addition of yttrium or titanium to $ZrB_2$ had almost no effect on the thermal conductivity of the resulting solid solutions. At room temperature the thermal conductivity was 87 W/m•K for $(Zr,Y)B_2$ and $(Zr,Ti)B_2$. The thermal conductivities decreased slightly as temperature increased to 200°C, with values of 86 W/m•K for both $(Zr,Y)B_2$ and $(Zr,Ti)B_2$. Apparently, small amounts of some transition metals do not impact the thermal properties of $ZrB_2$. Both Y and Ti have lower atomic numbers and masses than Zr and are positioned directly to the left (Y) and above (Ti) Zr in the periodic table.

The additions of hafnium and niobium decreased the thermal conductivities of the resulting ceramics. At 25°C, the thermal conductivities were 81 W/m•K for $(Zr,Hf)B_2$ and 74 W/m•K for $(Zr,Nb)B_2$. At 200°C, the values were 82 W/m•K and 76 W/m•K, respectively. Decreases between 4% and 16% compared to the nominally pure composition. In this case, both Hf, and Nb have higher atomic numbers and are heavier than Zr with Hf lying below and Nb to the right of Zr in the periodic table.

The most significant impact on thermal conductivity was observed when W was added. The room temperature thermal conductivity of $(Zr,W)B_2$ was 34 W/m•K, which increased slightly to 39 W/m•K at 200°C. Both are a decrease of more than 50% compared to nominally pure $ZrB_2$. Interestingly, $(Zr,W)B_2$ was the only composition to exhibit a noticeable increase in thermal conductivity with increasing temperature for the range of temperatures tested. Combined with the observations from the other additions, it appears that the effect of transition metals on thermal conductivity increases moving down and right across the periodic table. Moving across a row to the right appears to have a stronger effect than moving down in a column.

Figure 4 shows the electrical resistivity values that were measured for all of the compositions. The standard deviation was found to be less than 1% of the average, for 3 different test currents, for each composition at each temperature. The electrical resistivity values follow a trend similar to the inverse of the thermal conductivity. Whereas the room temperature thermal conductivity of $ZrB_2$ was the highest, the room temperature resistivity measurement of $ZrB_2$ was the lowest, 8.9 μΩ-cm. The hafnium, titanium, and yttrium additions also had the smallest impact, only raising the resistivity slightly to 9.2, 9.2, and 9.8 μΩ-cm respectively, (<10% increase). The niobium and tungsten additions

had a larger influence, raising the resistivity to 11.6, and 30.3 μΩ-cm respectively, (30 and 240% increases).

The electrical resistivity data were fit to linear trend lines (Equation 10). The values for *a* and *b* as well as the regression of the fits are listed in table IV. The resistivity fit was inverted to find the electrical conductivity, which was then used to calculate the electron contribution to the thermal conductivity using the theoretical Lorenz number, and the Wiedemann-Franz law (Equation 11).

The theoretical Lorenz number was originally derived by comparing the thermal and electrical conductivities of metals, where conduction is almost entirely electronic. Sommerfeld later calculated the theoretical Lorenz number using Fermi-Dirac statistics and got a value of: $L_o = \frac{\pi^2}{3}\left(\frac{K_b^2}{e^2}\right) = 2.44 \times 10^{-8}\, W \bullet \Omega/K^2$, where $K_b$ is Boltzmann's constant and $e$ is electron charge. However, this value only applies when the mean free path for electrical conduction ($l_e$) is equal to the mean free path for thermal conduction ($l_t$). The actual Lorenz number for any material can, therefore, be represented as: $L = L_o(\frac{l_t}{l_e})$.[22] Since the mean free paths of the boride ceramics in the present study are not known, $L_o$ was used to estimate the electron contribution to thermal conductivity.

Figure 5 summarizes the electron contribution to thermal conductivity calculated from the electrical resistivity fit (Equation 10) using the Wiedemann-Franz law (Equation 11).

Additives lowered the electron contribution to thermal conductivity of $ZrB_2$ in a trend that was similar to total thermal conductivity. The main difference was that any transition metal addition reduced the electron contribution to thermal conductivity, not just moving down or to the right on the periodic table. For example, the addition of

group IVb metals such as Ti and Hf (i.e., the same as zirconium) resulted in small (<5%), but repeatable decreases in the electron portion of thermal conductivity. For $ZrB_2$, the electron contribution was 88 W/m•K compared to 85 W/m•K for $(Zr,Hf)B_2$ and 87 W/m•K for $(Zr,Ti)B_2$. The addition of metals from different groups resulted in larger decreases in the electron contribution to thermal conductivity. The electron contributions to thermal conductivity were 81 W/m•K for $(Zr,Y)B_2$ (8% decrease, group IIIb), 67 W/m•K for $(Zr,Nb)B_2$ (24% decrease, group Vb), and 25 W/m•K for $(Zr,W)B_2$ (72% decrease, group VIb).

Figure 6 summarizes the phonon contribution to thermal conductivity that was estimated by subtracting the value for the electron contribution from the total thermal conductivity (Equation 12). For all of the specimens, the electron contribution was much larger than the phonon contribution.

The differences between the changes in total thermal conductivity and those of the electron and phonon portions indicate that certain additives have a larger impact on electron conduction, while others have a greater influence on phonon conduction. For example, yttrium and titanium additions decreased the electron contribution, but increased the phonon contribution by roughly equal amounts (7 and 1 W/m•K respectively). Although neither additive greatly changed the total thermal conductivity at room temperature, the addition of Y had a larger influence on the electron and phonon contributions to thermal conductivity than Ti. Tungsten decreased the electron contribution by ~60 W/m•K but increased the phonon contribution by ~10 W/m•K. Even though the addition of W increased the phonon contribution, similar to Y, it resulted in a significant decrease in the electron contribution, resulting in a net decrease in thermal

conductivity. The reason for the apparent increase in phonon conductivity with the addition of W is not clear, but it could be due to the use of the theoretical Lorenz number in the calculation of the electron contribution. It seems reasonable that the addition of W decreased both the electron and phonon contributions by changing the mean free paths for phonon and electron conduction, but measuring those quantities to determine the actual Lorenz number for $(Zr,W)B_2$ was beyond the scope of the present study.

In some cases, a negative phonon contribution to thermal conductivity was calculated. Obviously, negative phonon contributions are not physically possible. As with the addition of W discussed above, the Lorenz number for $ZrB_2$ and $ZrB_2$ with transition metal additives should have a smaller value than $L_o$.

XRD analysis was used to determine the lattice parameters for each composition produced in the present study. The measured lattice parameters are summarized in Table V. In addition, the unit cell volume and percent change in unit cell volume compared to nominally pure $ZrB_2$ were also calculated. Figure 7 shows the calculated volume change vs. the total thermal conductivity.

For the addition of Y, Hf, and Nb, the total thermal conductivity decreased in direct proportion to the volume change induced by substitution of the other metal into the $ZrB_2$ lattice. These additives change the lattice parameters of the $ZrB_2$ when they go into solid solution. The addition of Ti did not follow this trend, as the thermal conductivity of $(Zr,Ti)B_2$ was higher than expected based on the change in lattice parameter. Unlike the pure diborides of the other additives, the lattice parameters of $TiB_2$ are controlled by the B-B bond lengths, not the bonds in the close packed Ti layer (a-lattice parameter) or the Ti-B bonds (c-lattice parameter) due to the smaller size of the titanium atom compared to

zirconium.[1] The total thermal conductivity of $(Zr,W)B_2$ was lower than expected based on the measured change in the unit cell volume. The addition of W may have decreased the thermal conductivity more than expected due to the structure of W-borides. Unlike the diborides of the other additives examined in this study, the W-borides have a different structure, $P6_3/mmc$ for $W_2B_4$ compared to P6/mmm for the other diborides examined in the present study.[23] Thus, in addition to the change in lattice parameters and volume, the addition of W may be inducing additional strain into the $ZrB_2$ lattice due to the different structure of W-borides. Regardless, using the lattice parameters, especially combined with atom location on the periodic table, may be a suitable way for predicting the thermal properties of $ZrB_2$-based ceramics.

**IV. Summary**

The effect of transition metal boride additions on the thermal conductivity of $ZrB_2$ was studied. A series of dense $ZrB_2$ ceramics containing nominally 3 at% additions of various transition metals were produced by hot pressing. The transition metals dissolved into the $ZrB_2$ lattice to form solid solutions, as confirmed by XRD and microstructure analyses. The room temperature thermal conductivities decreased from 88 W/m•K for nominally pure $ZrB_2$ to 34 W/m•K for $(Zr,W)B_2$. The decrease in total thermal conductivity was stronger as transition metal additives were selected from farther down and to the right from Zr on the periodic table. For the addition of Y, Hf, and Nb, the total thermal conductivity values had a linear relationship with the change in unit cell volume that resulted from substitution of the transition metal atoms into the $ZrB_2$ structure. However, changes in thermal conductivity did not correlate to changes in lattice

parameters for the additions of Ti or W. For the addition of Ti, the lattice parameters are controlled by the B sublattice, so the addition of Ti into $ZrB_2$ did not decrease thermal conductivity as much as expected based on the change in unit cell volume. For W additions, the decrease in thermal conductivity was greater than expected based on the change in unit cell volume. This may be due to the stable structure of W-borides, which have buckled B planes. For W additions to $ZrB_2$, this may result in additional strain in the lattice and a stronger decrease in thermal conductivity than predicted by the change in lattice parameters alone. Electrical resistivity measurements were used to estimate the electron contribution to total thermal conductivity using the Wiedemann-Franz law, which revealed that electron transport dominated thermal conductivity for all compositions. The results of this study indicate that small amounts of transition metals, depending on their position on the periodic table and their effect on lattice parameters, influence the thermal properties of zirconium diboride.

**Acknowledgements**

This research was funded as part of the Aerospace Materials for Extreme Environments Program (Dr. Ali Sayir, Program Manager) in the U.S. Air Force Office of Scientific Research under contract number FA9550-09-1-0168. In addition, the authors would like to thank the Advanced Materials Characterization Laboratory in the Materials Research Center at Missouri S&T for the assistance with XRD (Eric Bohannan) and SEM (Clarissa Wisner).

## References

[1] B. Post, F. W. Glaser, and D. Moskowitz, "Transition metal diborides," *Acta Metallurgica,* **2**[1] 20-25 (1954).

[2] X. Zhang, X. Luo, J. Han, J. Li, and W. Han, "Electronic structure, elasticity and hardness of diborides of zirconium and hafnium: First principles calculations," *Computational Materials Science,* **44**[2] 411-21 (2008).

[3] R. A. Cutler, "Engineering Properties of Borides," pp. 787-803. in Ceramics and Glasses: Engineered Materials Handbook, **Vol. 4.** Edited by S. J. S. Jr. ASM International, Materials Park, OH, 1991.

[4] E. Wuchina, E. Opila, M. Opeka, W. Fahrenholtz, and I. Talmy, "UHTCs: Ultra-High Temperature Ceramic Materials for Extreme Environment Applications," *Interface,* **16**[4] 30-36 (2007).

[5] R. Telle, L. S. Sigl, and K. Takagi, "Boride-Based Hard Materials," pp. 802-945. in Handbook of Ceramic Hard Materials, Vol. 2, Edited by R. Riedel**,** Wiley-VCH Verlag GmbH, Weinheim, Germany, 2008.

[6] W. G. Fahrenholtz, G. E. Hilmas, I. G. Talmy, and J. A. Zaykoski, "Refractory Diborides of Zirconium and Hafnium," *Journal of the American Ceramic Society,* **90**[5] 1347-64 (2007).

[7] D. Kalish and E. V. Clougherty, "Densification Mechanisms in High-pressure Hot-Pressing of $HfB_2$," *Journal of the American Ceramic Society,* **52**[1] 26-30 (1969).

[8] M. Thompson, W. G. Fahrenholtz, and G. Hilmas, "Effect of Starting Particle Size and Oxygen Content on Densification of $ZrB_2$," *Journal of the American Ceramic Society,* **94**[2] 429-35 (2011).

[9] S. C. Zhang, G. E. Hilmas, and W. G. Fahrenholtz, "Pressureless Densification of Zirconium Diboride with Boron Carbide Additions," *Journal of the American Ceramic Society,* **89**[5] 1544-50 (2006).

[10] A. L. Chamberlain, W. G. Fahrenholtz, and G. E. Hilmas, "Pressureless Sintering of Zirconium Diboride," *Journal of the American Ceramic Society*, **89**[2] 450-56 (2006).

[11] L. Silvestroni, H.-J. Kleebe, S. Lauterbach, M. Müller, and D. Sciti, "Transmission electron microscopy on Zr- and Hf-borides with $MoSi_2$ addition: Densification mechanisms," *Journal of Materials Research*, **25**[05] 828-34 (2010).

[12] L. Zhang, D. A. Pejaković, J. Marschall, and M. Gasch, "Thermal and Electrical Transport Properties of Spark Plasma-Sintered $HfB_2$ and $ZrB_2$ Ceramics," *Journal of the American Ceramic Society*, **94**[8] 2562-70 (2011).

[13] J. W. Zimmermann, G. E. Hilmas, W. G. Fahrenholtz, R. B. Dinwiddie, W. D. Porter, and H. Wang, "Thermophysical Properties of $ZrB_2$ and $ZrB_2$–SiC Ceramics," *Journal of the American Ceramic Society*, **91**[5] 1405-11 (2008).

[14] H. J. Juretschke and R. Steinitz, "Hall effect and electrical conductivity of transition-metal diborides," *Journal of Physics and Chemistry of Solids*, **4**[1–2] 118-27 (1958).

[15] ASTM Standard C830, 2000 (2011), "Standard Test Methods for Apparent Porosity, Liquid Absorption, Apparent Specific Gravity, and Bulk Density of Refractory Shapes by Vacuum Pressure," ASTM International, West Conshohocken, PA, 2012, DOI: 10.1520/C0830-06R11, www.astm.org.

[16] Y. Touloukian, C. Ho, and D. Dewitt, "Thermal Expansion: Nonmetallic Solids," pp. 784-9 in Thermophysical Properties of Matter, **Vol. 13.** Edited by Touloukian. IFI/Plenum, New York, 1977.

[17] ASTM Standard E1461, 2011 "Standard Test Method for Thermal Diffusivity by the Flash Method," ASTM International, West Conshohocken, PA, 2006, DOI: 10.1520/E1461-11, www.astm.org.

[18] M. W. Chase, S. National Institute of, and Technology, "NIST-JANAF thermochemical tables," **Vol. no. 9.** American Chemical Society: Woodbury, N.Y, (1998).

[19] G. Ondracek and B. Schulz, "The porosity dependence of the thermal conductivity for nuclear fuels," *Journal of Nuclear Materials,* **46**[3] 253-58 (1973).

[20] ASTM Standard F76, 2008, "Standard Test Methods for Measuring Resistivity and Hall Coefficient and Determining Hall Mobility in Single-Crystal Semiconductors," ASTM International, West Conshohocken, PA, 2006, DOI: 10.1520/F0076-08, www.astm.org

[21] M. J. Thompson, "Densification and Thermal Properties of Zirconium Diboride Based Ceramics," Ph.D. Disertation, Missouri University of Science and Technology, Rolla, MO 2012.

[22] G. S. Kumar, G. Prasad, and R. O. Pohl, "Experimental determinations of the Lorenz number," *J Mater Sci,* **28**[16] 4261-72 (1993).

[23] M. Frotscher, W. Klein, J. Bauer, C.-M. Fang, J.-F. Halet, A. Senyshyn, C. Baehtz, and B. Albert, "$M_2B_5$ or $M_2B_4$? A Reinvestigation of the Mo/B and W/B System," *Zeitschrift für anorganische und allgemeine Chemie,* **633**[15] 2626-30 (2007).

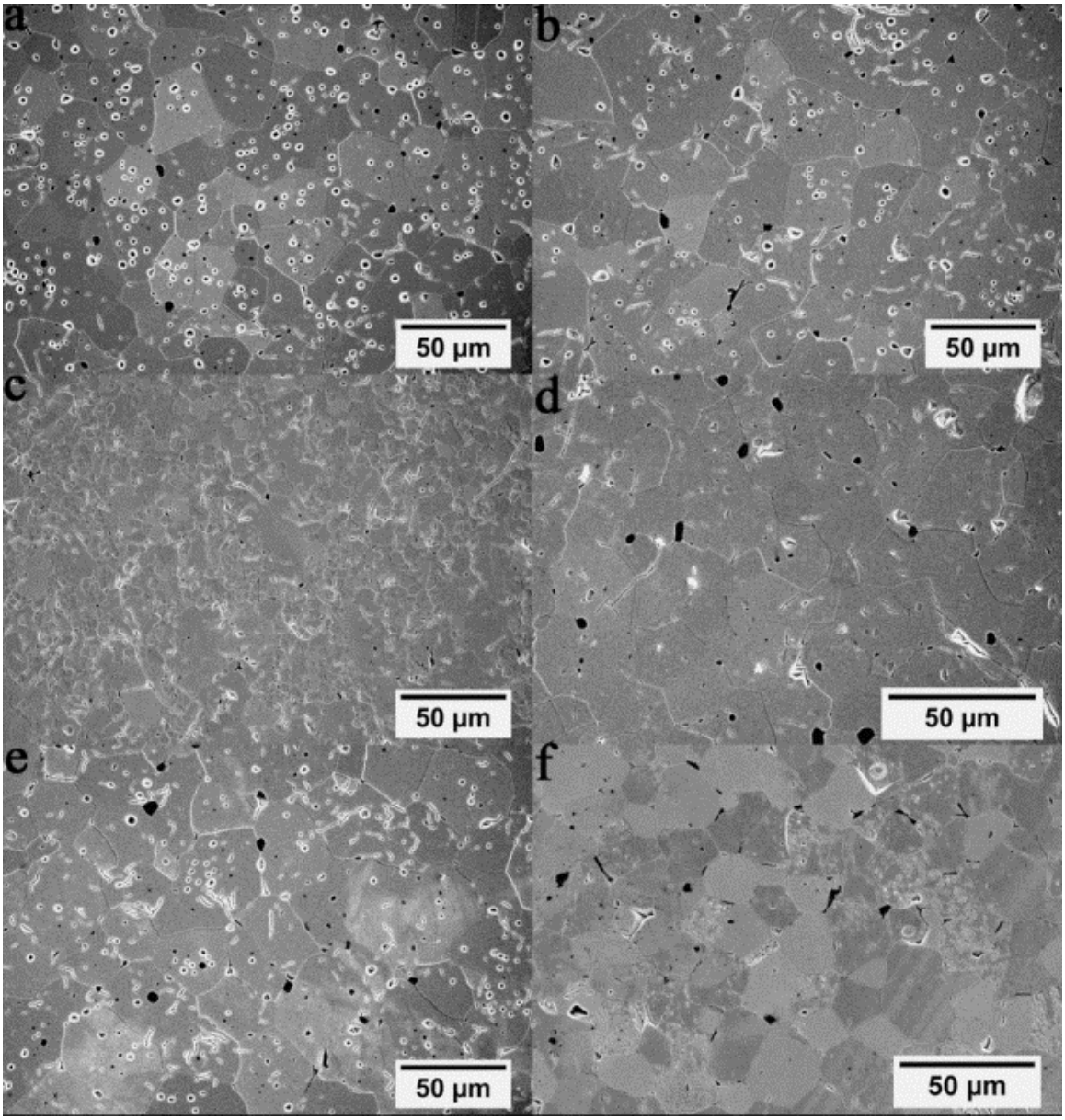


**Figure 1:** SEM micrographs of etched ceramics (a) $ZrB_2$, (b) $(Zr,Hf)B_2$, (c) $(Zr,Nb)B_2$, (d) $(Zr,W)B_2$, (e) $(Zr,Ti)B_2$, and (f) $(Zr,Y)B_2$.

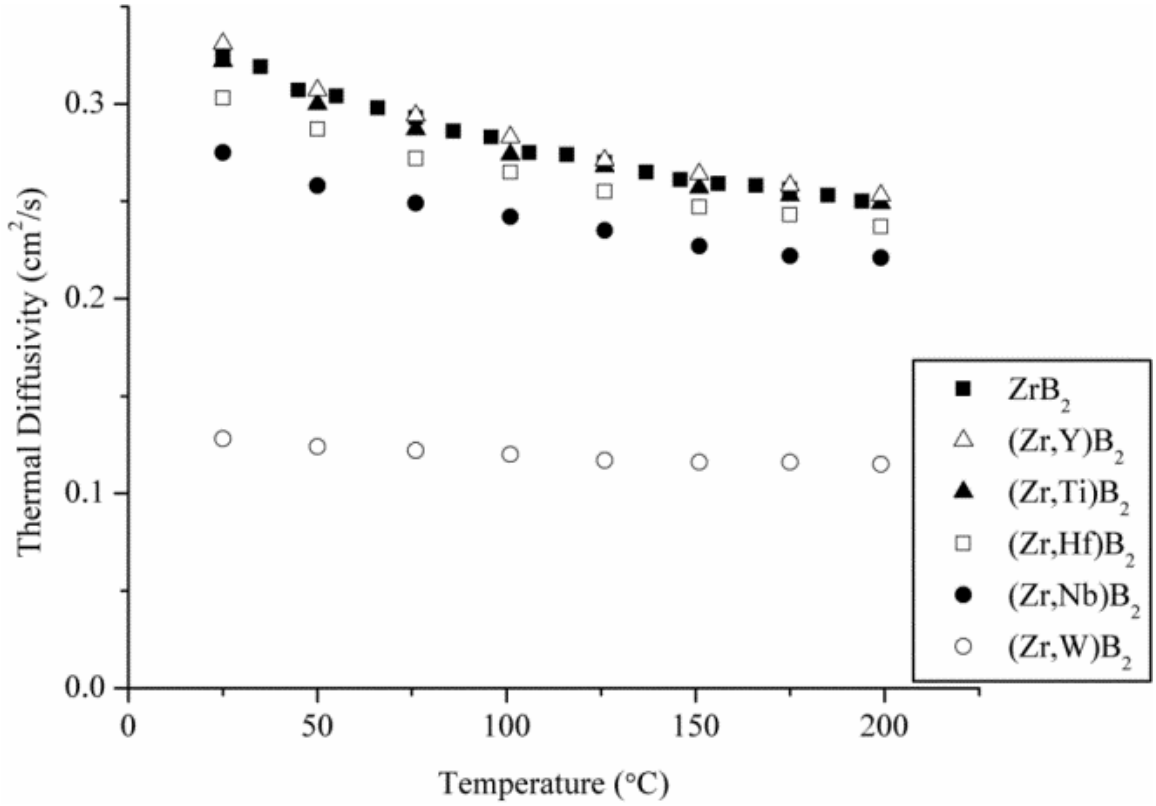


**Figure 2:** Measured thermal diffusivity as a function of temperature for $ZrB_2$ with transition metal additions.

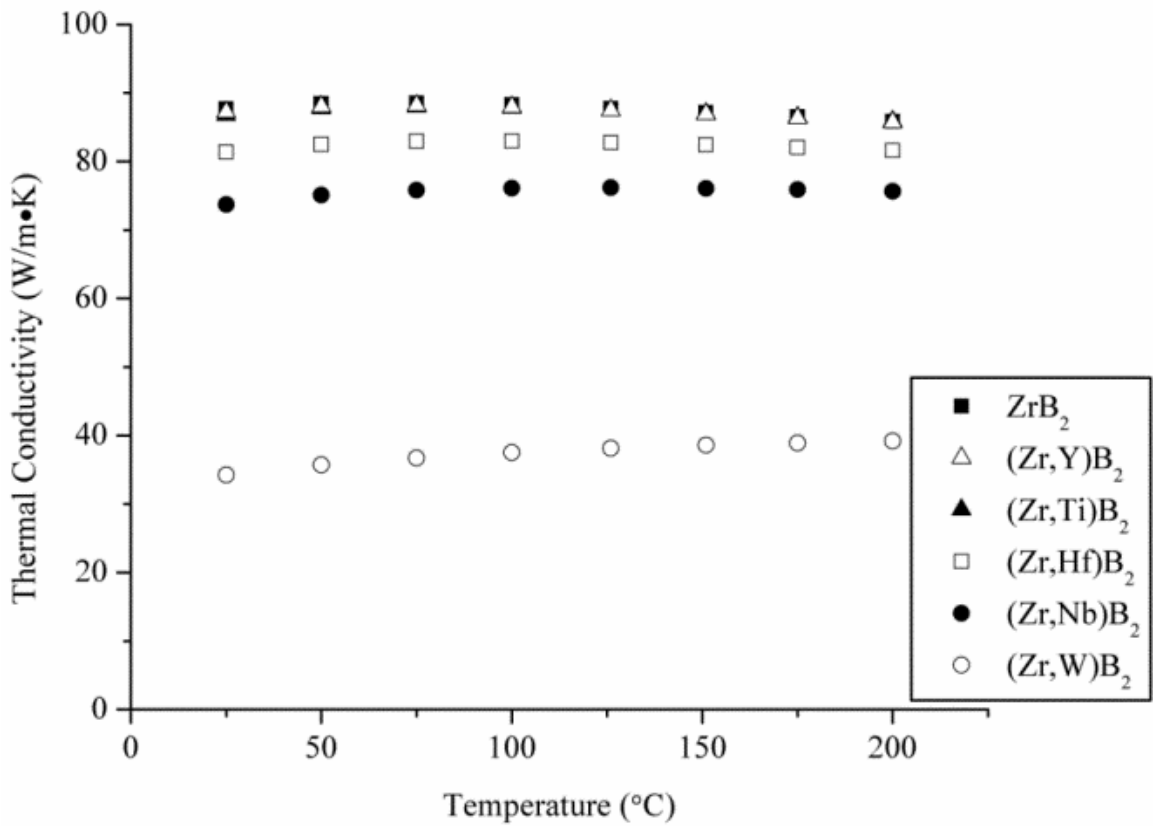


**Figure 3:** Thermal conductivity as a function of temperature for $ZrB_2$ with various transition metal additions.

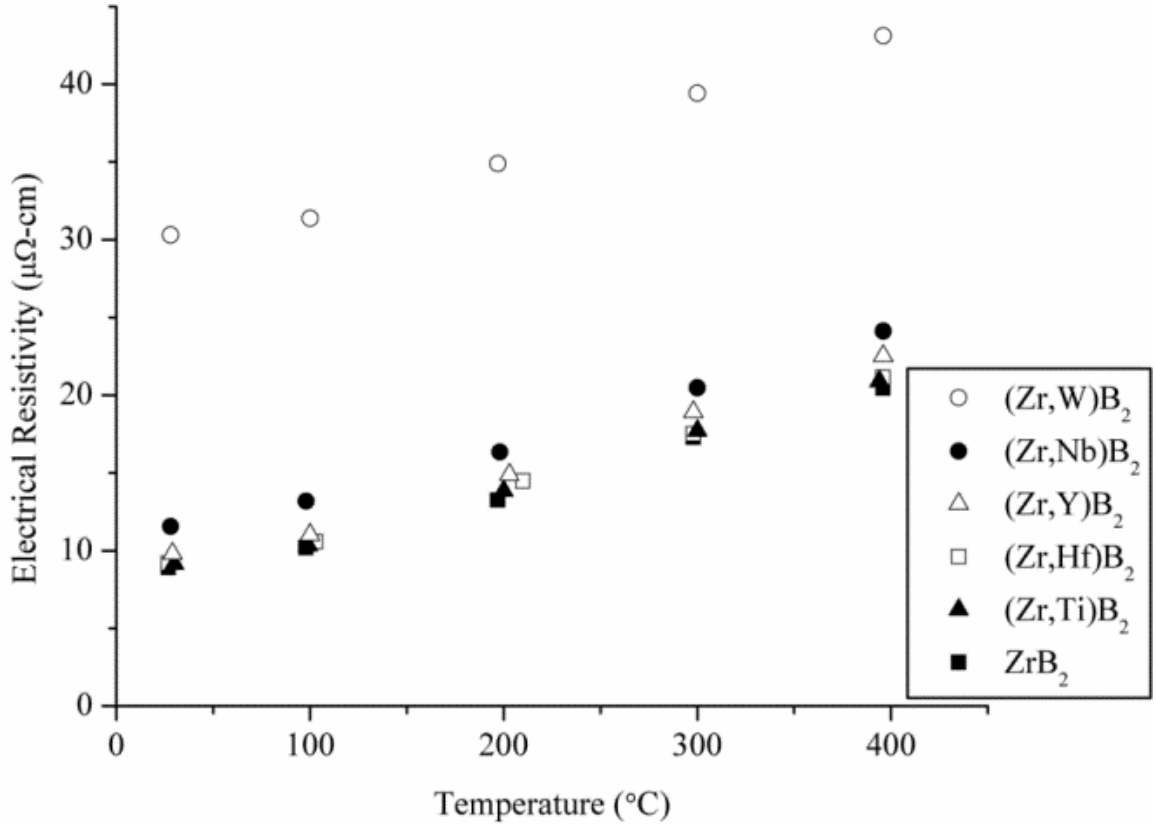


**Figure 4:** Electrical resistivity as a function of temperature for $ZrB_2$ with various transition metal additions.

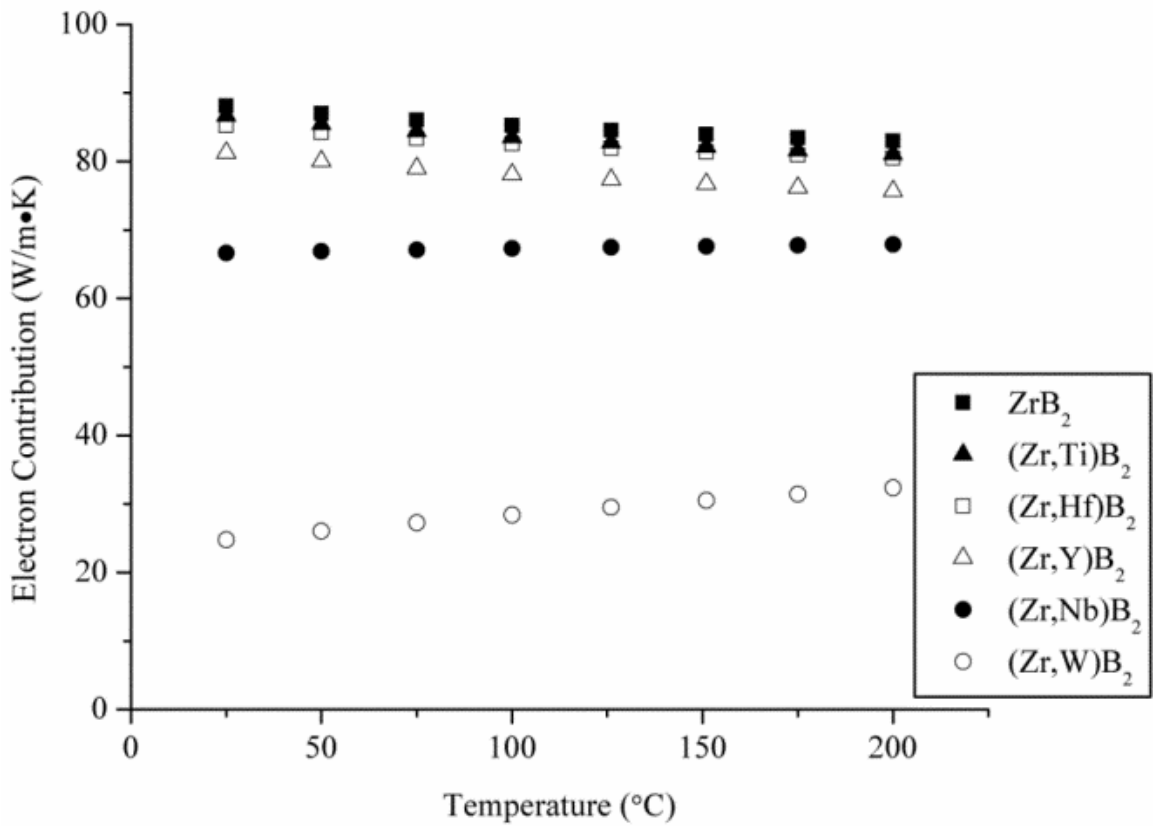


**Figure 5:** Electron contribution to thermal conductivity.

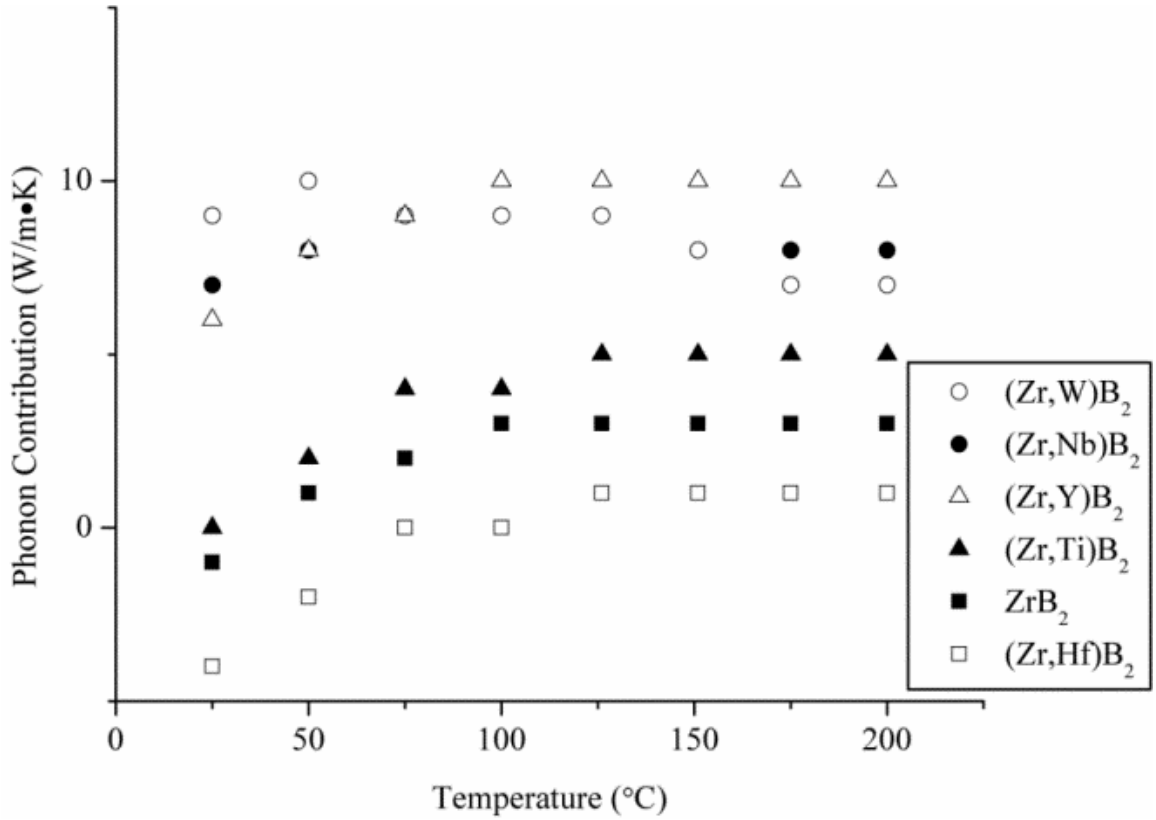


**Figure 6:** Phonon contribution to thermal conductivity.

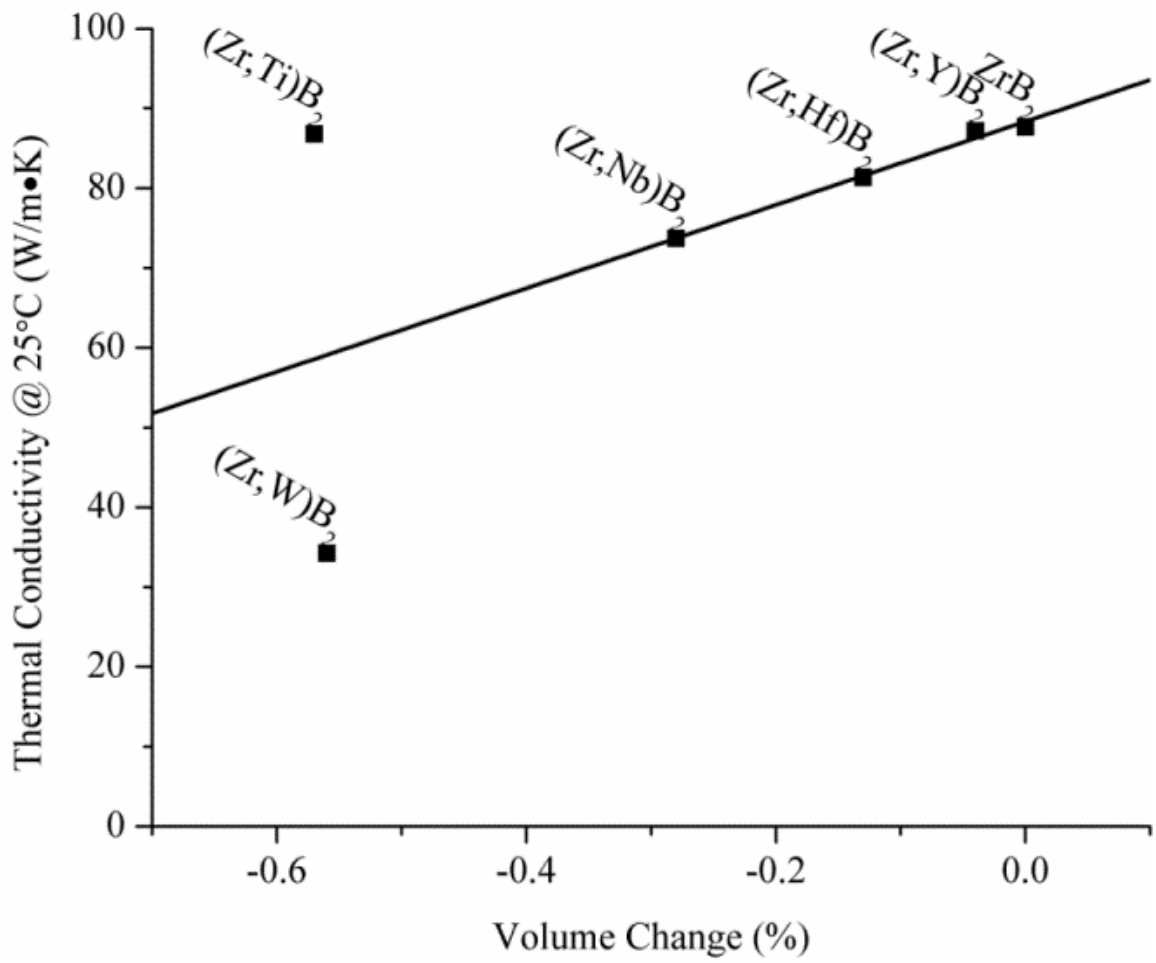


**Figure 7:** Relationship between volume change and the total thermal conductivity.

**Table I:** Designation and composition after milling for tested ceramics.

| Designation | Weight % | | | Atomic % | | | | | |
|---|---|---|---|---|---|---|---|---|---|
| | $ZrB_2$ | Carbon | TMB | Zr | TM | B | C | TM in Metal Sublattice | Metal to Boron Ratio |
| $ZrB_2$ | 99.5 | 0.5 | 0.0 | 32.8 | 0.0 | 65.7 | 1.5 | 0.0 | 50.0 |
| $(Zr,Hf)B_2$ | 94.3 | 0.5 | 5.2 | 31.8 | 1.0 | 65.6 | 1.5 | 3.0 | 50.0 |
| $(Zr,Nb)B_2$ | 96.3 | 0.5 | 3.2 | 31.8 | 1.0 | 65.7 | 1.5 | 3.2 | 50.0 |
| $(Zr,W)B_2$ | 94.0 | 0.5 | 5.5 | 31.7 | 1.0 | 65.8 | 1.5 | 3.0 | 49.7 |
| $(Zr,Ti)B_2$ | 97.1 | 0.6 | 2.3 | 31.5 | 1.2 | 65.5 | 1.7 | 3.7 | 50.0 |
| $(Zr,Y)B_2$ | 96.7 | 0.4 | 2.9 | 31.9 | 1.0 | 65.7 | 1.4 | 2.9 | 50.0 |

**Table II:** Designation, density, porosity, and average grain size for tested compositions.

| Designation | Theoretical Density | Bulk Density | Relative Density | Porosity | Grain Size |
|---|---|---|---|---|---|
| | $g/cm^3$ | $g/cm^3$ | % | % | μm |
| $ZrB_2$ | 6.05 | 5.97 | 98.6 | 1.4 | 22 +/- 20 |
| $(Zr,Hf)B_2$ | 6.20 | 6.17 | 99.5 | 0.5 | 29 +/- 27 |
| $(Zr,Nb)B_2$ | 6.08 | 6.04 | 99.3 | 0.7 | 8 +/- 10 |
| $(Zr,W)B_2$ | 6.23 | 6.29 | 99.9 + | 0.0 | 19 +/- 17 |
| $(Zr,Ti)B_2$ | 6.00 | 5.95 | 99.2 | 0.8 | 27 +/- 25 |
| $(Zr,Y)B_2$ | 6.02 | 6.01 | 99.8 | 0.2 | 19 +/- 16 |

**Table III:** Fitting parameters for thermal diffusivity data for all of the compositions.

| | Composition | | | | | |
|---|---|---|---|---|---|---|
| | $ZrB_2$ | $(Zr,Hf)B_2$ | $(Zr,Nb)B_2$ | $(Zr,W)B_2$ | $(Zr,Ti)B_2$ | $(Zr,Y)B_2$ |
| *a* ($cm^2/s$) | 0.1572 | 0.1561 | 0.1502 | 0.0943 | 0.1588 | 0.1602 |
| *b* (K) | 215.85 | 196.41 | 177.91 | 89.89 | 207.40 | 212.66 |
| Regression | 0.9967 | 0.9975 | 0.9918 | 0.9897 | 0.9940 | 0.9950 |

**Table IV:** Fitting parameters for electrical resistivity of all of the compositions.

| | Composition | | | | | |
|---|---|---|---|---|---|---|
| | $ZrB_2$ | $(Zr,Hf)B_2$ | $(Zr,Nb)B_2$ | $(Zr,W)B_2$ | $(Zr,Ti)B_2$ | $(Zr,Y)B_2$ |
| a | 0.0323 | 0.0332 | 0.0348 | 0.0363 | 0.0334 | 0.0360 |
| b | -1.3836 | -1.3696 | 0.5539 | 18.5220 | -1.5723 | -1.7768 |
| Regression | 0.99 | 0.9919 | 0.9926 | 0.9847 | 0.9915 | 0.9896 |

**Table V:** Summary of lattice parameters and unit cell volumes.

| Composition | Measured Lattice Parameters | | | |
|---|---|---|---|---|
| | a (Å) | c (Å) | Volume ($Å^3$) | Volume Change (%) |
| $ZrB_2$ | 3.16814(2) | 3.52992(5) | 30.683 | 0 |
| $(Zr,Hf)B_2$ | 3.16689(2) | 3.52828(5) | 30.645 | -0.13 |
| $(Zr,Nb)B_2$ | 3.16565(5) | 3.52552(11) | 30.597 | -0.28 |
| $(Zr,W)B_2$ | 3.16296(2) | 3.52161(5) | 30.511 | -0.56 |
| $(Zr,Ti)B_2$ | 3.16283(2) | 3.52163(7) | 30.509 | -0.57 |
| $(Zr,Y)B_2$ | 3.16754(2) | 3.52986(5) | 30.671 | -0.04 |

# 2. THERMAL PROPERTIES OF (Zr,TM)$B_2$ SOLID SOLUTIONS WITH TM = Ta, Mo, Re, V, AND Cr

Devon L. McClane*, William G. Fahrenholtz, and Gregory E. Hilmas

Materials Science and Engineering Department, Missouri University of Science and Technology, Rolla, Missouri 65409

## Abstract

The thermal properties were investigated for hot pressed zirconium diboride containing solid solution additions of tantalum, molybdenum, rhenium, vanadium, and chromium. The nominal additions were equivalent to 3 at% of each metal with respect to zirconium. Using 0.5 wt% carbon as a sintering aid, powders were hot-pressed to near full density at 2150°C. Reitveld refinement of x-ray diffraction data was used to measure lattice parameters and to ensure that the additives formed solid solutions. Thermal conductivities were calculated from measured thermal diffusivities and temperature-dependent values for density and heat capacity. Thermal conductivities at 25°C ranged from 88 W/m•K for nominally pure $ZrB_2$ down to 28 W/m•K for (Zr,Cr)$B_2$. Electron contributions to thermal conductivity were calculated from electrical resistivity measurements using the Wiedemann-Franz law. Decreases in phonon and electron conduction correlated to the size of the metallic additive, indicating that changes in atom size in the Zr lattice positions reduced thermal transport.

## I. Introduction

Zirconium diboride ($ZrB_2$) is a transition metal (TM) boride that belongs to the ultra-high temperature ceramic (UHTC) class of materials.[1] These materials are characterized by having melting temperatures in excess of 3000°C, as well as high strengths and chemical inertness.[2] Because of their high melting temperatures, these materials have been proposed for use as high temperature electrodes, refractory linings, and leading edges on hypersonic vehicles.[3] In applications such as leading edges on hypersonic vehicles, it is necessary for the material to also have a high thermal conductivity. A high thermal conductivity allows for heat to be transported away from the leading edge so that it can be dissipated.[1]

$ZrB_2$, as well as several other TM borides, have been reported to have high thermal and electrical conductivities.[4] However, it is often difficult to produce fully dense parts from these ceramics without incorporating sintering aids, or introducing other impurities as part of processing steps. To date, few studies have systematically investigated the effects of solid solution formation on thermal transport or other properties.

One recent study by our group investigated the effects of hafnium, niobium, tungsten, titanium, and yttrium additions on the thermal conductivity of $ZrB_2$ ceramics.[5] All of the additions formed solid solutions, with the transition metal substituting onto Zr sites in the lattice. The resulting ceramics were designated using the notation $(Zr,TM)B_2$ to indicate the specific TM that was dissolved into the $ZrB_2$. Different additives, summarized in Table I, had varying impacts on thermal conductivity. For example, the additions of Y or Ti had almost no effect on thermal conductivity, with room temperature

thermal conductivities of ~87 W/m•K compared to 88 W/m•K for nominally pure $ZrB_2$. In contrast, the addition of W decreased thermal conductivity to 34 W/m•K. The position of the additive relative to Zr on the periodic table was correlated to the effect on thermal conductivity, with the effect becoming larger for transition metals located farther down and to the right of Zr on the periodic table. X-ray diffraction analysis revealed that the unit cell volume for the $ZrB_2$-based ceramics decreased when these TMs were added to $ZrB_2$. The decrease in unit cell volume correlated to the reduction in thermal conductivity. Therefore, it was concluded that lattice strain, caused by the substitution of transition metal atoms for Zr in the lattice, affected both phonon and electron conduction, and lead to the observed decreases in thermal conductivity.[5]

The purpose of the present study was to investigate the effect of other transition metal additions on the thermal conductivity of $ZrB_2$. The additives investigated in the present study include tantalum, molybdenum, rhenium, vanadium, and chromium. This was done to determine if the trends identified in the previous study were generally applicable to other transition metals.

## II. Experimental Procedure

The procedures used in the present study were nominally identical to those described in Reference 5. The goal was to produce ceramics with similar relative densities and grain sizes to the previous study, so that the results could be directly compared. Briefly, zirconium diboride was batched with phenolic resin and either a transition metal boride or with elemental transition metal and boron powders to produce the $(Zr,TM)B_2$ compositions shown in Table II. The starting powders were: $ZrB_2$ (Grade

B, H.C. Starck, Newton, MA), tantalum (1-5um, 99.8%, Atlantic Equipment Engineers, Bergenfield, NJ), molybdenum (2-4um, 99.95%, Cerac, Milwaukee, WI), rhenium (-325 mesh, 99.98%, Colonial Metals, Elkton, MD), vanadium (-325 mesh, 99.5%, Alfa Aesar, Ward Hill, MA), $CrB_2$ (99%, Alfa Aesar), and amorphous boron (SB Boron Corporation, Bellwood, IL). Phenolic resin (Georgia Pacific, Atlanta, GA) was added as a carbon source, which acted as a densification aid.

The powder mixing method and sintering temperature schedule were the same as those described in RReference 5, with the exception of the final pressing temperature for $(Zr,Re)B_2$. For most of the compositions, ceramics were hot pressed at 2150°C under argon. However, a temperature of 2250°C was used for $(Zr,Re)B_2$ since the $ReB_2$ did not go into solution at 2150°C, confirmed by X-ray diffraction and microstructural analysis.

The resulting billets were cut and ground to produce either 12.7 mm by 12.7 mm by 2.5 mm rectangular prisms or 25.4 mm diameter by 1 mm tall cylinders with parallel faces. Archimedes method (ASTM standard C830-00)[6] was used to determine the bulk density and apparent porosity of the specimens using vacuum infiltration with distilled water as the immersing medium. The bulk and crystallographic densities were then used to determine the relative densities. Crystallographic densities were estimated from nominal compositions and lattice parameters determined using x-ray diffraction (XRD) analysis. Temperature dependent densities were estimated by using the linear expansion data for polycrystalline $ZrB_2$ from Touloukian[7], and the measured bulk densities, similar to the method described in Reference 5. Part of a billet of each composition was crushed, ground in an alumina mortar, and sieved through a 200 mesh screen. X-ray diffraction

analysis was used to identify crystalline phases, and Rietveld refinement was used to determine the lattice parameters.

The specimens were polished with diamond abrasive slurry (South Bay Technologies, San Clemente, CA) to 0.25 μm and etched with potassium hydroxide (Fisher Scientific, Fair Lawn, NJ) at 210°C, for microstructure analysis. The microstructure was investigated by imaging with scanning electron microscopy (SEM; S570 or S4700, Hitachi, Japan) and the grain size was determined by examining at least 625 grains per composition with image analysis software (ImageJ, National Institutes of Health, Bethesda, MD).

The rectangular prisms were coated with graphite (Sprayon, Cleveland, OH) and used for measuring the thermal diffusivity. The diffusivity was measured from room temperature to 2000°C using the laser flash technique (Flashline 5000, Anter Corp, Pittsburgh, PA) according to ASTM standard E1461-13.[8] The Clark and Taylor method was used to calculate thermal diffusivity from measured temperature rise.[8]

Similar to RReference 5, the thermal diffusivity data up to 200°C were fit with an exponential trend line (Equation 1) where α is the diffusivity ($cm^2/s$) and T is the temperature in Kelvin.

$$\alpha = ae^{b/T} \tag{1}$$

The thermal conductivity was calculated using Equation 2 from the resulting trend lines for thermal diffusivity, the temperature-dependent bulk densities, and the heat

capacity values for $ZrB_2$ from the NIST-JANAF tables[9], where $k_t$ is the thermal conductivity (W/m•K), α is the thermal diffusivity ($cm^2/s$), $\rho$ is the density ($g/cm^3$), *Cp* is the heat capacity (J/mol•K), and *M* is the molar mass (g/mol).[10] The thermal conductivities were then corrected for porosity using the Maxwell equation,[11] shown in Equation 3, where k is the intrinsic thermal conductivity (W/m•K), and P is the volume fraction of porosity.

$$k_t = \frac{\left(\frac{100cm}{m}\right)\alpha\rho C_p}{M} \tag{2}$$

$$k = k_t \frac{(1+0.5\,P)}{(1-P)} \tag{3}$$

The electrical resistivity ($\rho_e$) was measured according to the van der Pauw method described in ASTM standard F76-08[12] using the cylindrical specimens. A linear trend line was fit to the measured values, shown in Equation 4.

$$\rho_e = aT + b \tag{4}$$

The electron contribution to the thermal conductivity was estimated using the Wiedemann-Franz law, shown in Equation 5, where $k_e$ is the electron contribution to the thermal conductivity (W/m•K), $L_o$ is the theoretical Lorentz number ($2.44 \times 10^{-8}$ W•Ω/$K^2$), T is the temperature (K), and σ is the electrical conductivity, which is the inverse of the electrical resistivity from Equation 4 (S/m).[10]

$$k_e = L_o T \sigma \quad (5)$$

The phonon contribution to thermal conductivity, $k_{p,}$ was determined by subtracting the electron portion from the total thermal conductivity, after porosity was corrected for (Equation 3), as shown in Equation 6.

$$k_p = k - k_e \quad (6)$$

**III. Results and Discussion**

Table III summarizes the calculated crystallographic densities, measured bulk densities, porosities, and average grain sizes of the ceramics tested in this study. All of the ceramics reached >98% relative density. Archimedes measurements indicated that the specimens had negligible open porosity.

Figure 1 shows SEM micrographs of thermally etched cross sections. The molten salt etch used to highlight the grain structure exaggerated the size of the pores, but the micrographs still allow grain size measurements along with identification of pore locations. Similar to the previous study, all of the transition metal additives appeared to dissolve into the $ZrB_2$ matrix as no residual metal-rich phases were observed. This was confirmed by XRD analysis (not shown), which indicated that all of the ceramics were single phase $ZrB_2$. The amount of porosity was minimal, the pores were primarily round in shape, and intragranular. The range of porosity values among the compositions was small, ranging from 0 to 1.7 vol%. The black phase, which was primarily located on the

grain boundaries, was residual carbon that was not removed by reaction with oxides or did not go into solution. The carbon contents were approximately the same in all compositions, ~1 vol%. Because the contents and morphologies were similar, carbon was expected to have the same influence on the thermal properties of each composition and, therefore, not complicate comparison of the effects of transition metal additives. The measured average grain sizes ranged from 6 to 12 um. This range is smaller than the previous study, which had grain sizes up to ~30 μm. However, all of the grain sizes from both studies are in a range that should not have a strong effect on thermal properties.[10] Overall, the materials that were produced as part of the present study have comparable relative densities, grain sizes, and microstructures, which should allow direct comparison of their thermal properties to those from Reference 5.

Figure 2 shows the measured thermal diffusivity values for all of the compositions from the present study. The standard deviation was less than 1.5% of the average diffusivity for temperatures below 200°C and less than 5% of the average diffusivity for temperatures above 200°C. The standard deviation was based on three rise time measurements at each temperature for all compositions. The measured thermal diffusivities at 25°C ranged from as high as 0.265 $cm^2/s$ for $(Zr,Ta)B_2$ to as low as 0.105 $cm^2/s$ for $(Zr,Cr)B_2$. Likewise at 200°C, diffusivities ranged from 0.214 $cm^2/s$ for $(Zr,Ta)B_2$, to 0.088 $cm^2/s$ for $(Zr,Cr)B_2$. The diffusivity values for all of the compositions decreased with temperature, up to 200°C, although each had a different temperature dependency. At temperatures above ~1600°C, the thermal diffusivities of all of the specimens converged to ~0.155 $cm^2/s$. These trends indicated that small amounts of transition metals had a large impact on thermal transport in $ZrB_2$, affecting both the

magnitude of thermal diffusivity and the temperature dependence of thermal diffusivity. However, transition metal additions had the strongest effect on diffusivity at lower temperatures. Hence, the remainder of this paper will focus on thermal transport for temperatures below 200°C.

The diffusivity data, from room temperature to 200°C, were fit with an exponential trend line, (Equation 1). The values for *a* and *b*, as well as the regression of the fits, are shown in Table IV.

Figure 3 shows the thermal conductivities of the (Zr,TM)$B_2$ ceramics that were calculated using Equation 3. The baseline $ZrB_2$ composition previously reported in Reference 5 had a thermal conductivity that was similar to other dense $ZrB_2$ produced from commercially available powders, with a value of 88 W/m•K at 25°C and a value of 86 W/m•K at 200°C.[13] All of the transition metal additives tested in the present study had a lower thermal conductivity, compared to nominally pure $ZrB_2$.

The addition of Ta had the smallest effect. The thermal conductivity of (Zr,Ta)$B_2$ was 71 W/m•K at 25°C and 74 W/m•K at 200°C which represented decreases between 10% and 20% compared to nominally pure $ZrB_2$. These decreases were similar to what was previously observed for (Zr,Nb)$B_2$ which had a thermal conductivity of 74 W/m•K at 25°C.[5] Based on previous analysis, the effects of Nb and Ta additions were expected to be similar since both Ta and Nb belong to group Vb. Whereas Nb is directly to the right of Zr, Tantalum has a higher atomic number and is heavier, lying below and to the right of Zr in the periodic table meaning it should decrease the thermal conductivity of $ZrB_2$ more than Nb.

The addition of Re or V decreased thermal conductivity between 30 and 40% compared to the baseline $ZrB_2$. At room temperature the thermal conductivity of $(Zr,Re)B_2$ was 53 W/m•K and the thermal conductivity of $(Zr,V)B_2$ was 45 W/m•K. At 200°C, $(Zr,Re)B_2$ had a thermal conductivity of 59 W/m•K while $(Zr,V)B_2$ had a value of 48 W/m•K. These thermal conductivities are between those observed for $(Zr,Nb)B_2$ and $(Zr,W)B_2$ in the previous study. Rhenium lies below and several groups to the right of Zr in group VIIb, while vanadium lies above and to the right of Zr on the periodic table.

The addition of Mo had an effect that was very similar to what was previously seen for W. $(Zr,Mo)B_2$ had a thermal conductivity of 34 W/m•K at 25°C and 38 W/m•K at 200°C, which were decreases of ~60% compared to the baseline composition. In comparison, $(Zr,W)B_2$ had a thermal conductivity of 34 W/m•K at room temperature and 39 W/m•K at 200°C.[5] Molybdenum lies in group VIb, directly above W on the periodic table, so its effect was expected to be similar.

The addition of Cr had the largest impact on thermal conductivity of any of the additives examined in either study. The thermal conductivity of $(Zr,Cr)B_2$ was more than 65% lower than the baseline $ZrB_2$. At 25°C, $(Zr,Cr)B_2$ had a thermal conductivity of 28 W/m•K and the value was 30 W/m•K at 200°C. Chromium is in the same group as Mo and W, but lies above Zr on the periodic table. Based on the previous analysis, Cr had a stronger impact on thermal conductivity than expected.

While the observed thermal conductivity values decreased as the TM moved to the right on the periodic table for all of the specimens, excluding Re, conductivity did not decrease as the TM moved down within a group. For example both $(Zr,V)B_2$ and $(Zr,Cr)B_2$ had lower conductivities than other $(Zr,TM)B_2$ ceramics with TMs that were

lower in their respective groups. Hence, the previous trend that indicated that thermal conductivity was more strongly affected by the TM additive moving down within a group and to the right in a row on the periodic table did not hold for this study.

Figure 4 shows the electrical resistivity of the $(Zr,TM)B_2$ ceramics. The standard deviation was less than 1% of the average based on measurements using 3 different test currents for each composition at each temperature. The electrical resistivity values follow a trend that is similar to the opposite of the thermal conductivity. The electrical resistivity at 25°C increased with TM additions where the thermal conductivity decreased. For example, the electrical resistivity increased from 8.9 μΩ-cm for the baseline $ZrB_2$ to 11.2 μΩ-cm for $(Zr,Ta)B_2$, an increase of ~25% compared to a decrease of ~20% in the thermal conductivity. All of the other additives had a much greater impact on the electrical resistivity. At 25°C, the electrical resistivities were 18.5 μΩ-cm for $(Zr,Re)B_2$, 26.0 μΩ-cm for $(Zr,V)B_2$, and 35.1 μΩ-cm for $(Zr,Mo)B_2$, which represented increases of 108%, 192% and 294%, respectively, compared to nominally pure $ZrB_2$. The addition of chromium had the largest impact, increasing the electrical resistivity by more than 500% to 58.8 μΩ-cm for $(Zr,Cr)B_2$.

Linear trend lines were fit to the electrical resistivity values using Equation 4. The values for *a* and *b* as well as the regression of the fits are listed in Table V. The resistivity fit was inverted to calculate the electrical conductivity, which was then used to estimate the electron contribution to the thermal conductivity (Figure 5). The electron contribution to thermal conductivity was estimated using the theoretical Lorenz number ($L_o$) and the Wiedemann-Franz law (Equation 5). Previous results have indicated that the theoretical Lorenz number of $2.44 \times 10^{-8} W \bullet \Omega / K^2$ may not be appropriate to estimate

the electron contribution to thermal conductivity for $ZrB_2$ and (Zr,TM)$B_2$ ceramics.[5] Unfortunately, the Lorenz numbers for borides have not been measured, so the theoretical value was used in this analysis to compare the potential impact of TM additions on the electron contribution to thermal conductivity.

The addition of transition metals to $ZrB_2$ lowered the electron contribution to thermal conductivity in the same general trend that the total thermal conductivity was reduced. However, TM additions generally decreased the electron contribution to thermal conductivity by a higher percentage than the total thermal conductivity. For example, the electron contribution to thermal conductivity was 21 W/m•K for (Zr,Mo)$B_2$ at 25°C, a decrease of ~75% compared to the electron contribution of 88 W/m•K for the baseline $ZrB_2$. Thus, the decrease in the electron contribution to thermal conductivity was more than the 60% decrease to the total thermal conductivity. If the theoretical Lorenz number were valid for all of the compositions, or even if the same value of the Lorenz number were valid for all compositions, these trends would indicate that the addition of TMs to $ZrB_2$ increased the phonon contribution to thermal conductivity. In contrast, any impurity atoms in the lattice disrupt phonon transport, especially heavier transition metal additions, and should decrease the phonon contribution to thermal conductivity. Hence, Lorenz numbers need to be measured for $ZrB_2$ and each of the (Zr,TM)$B_2$ ceramics to elucidate the effects of TM additives on the electron contribution to thermal conductivity.

The phonon contribution to the thermal conductivity (Figure 6) was estimated by subtracting the electron contribution from the total thermal conductivity (Equation 6). The electron contribution dominated thermal conduction for most of the (Zr,TM)$B_2$

across the entire temperature range. The exception to the trend was (Zr,Cr)$B_2$, which had a phonon contribution making up 55% of the total thermal conductivity at 25°C.

XRD analysis was used to determine the lattice parameters for each (Zr,TM)$B_2$ composition produced in the study. The measured lattice parameters are summarized in Table VI. Additionally, the unit cell volume and change in unit cell volume compared to nominally pure $ZrB_2$ were also calculated. Figure 7 shows the total thermal conductivity for the (Zr,TM)$B_2$ ceramics as a function of the calculated volume change. The trend line on the plot is based on analysis in the previous study,[5] which identified a trend for the decrease in thermal conductivity related to the lattice strain resulting from TM additions.

From the TM additions examined in the present study, only (Zr,Ta)$B_2$ falls near the trend line from the previous study[5], the rest of the additives do not. However, similar to titanium diboride, the lattice parameters of both vanadium diboride and chromium diboride are controlled by the boron-boron bond lengths, due to the smaller size of the transition metals.[14] Additionally, $ReB_2$ has $P6_3/mmc$ symmetry,[15] and $Mo_2B_4$ has $R\bar{3}m$ symmetry.[16] Both of these are different than the P6/mmm symmetry of $ZrB_2$, and, like $W_2B_4$, may induce additional changes in the lattice that reduce thermal conductivity more than expected based solely on measured lattice volume. Hence, the analysis presented in Reference 5 suggests that these compositions would not be expected to follow the trend related to lattice volume change.

Another potential method for analyzing the effect of transition metal substitutions into the $ZrB_2$ lattice is to directly compare the size of the transition metal atoms. The total thermal conductivity was compared to the Linus Pauling metallic radii for each of the TM additives.[17] As shown in Figure 8, a trend is evident. The equation for the best

fit line is shown in Equation 7, where k is the total thermal conductivity (W/m•K), and r is the Linus Pauling metallic radius (Å).

$$k = -323.71r^2 + 1132.2r - 884.49 \text{ (W/m•K)} \quad (7)$$

The only composition that did not appear to follow the trend based on metallic radius was (Zr,Mo)$B_2$, which had a thermal conductivity that was lower than predicted based on its reported radius. The deviation may be due to the tendency of Mo to form $Mo_2B_n$ compounds[16] in contrast to the other TMs, which all form stoichiometric $TMB_2$ compounds.

Using Equation 7, the trend line predicted from the size of the metal atoms was compared to the thermal conductivities of the (Zr,TM)$B_2$ ceramics that were tested in the current study as well as the TM additions investigated in RReference 5. Table VII summarizes the room temperature conductivities that were calculated from the TM radii, as well as the difference between the predicted and measured values.

The predicted values matched closely for most of the specimens, with differences of less than ~5% for the majority of the compositions. For example, the predicted value for (Zr,Re)$B_2$ was 55 W/m•K and the actual value was 52 W/m•K, an ~4% difference. Since the trend line was only based on data from the current study, the conductivity predicted for (Zr,Y)$B_2$ was significantly higher than the measured value, since Y is the only additive that has a larger metallic radius than Zr. Similar to Mo described above, W forms $W_2B_n$ compounds instead of stoichiometric diborides[16], which may contribute to

the discrepancy between the predicted and measured values for $(Zr,W)B_2$. Finally, Ti does not follow the trend. This may be due to the fact that it lies in the same group as Zr. Unlike the other smaller additives such as V, Cr, and Re, Ti exhibits complete solubility in $(Zr,B)_2$, and therefore, may not induce as much strain. Overall, Equation 7 appears to predict the thermal conductivity of $(Zr_{0.97},TM_{0.03})B_2$ ceramics for TMs that are smaller than Zr and that form $TMB_2$ compounds.

**IV. Summary**

The effect of transition metal additions on the thermal conductivity of $ZrB_2$ was studied. Dense $ZrB_2$ ceramics containing nominally 3 at% additions of various transition metals were produced by hot pressing. The transition metals dissolved into the $ZrB_2$ lattice to form solid solutions, as confirmed by XRD and microstructure analyses. The room temperature thermal conductivities decreased from 88 W/m•K for nominally pure $ZrB_2$ to 28 W/m•K for $(Zr,Cr)B_2$, but converged to similar values as temperatures approached 2000°C. The decrease in total thermal conductivity was stronger as transition metal additives were farther to the right on the periodic table, with the exception of Re. While the addition of Ta resulted in thermal conductivity values that were close to the trend line relating lattice volume change and conductivity that was previously found for Y, Hf, and Nb additives, the additions of Mo, Re, V, and Cr did not follow the trend. Instead, thermal conductivities for most of the $(Zr,TM)B_2$ ceramics followed a trend relating to the metallic radii. As a result, a parabolic trend line was used to predict the thermal conductivity for several other $(Zr,TM)B_2$ ceramics from the metallic radii of the TM additive. The results of this study indicate that small amounts of transition metals,

depending on their size and preferred boride structure, influence the thermal properties of zirconium diboride.

**Acknowledgements**

This research was funded as part of the Aerospace Materials for Extreme Environments Program (Dr. Ali Sayir, Program Manager) in the U.S. Air Force Office of Scientific Research under contract number FA9550-09-1-0168. In addition, the authors would like to thank the Advanced Materials Characterization Laboratory in the Materials Research Center at Missouri S&T for the assistance with XRD (Eric Bohannan) and SEM (Clarissa Wisner).

**References**

[1] E. Wuchina, E. Opila, M. Opeka, W. Fahrenholtz, and I. Talmy, "UHTCs: Ultra-High Temperature Ceramic Materials for Extreme Environment Applications," *Interface*, **16**[4] 30-36 (2007).

[2] R. Telle, L. S. Sigl, and K. Takagi, "Boride-Based Hard Materials," pp. 802-945. in Handbook of Ceramic Hard Materials, Vol. 2, Edited by R. Riedel. Wiley-VCH Verlag GmbH, Weinheim, Germany, 2008.

[3] W. G. Fahrenholtz, G. E. Hilmas, I. G. Talmy, and J. A. Zaykoski, "Refractory Diborides of Zirconium and Hafnium," *Journal of the American Ceramic Society*, **90**[5] 1347-64 (2007).

[4] H. J. Juretschke and R. Steinitz, "Hall effect and electrical conductivity of transition-metal diborides," *Journal of Physics and Chemistry of Solids*, **4**[1–2] 118-27 (1958).

[5] D. L. McClane, W. G. Fahrenholtz, and G. E. Hilmas, "Thermal Properties of (Zr,TM)$B_2$ Solid Solutions with TM = Hf, Nb, W, Ti, and Y," *J. Am. Ceram. Soc*. (2014).

[6] ASTM Standard C830, 2000 (2011), "Standard Test Methods for Apparent Porosity, Liquid Absorption, Apparent Specific Gravity, and Bulk Density of Refractory Shapes by Vacuum Pressure," ASTM International, West Conshohocken, PA, 2012, DOI: 10.1520/C0830-06R11, www.astm.org.

[7] Y. Touloukian, C. Ho and D. Dewitt, "Thermal Expansion: Nonmetallic Solids," pp. 784-9 in Thermophysical Properties of Matter, **Vol. 13**. Edited by Touloukian. IFI/Plenum, New York, 1977.

[8] ASTM Standard E1461, 2013 "Standard Test Method for Thermal Diffusivity by the Flash Method," ASTM International, West Conshohocken, PA, 2006, DOI: 10.1520/E1461-13, www.astm.org.

[9] M. W. Chase, S. National Institute of, and Technology, "NIST-JANAF thermochemical tables," **Vol. no. 9**. American Chemical Society: Woodbury, N.Y, (1998).

[10] J. W. Zimmermann, G. E. Hilmas, W. G. Fahrenholtz, R. B. Dinwiddie, W. D. Porter, and H. Wang, "Thermophysical Properties of $ZrB_2$ and $ZrB_2$–SiC Ceramics," *Journal of the American Ceramic Society*, **91**[5] 1405-11 (2008).

[11] G. Ondracek and B. Schulz, "The porosity dependence of the thermal conductivity for nuclear fuels," *Journal of Nuclear Materials*, **46**[3] 253-58 (1973).

[12] ASTM Standard F76, 2008, "Standard Test Methods for Measuring Resistivity and Hall Coefficient and Determining Hall Mobility in Single-Crystal Semiconductors," ASTM International, West Conshohocken, PA, 2006, DOI: 10.1520/F0076-08, www.astm.org.

[13] M. J. Thompson, "Densification and Thermal Properties of Zirconium Diboride Based Ceramics." in. Missouri University of Science and Technology, Rolla, MO 2012.

[14] B. Post, F. W. Glaser, and D. Moskowitz, "Transition metal diborides," *Acta Metallurgica*, **2**[1] 20-25 (1954).

[15] O. J. Żogał, Z. Fojud, P. Herzig, A. Pietraszko, A. B. Lyashchenko, S. Jurga, and V. N. Paderno, "Crystal structure, electric field gradient, and electronic charge densities in $ReB_2$: A single crystal x-ray, B11 nuclear magnetic resonance, and first-principles study," *Journal of Applied Physics*, **106**[3] - (2009).

[16] M. Frotscher, W. Klein, J. Bauer, C.-M. Fang, J.-F. Halet, A. Senyshyn, C. Baehtz, and B. Albert, "$M_2B_5$ or $M_2B_4$? A Reinvestigation of the Mo/B and W/B System," *Zeitschrift für anorganische und allgemeine Chemie*, **633**[15] 2626-30 (2007).

[17] L. Pauling and B. Kamb, "A Revised Set of Values of Single-Bond Radii Derived from the Observed Interatomic Distances in Metals by Correction for Bond Number and Resonance Energy," *Proceedings of the National Academy of Sciences of the United States of America*, **83**[11] 3569-71 (1986).

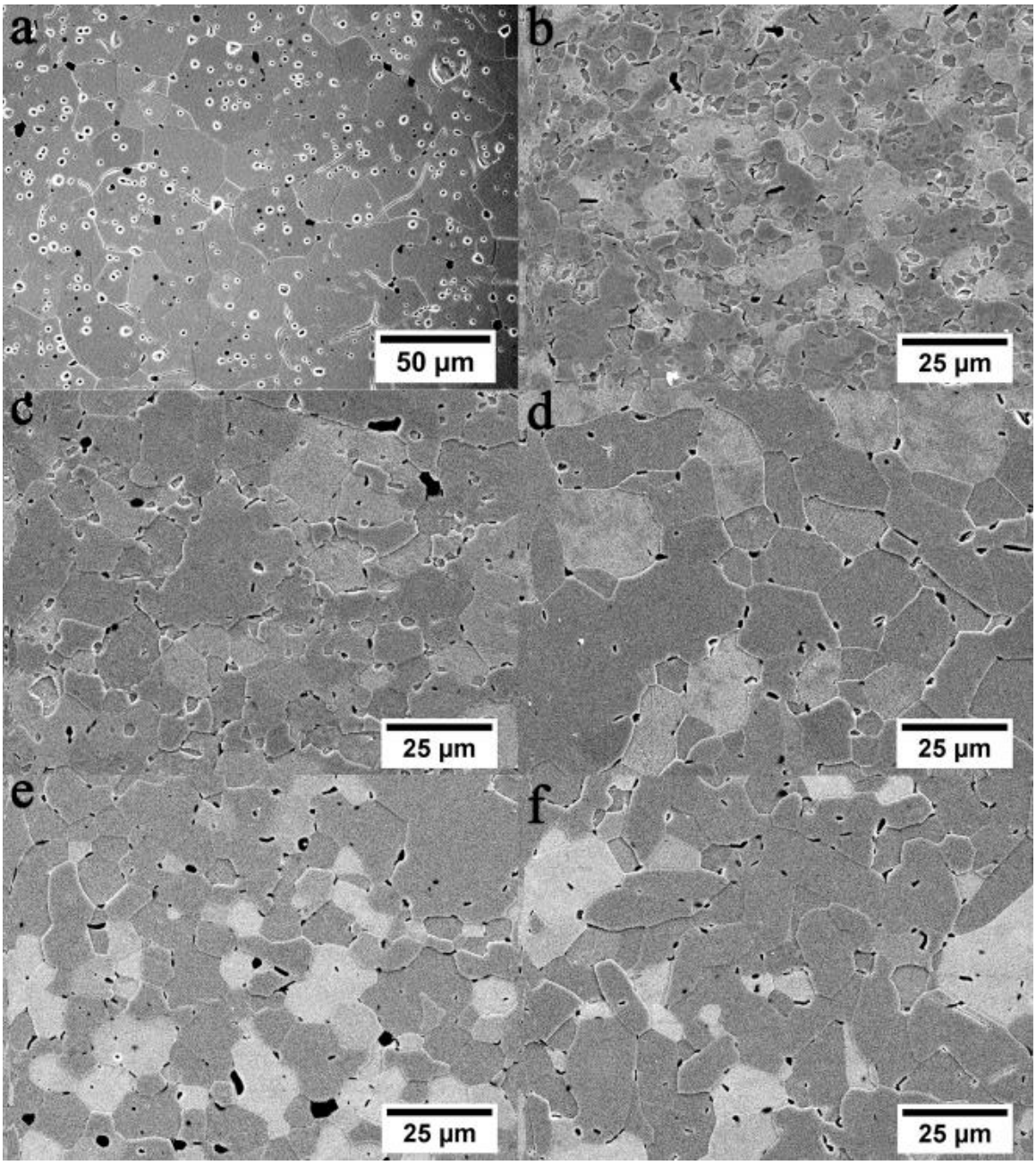


**Figure 1:** SEM micrographs of polished, chemically-etched cross sections of (a) $ZrB_2$, (b) $(Zr,Ta)B_2$, (c) $(Zr,Mo)B_2$, (d) $(Zr,Re)B_2$, (e) $(Zr,V)B_2$, and (f) $(Zr,Cr)B_2$.

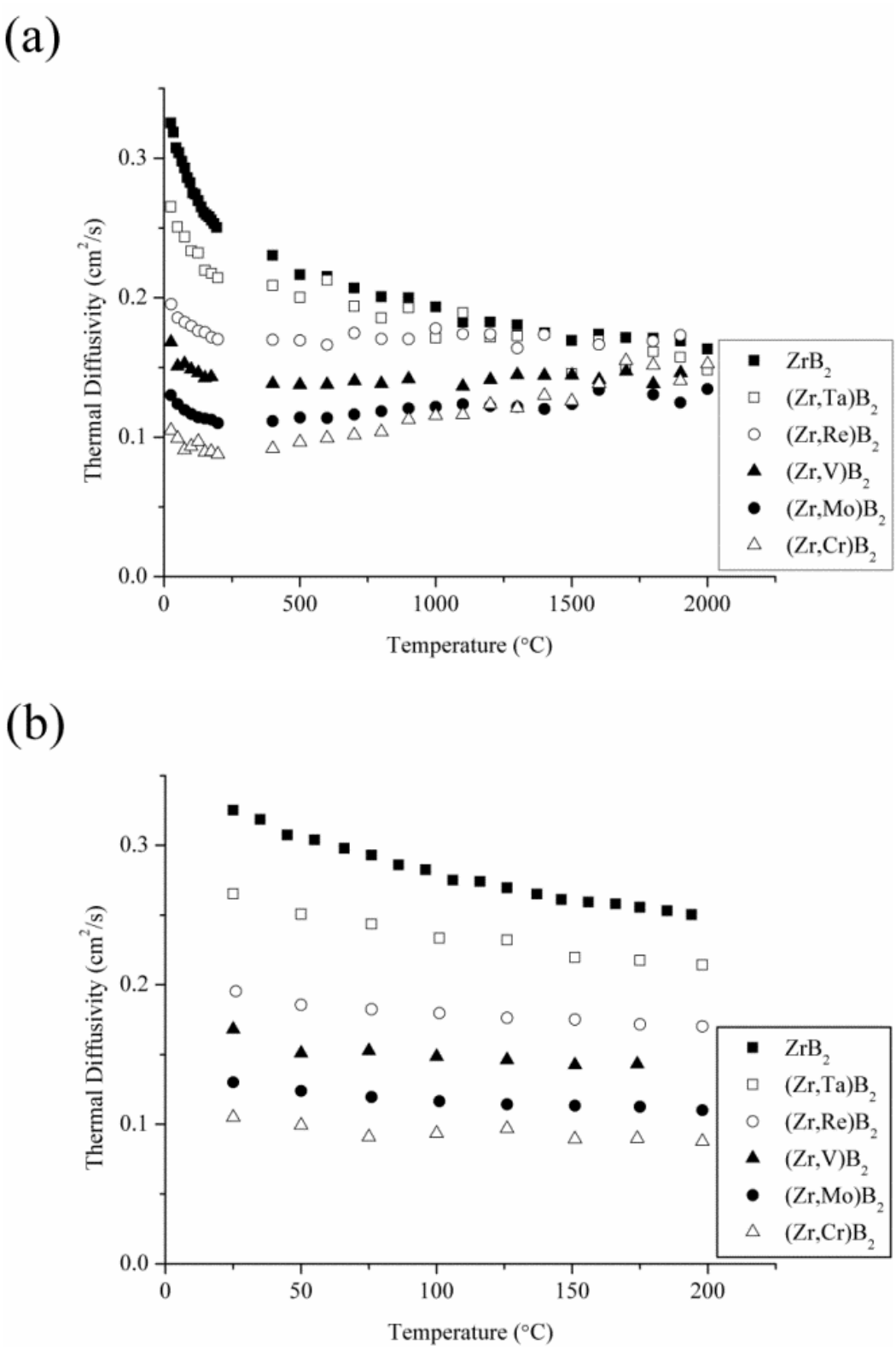


**Figure 2:** Thermal diffusivity as a function of temperature for (Zr,TM)$B_2$ ceramics from (a) room temperature to 2000°C and (b) room temperature to 200°C. Note that the data for $ZrB_2$ were reproduced from Reference 5.

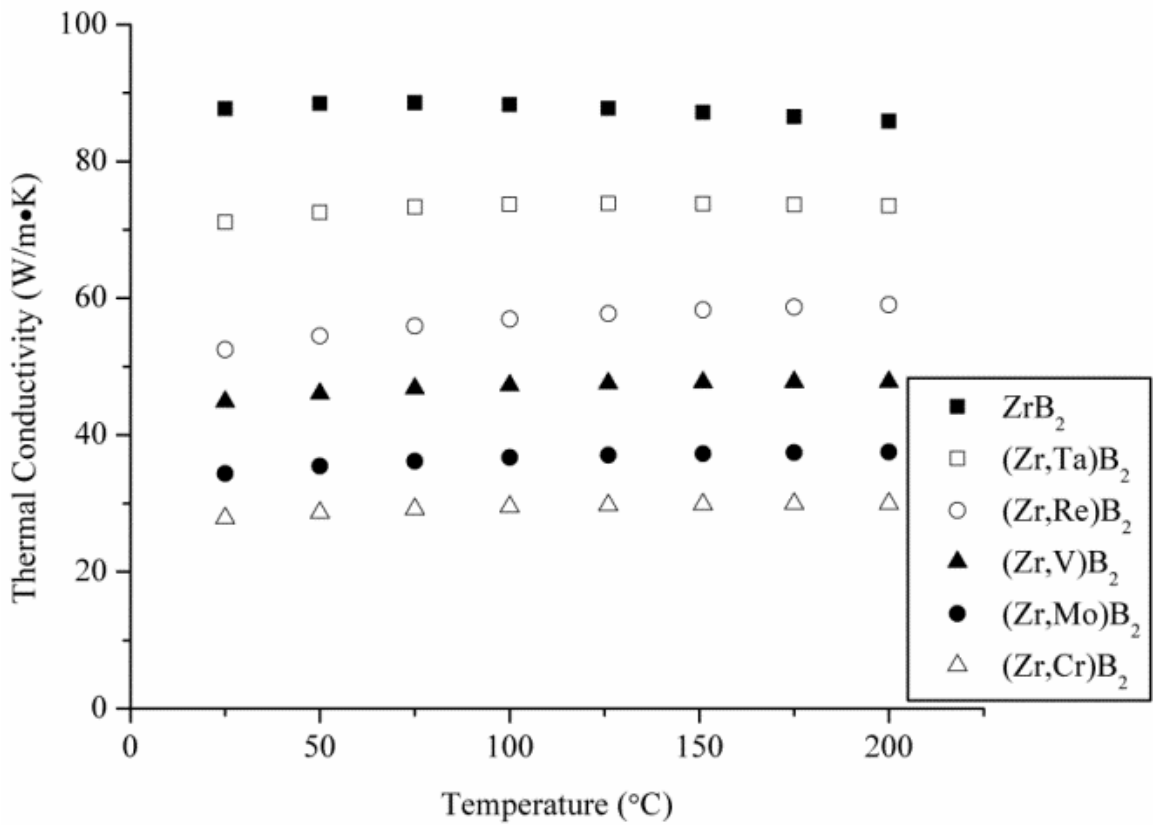


**Figure 3:** Thermal conductivity as a function of temperature for (Zr,TM)$B_2$ ceramics. Note that the data for $ZrB_2$ were reproduced from Reference 5.

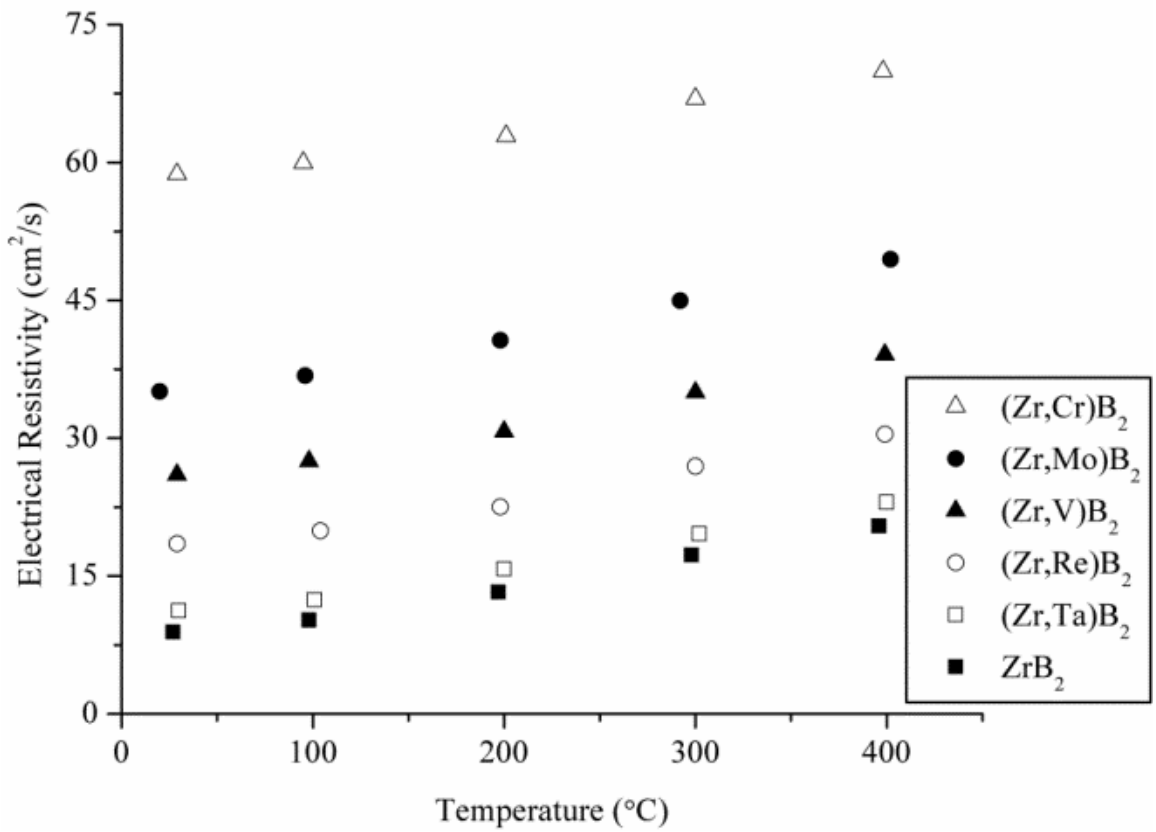


**Figure 4:** Electrical resistivity as a function of temperature for $(Zr,TM)B_2$ ceramics. Note that the data for $ZrB_2$ were reproduced from Reference 5.

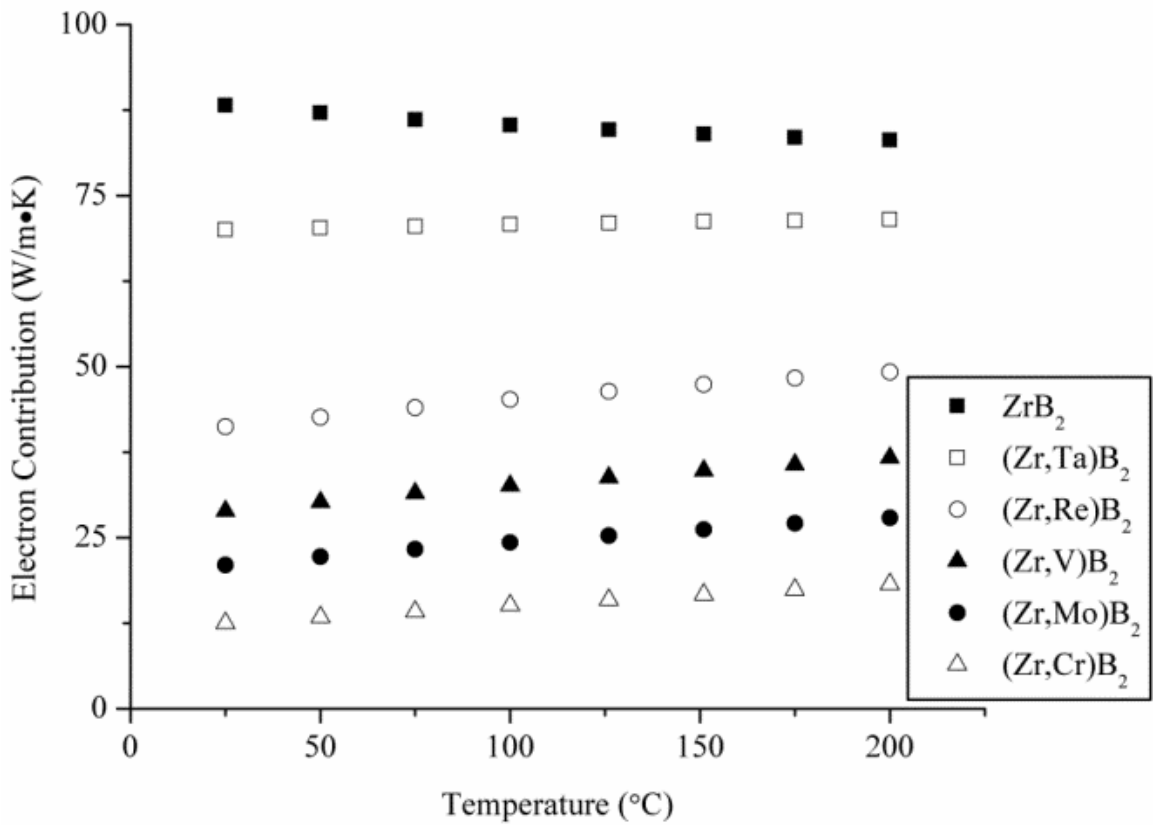


**Figure 5:** Electron contribution to thermal conductivity for $(Zr,TM)B_2$ ceramics estimated using the theoretical Lorenz number. Note that the data for $ZrB_2$ were reproduced from Reference 5.

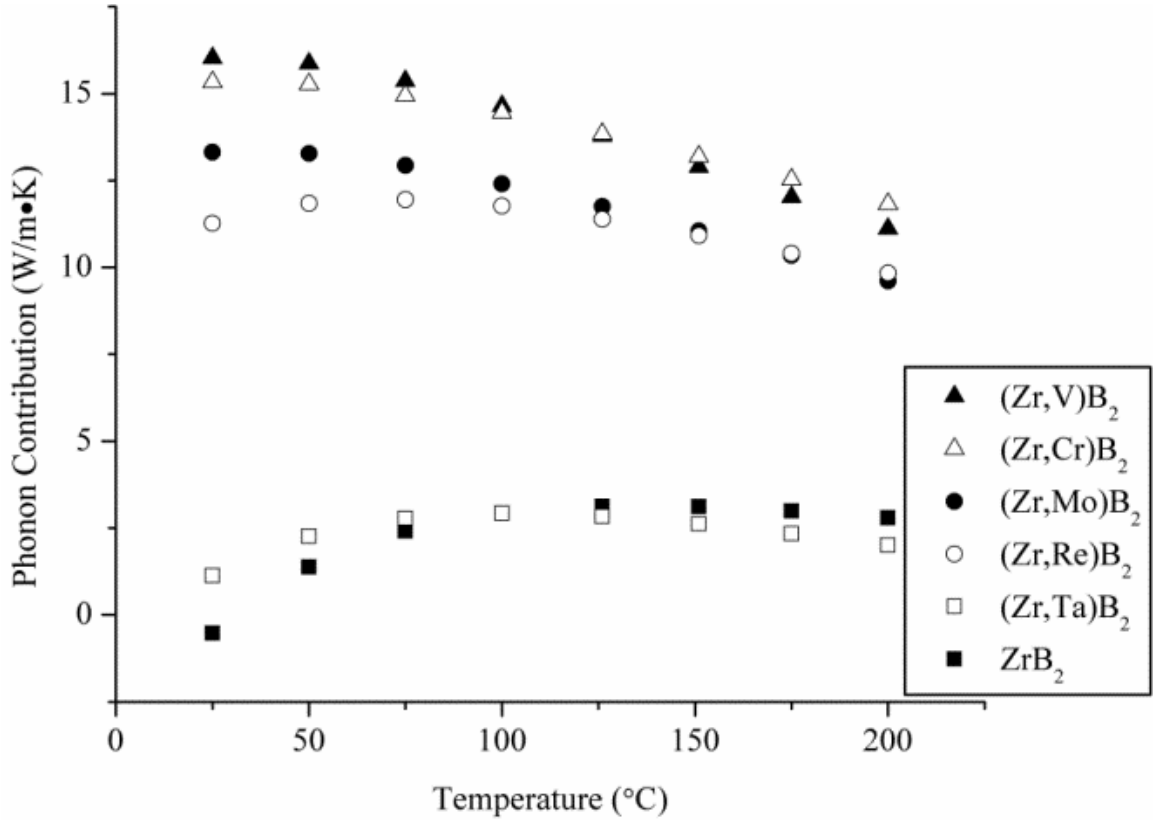


**Figure 6:** Phonon contribution to thermal conductivity for (Zr,TM)$B_2$ ceramics. Note that the data for $ZrB_2$ were reproduced from Reference 5.

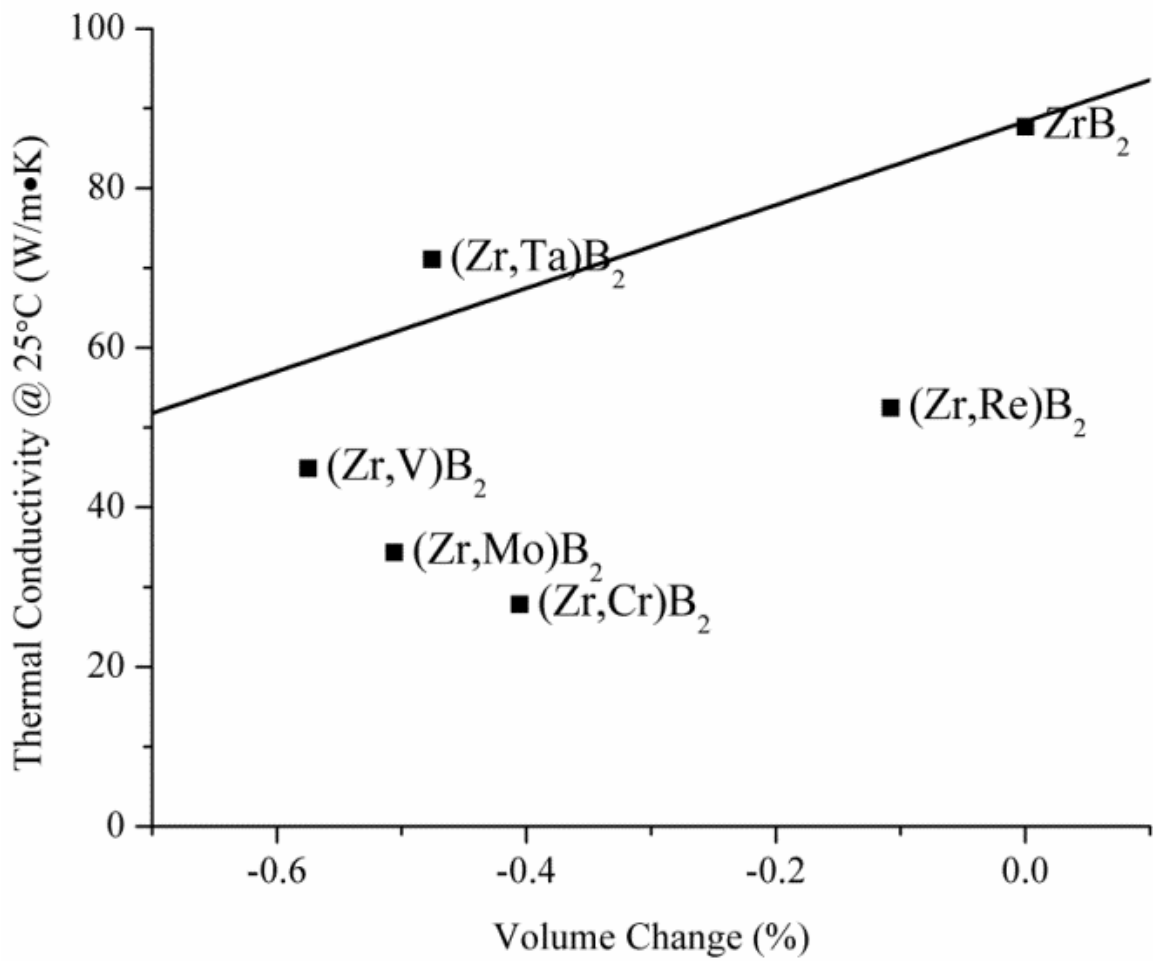


**Figure 7:** Relationship between volume change and the total thermal conductivity for $(Zr,TM)B_2$ ceramics. Note that the trend line shown was identified in Reference 5.

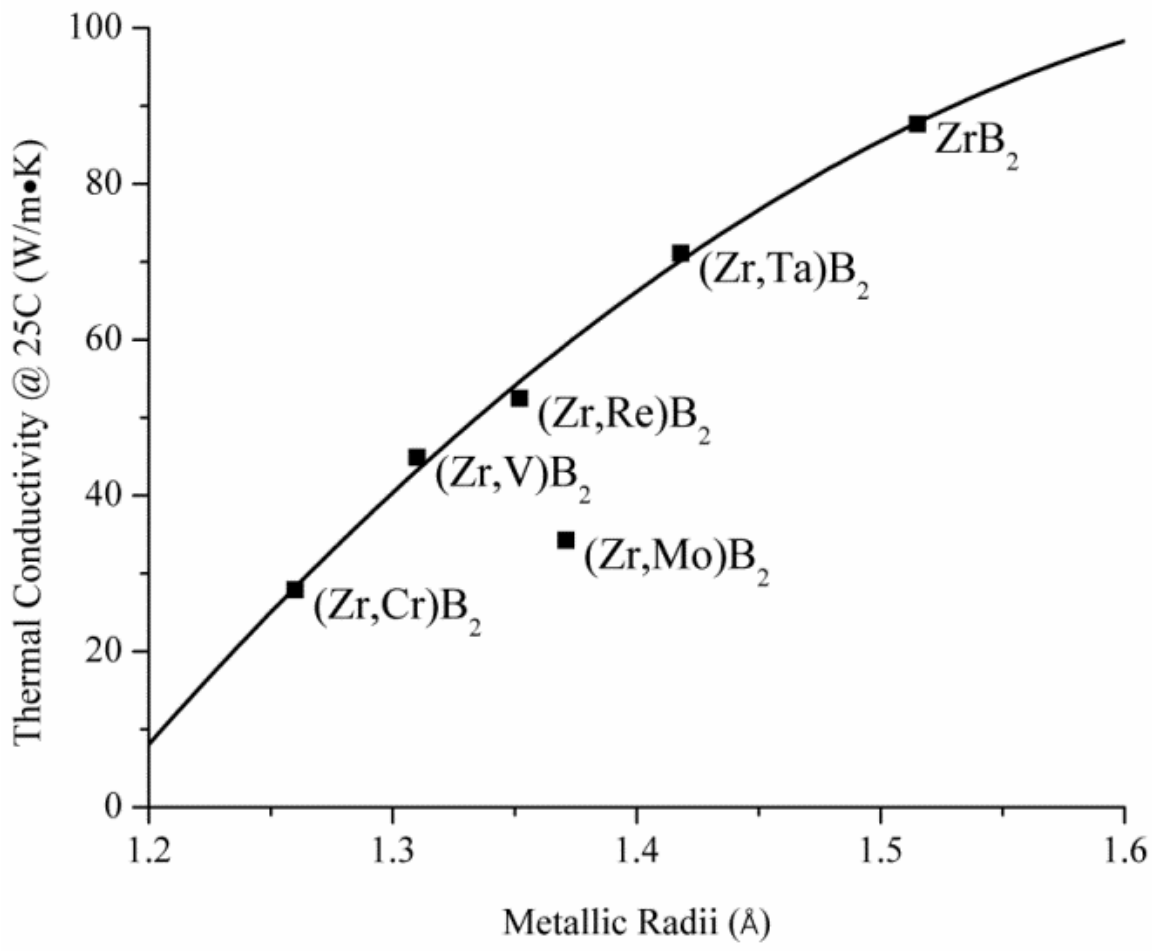


**Figure 8:** Relationship between metallic radii and thermal conductivity for (Zr,TM)$B_2$ ceramics.

**Table I:** Composition and room temperature thermal conductivity for (Zr,TM)$B_2$ ceramics from Reference 5.

| Designation | Atomic % | | | | Thermal Conductivity (W/m•K) |
|---|---|---|---|---|---|
| | Zr | TM | B | C | |
| $ZrB_2$ | 32.8 | 0.0 | 65.7 | 1.5 | 88 |
| (Zr,Hf)$B_2$ | 31.8 | 1.0 | 65.6 | 1.5 | 81 |
| (Zr,Nb)$B_2$ | 31.8 | 1.0 | 65.7 | 1.5 | 74 |
| (Zr,W)$B_2$ | 31.7 | 1.0 | 65.8 | 1.5 | 34 |
| (Zr,Ti)$B_2$ | 31.5 | 1.2 | 65.5 | 1.7 | 87 |
| (Zr,Y)$B_2$ | 31.9 | 1.0 | 65.7 | 1.4 | 87 |

**Table II:** Specimen designations and compositions for the $(Zr,TM)B_2$ ceramics. Note that the data for $ZrB_2$ is from Reference 5.

| Designation | Weight % | | | Atomic % | | | | | |
|---|---|---|---|---|---|---|---|---|---|
| | $ZrB_2$ | Carbon | TMB | Zr | TM | B | C | TM in Metal Sublattice | Metal to Boron Ratio |
| $ZrB_2$ | 99.5 | 0.5 | 0.0 | 32.8 | 0.0 | 65.7 | 1.5 | 0.0 | 50.0 |
| $(Zr,Ta)B_2$ | 94.2 | 0.5 | 5.3 | 31.9 | 1.0 | 65.6 | 1.6 | 3.1 | 50.2 |
| $(Zr,Mo)B_2$ | 96.2 | 0.5 | 3.3 | 31.7 | 1.0 | 65.8 | 1.5 | 3.0 | 49.6 |
| $(Zr,Re)B_2$ | 94.0 | 0.5 | 5.5 | 31.9 | 1.0 | 65.6 | 1.5 | 3.1 | 50.2 |
| $(Zr,V)B_2$ | 97.4 | 0.5 | 2.1 | 31.7 | 1.1 | 65.6 | 1.5 | 3.3 | 50.0 |
| $(Zr,Cr)B_2$ | 97.6 | 0.5 | 2.0 | 31.9 | 1.0 | 65.7 | 1.4 | 3.0 | 50.0 |

**Table III:** Specimen designations, density values, and average grain sizes for the $(Zr,TM)B_2$ ceramics. Note that the data for $ZrB_2$ is from Reference 5.

| Designation | Theoretical Density | Bulk Density | Relative Density | Porosity | Grain Size |
|---|---|---|---|---|---|
| | $g/cm^3$ | $g/cm^3$ | % | % | μm |
| $ZrB_2$ | 6.05 | 5.97 | 98.6 | 1.4 | 22 +/- 20 |
| $(Zr,Ta)B_2$ | 6.22 | 6.25 | 99.9+ | 0.0 | 6 +/- 6 |
| $(Zr,Mo)B_2$ | 6.10 | 6.18 | 99.9+ | 0.0 | 10 +/- 9 |
| $(Zr,Re)B_2$ | 6.23 | 6.13 | 98.3 | 1.7 | 12 +/- 12 |
| $(Zr,V)B_2$ | 6.03 | 6.05 | 99.9+ | 0.0 | 10 +/- 11 |
| $(Zr,Cr)B_2$ | 6.04 | 6.10 | 99.9+ | 0.0 | 11 +/- 10 |

**Table IV:** Fitting parameters for thermal diffusivity data for $(Zr,TM)B_2$ ceramics. Note that the data for $ZrB_2$ were reproduced from Reference 5.

| | Composition | | | | | |
|---|---|---|---|---|---|---|
| | $ZrB_2$ | $(Zr,Ta)B_2$ | $(Zr,Mo)B_2$ | $(Zr,Re)B_2$ | $(Zr,V)B_2$ | $(Zr,Cr)B_2$ |
| *a* ($cm^2/s$) | 0.1572 | 0.1482 | 0.0838 | 0.1363 | 0.1010 | 0.0650 |
| *b* (K) | 215.85 | 172.25 | 127.2 | 103.72 | 148.31 | 139.37 |
| Regression | 0.9967 | 0.9851 | 0.9738 | 0.9709 | 0.9609 | 0.9782 |

**Table V:** Fitting parameters for electrical resistivities of $(Zr,TM)B_2$ ceramics. Note that the data for $ZrB_2$ were reproduced from Reference 5.

| | Composition | | | | | |
|---|---|---|---|---|---|---|
| | $ZrB_2$ | $(Zr,Ta)B_2$ | $(Zr,Mo)B_2$ | $(Zr,Re)B_2$ | $(Zr,V)B_2$ | $(Zr,Cr)B_2$ |
| a | 0.0323 | .0329 | 0.0386 | 0.0332 | 0.0359 | 0.0312 |
| b | -1.3836 | 0.5903 | 23.069 | 7.7569 | 14.503 | 48.78 |
| Regression | 0.99 | 0.9908 | 0.9914 | 0.9842 | 0.9882 | 0.9891 |

**Table VI:** Summary of lattice parameters and unit cell volumes. Note that the data for $ZrB_2$ were reproduced from Reference 5.

| Composition | Measured Lattice Parameters | | | |
|---|---|---|---|---|
| | a (Å) | c (Å) | Volume ($Å^3$) | Volume Change (%) |
| $ZrB_2$ | 3.16814(2) | 3.52992(5) | 30.683 | 0 |
| $(Zr,Ta)B_2$ | 3.16435(3) | 3.52155(7) | 30.538 | -0.48 |
| $(Zr,Mo)B_2$ | 3.16334(1) | 3.52273(4) | 30.528 | -0.51 |
| $(Zr,Re)B_2$ | 3.16681(2) | 3.52908(5) | 30.650 | -0.11 |
| $(Zr,V)B_2$ | 3.16262(3) | 3.52191(8) | 30.507 | -0.57 |
| $(Zr,Cr)B_2$ | 3.16405(2) | 3.52471(6) | 30.559 | -0.41 |

**Table VII:** Predicted vs. measured thermal conductivity for $(Zr,TM)B_2$ ceramics. Note that the measured conductivities for $ZrB_2$, $(Zr,Hf)B_2$, $(Zr,Nb)B_2$, $(Zr,W)B_2$, $(Zr,Ti)B_2$, and $(Zr,Y)B_2$ are from Reference 5.

| Composition | Metallic Radii (Å) | Predicted Thermal Conductivity (W/m•K) | Measured Thermal Conductivity (W/m•K) | Difference (%) |
|---|---|---|---|---|
| $ZrB_2$ | 1.515 | 88 | 88 | 0.1% |
| $(Zr,Ta)B_2$ | 1.418 | 70 | 71 | 1.4% |
| $(Zr,Mo)B_2$ | 1.371 | 59 | 34 | 72.7% |
| $(Zr,Re)B_2$ | 1.352 | 55 | 52 | 3.9% |
| $(Zr,V)B_2$ | 1.31 | 43 | 45 | 3.8% |
| $(Zr,Cr)B_2$ | 1.26 | 28 | 28 | 1.1% |
| $(Zr,Hf)B_2$ | 1.503 | 86 | 81 | 5.6% |
| $(Zr,Nb)B_2$ | 1.417 | 70 | 74 | 5.2% |
| $(Zr,W)B_2$ | 1.378 | 61 | 34 | 78.1% |
| $(Zr,Ti)B_2$ | 1.384 | 62 | 87 | 28.1% |
| $(Zr,Y)B_2$ | 1.659 | 103 | 87 | 18.0% |

# SECTION

# 3. CONCLUSIONS

The research presented in this thesis focused on the thermal properties of zirconium diboride ($ZrB_2$) based ceramics, more specifically, the influence that transition metal (TM) additives have on thermal transport in $ZrB_2$ solid solutions. This was done in an attempt to answer the questions that were presented in the Introduction section of this document. The procedures and results that were discussed in Papers 1 and 2 were used to answer the questions accordingly:

1. *What transition metal impurities have the greatest influence on the thermal conductivity of $ZrB_2$?*

   While all of the TM additions to $ZrB_2$ that were examined lowered the thermal conductivity compared to nominally pure $ZrB_2$, different additives had varying effects. The effect was generally stronger for TMs located farther to the right on the periodic table. For example, adding Ti, which is in the same group (IVb) as Zr, only decreased the room temperature thermal conductivity by 1 W/m•K from 88 W/m•K to 87 W/m•K. In comparison, adding Ta, which is in group Vb, decreased the room temperature thermal conductivity to 71 W/m•K and adding Cr, which is in group VIb, decreased the room temperature thermal conductivity to 28 W/m•K. Interestingly, all of the thermal conductivities converged to similar values as temperature increased. For example, at 200°C nominally pure $ZrB_2$ had a thermal conductivity of 86 W/m•K compared to 74 W/m•K for the specimen with Ta added, and 30 W/m•K for the specimen with Cr

added, which are differences of 12 W/m•K and 56 W/m•K respectively. At temperatures above 1600°C, the thermal conductivities of all of the compositions were approximately 70 W/m•K.

2. *How does the presence of an impurity in solid solution affect electron and phonon conduction?*

The electron contribution to thermal conductivity was determined from measured electrical resistivity values using the Wiedemann-Franz law. The electron contribution dominated thermal conduction in all of the compositions, especially at high temperatures. Similar to the effect seen in total thermal conductivity, all of the TM additives decreased the electron portion of thermal conductivity. In general, as the TM moved away from group IVb, the decrease became larger. For example, the addition of Ti, group IVb, only decreased electron conduction by 1W/m•K from 88 W/m•K to 87 W/m•K at 25°C, whereas the addition of Cr, group VIb, decreased the electron conduction by 76 W/m•K to 12W/m•K at 25°C.

The phonon contribution to thermal conductivity was determined by subtracting the electron contribution from the total thermal conductivity. The phonon contribution was negative for some specimens, and was higher than the nominally pure $ZrB_2$ for the majority of the compositions. Since negative values are not physically possible, and it seems likely that any additive should decrease phonon conduction due to scattering, it was concluded that the Sommerfield Lorenz number was not appropriate for $ZrB_2$ based ceramics, especially those with TM additions.

3. *What factors contribute to reducing thermal transport in (Zr,TM)$B_2$ ceramics?*

Several factors contribute to the reduction in thermal transport in (Zr,TM)$B_2$ ceramics. As the size of the transition metal that substituted onto Zr lattice sites decreased, the thermal conductivity also decreased. A parabolic trend line was fit to the thermal conductivities of the different compositions that related the measured thermal conductivity to the Linus Pauling metallic radii of the metal additive. This trend seemed to correlate with the solubility limits of the TM boride and $ZrB_2$. In addition, the differences in metallic radius were expected to produce strain in the lattice, which contributed to the decrease in thermal and electrical conductivities. However, the thermal conductivity was lower than predicted by this trend for TM borides that form different crystal structures (i.e., not the P6/mmm crystal structure observed for $ZrB_2$ and several other TM diborides). The structural differences may produce additional strain in the lattice, beyond that due simply to metallic radius, which could lower the thermal conductivity more than for other additives.

# 4. FUTURE WORK

The goal of the research presented in this thesis was to investigate the effects that transition metal additives have on thermal transport in zirconium diboride. During the course of this research, several areas that could be the subject of additional investigation arose. Some of these include:

1. The effect that other additives have on the thermal conductivity of $ZrB_2$ could be examined further. While this study characterized the effect of transition metal boride additions, more investigation into the influence of carbide, or silicide additions would be useful. This would be advantageous since much research has been done on $MoSi_2$, SiC, and $B_4C$ additions for improving densification, oxidation resistance, and mechanical properties at high temperatures.[74, 75, 81]
2. The effect of varying the amount of the TM additive should be studied. This study investigated additions of ~1 atomic percent TM with respect to zirconium, but further investigation of thermal conductivity decreases as a function of additive concentration would be useful. To date, the effect of different additions of SiC and $TiB_2$ have been investigated.[12, 44] However, it is currently not known how the thermal conductivity changes as a function of concentration of other additives. The thermal conductivity could decrease rapidly and then level off, or could require a certain impurity concentration to be reached before any effect is noticed. This study would be beneficial in determining what additive levels are acceptable in $ZrB_2$ for select applications.

3. The effect that multiple TM additives in solid solution have on the thermal conductivity of $ZrB_2$ should be studied. The present investigation studied the influence of individual TM additives to commercially available powders, but it would be beneficial to know how multiple additives influence thermal conductivity. Since Hf is present in commercial powders, the effects on thermal conductivity for additives, such as Ti and Y, could have been overshadowed by the effect of Hf. Additionally, more additives could compound, and have an even larger influence than what was seen in this study.
4. The Lorenz number for $ZrB_2$, as well as other ultra-high temperature ceramics, needs to be determined. This study used the theoretical Lorenz number and the Weidemann-Franz law to estimate the electron and phonon contributions to thermal conductivity. It was found that the theoretical value was not a good fit for $ZrB_2$. The results indicated that not only was the theoretical Lorenz number not appropriate, but the Lorenz number should vary with additive content. Because of this, more investigation is necessary for a better understanding of thermal transport in $ZrB_2$.

# APPENDIX

## A.1 UNPUBLISHED DATA

**A1.1 High Temperature Thermal Diffusivity.** The thermal diffusivity of the compositions tested in Papers 1 and 2 were measured up to 2000°C, Figure A1. The measured values vary widely at room temperature, discussed in Papers 1 and 2, but converge at high temperatures, above 1600°C. Although this was noted in Paper 2, the data for the compositions discussed in Paper 1 were not previously shown above 200°C.

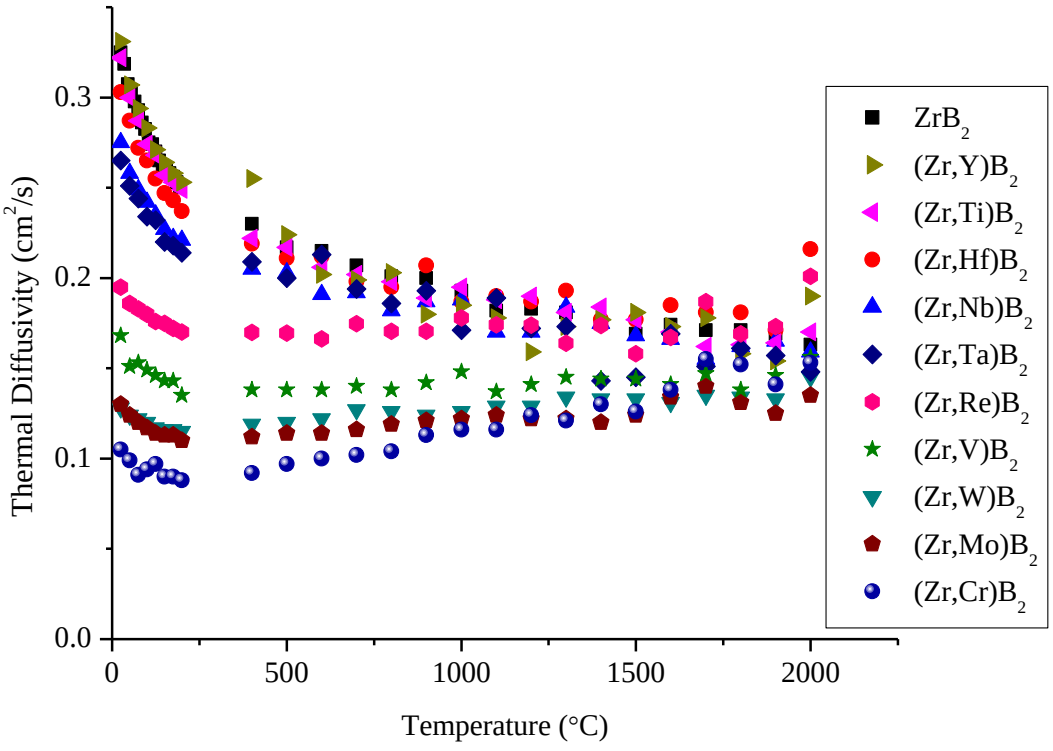


**Figure A1:** Thermal diffusivity of (Zr,TM)$B_2$ ceramics.

**A1.2 High Temperature Thermal Conductivity.** In Papers 1 and 2, the thermal diffusivity up to 200°C was fit with an exponential trend line and used to calculate the thermal conductivity. Figure A2, shows the thermal conductivities calculated from the raw diffusivity data for all measured temperatures up to 2000°C. As was noted with the thermal diffusivity, the conductivity varies at low temperatures but converges around 70 W/m•K for temperatures above 1600°C.

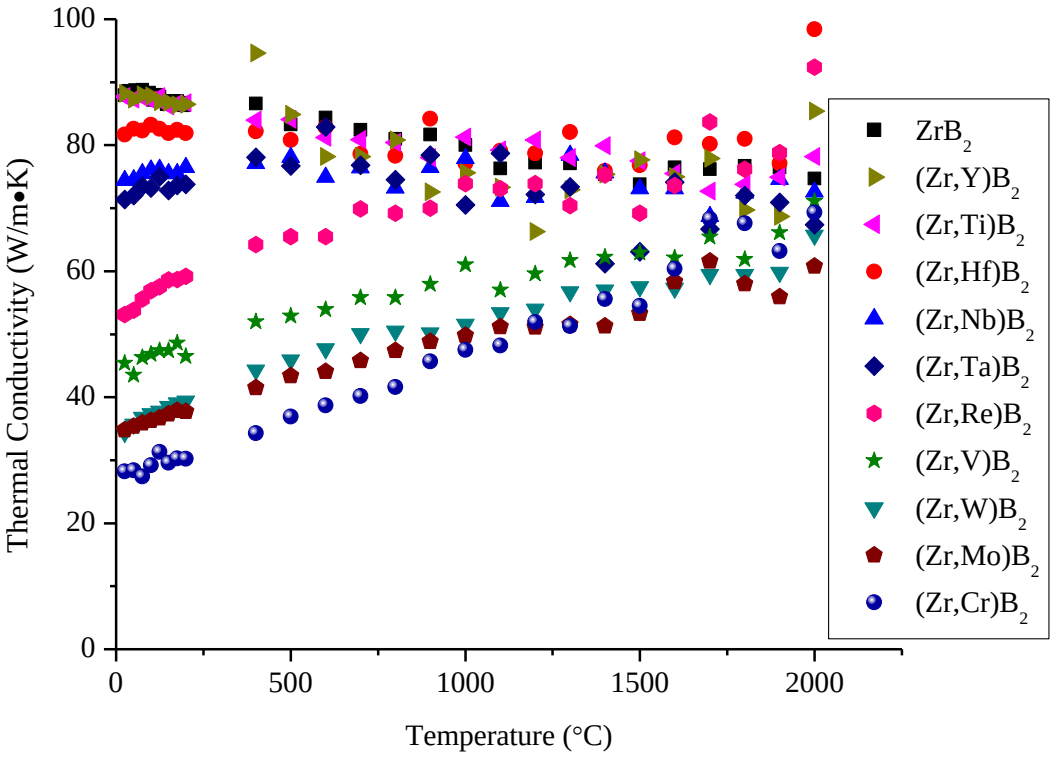


**Figure A2:** Thermal conductivity of (Zr,TM)$B_2$ ceramics.

**A1.3 Heat Capacity.** Heat capacity data was collected using the laser flash method. The data for the compositions tested in Papers 1 and 2 as well as the data for $ZrB_2$ from the NIST-JANAF tables[82] are shown in Figure A3. The measured values of all of the compositions were lower than that from NIST-JANAF at room temperature. Although the measured values for all of the compositions are relatively close to one another, the presence of an additive increased the heat capacity of $ZrB_2$ for almost all of the compositions. This was slightly unexpected since the presence of an impurity primarily changes the mean free path for conduction, but generally does not have a large effect on the constant volume heat capacity, or velocity of sound through a solid.[26] Additionally, the literature values for all of the transition metal borides that were found were relatively close.[59, 60, 82]

(a)

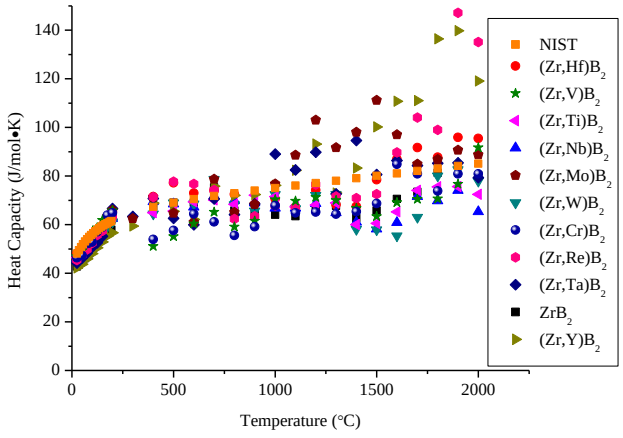

(b)

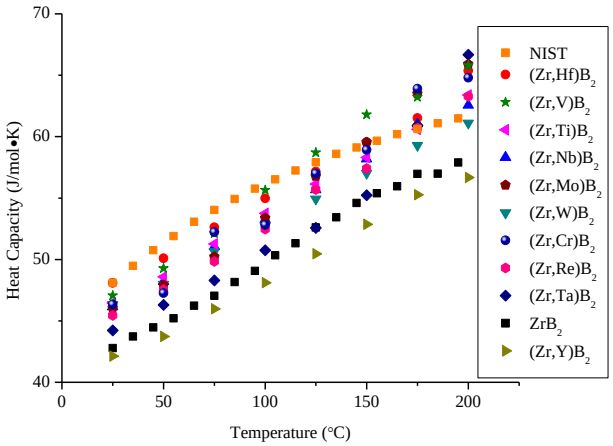


**Figure A3:** Measured heat capacity of $(Zr,TM)B_2$ ceramics using the laser flash method from (a) 25-2000°C and (b) 25-200°C, compared to the NIST-Janaf database heat capacity of $ZrB_2$.[82]

**A1.4 Lorenz Number Determination.** Using the method for determining the Lorenz number of a material graphically, proposed by Sharma[38] and described in the introduction, was used to determine the Lorenz number for the $(Zr,TM)B_2$ ceramics that were discussed in Papers 1 and 2. Only the data for temperatures between 1000°C and 1600°C were used in these calculations. These temperatures were chosen since 1000°C is above all reported values for the Debye temperature of $ZrB_2$[56, 67, 83, 84, 85] and it was observed that the conductivity did not seem to change with temperature above 1600°C. Therefore, the conductivity data for this range should fall in the 1/T temperature dependency regime, where this graphical method is valid. The trend lines for the electrical resistivity were extrapolated through this temperature range. The values for the Lorenz numbers, added term that relates to phonon conduction, and the regressions of the linear trend lines for the tested compositions are shown in Table A1.

**Table A1:** Linear trend line parameters used to determine Lorenz number for $(Zr,TM)B_2$ ceramics.

| Composition | Lorenz Number ($10^{-8}$ $V^2 \bullet K^{-2}$) | Added Constant (W/m) | Linear Regression |
|---|---|---|---|
| $ZrB_2$ | 2.185 | 10,890 | 0.9802 |
| $(Zr,Hf)B_2$ | 2.706 | -7,789 | 0.9558 |
| $(Zr,Nb)B_2$ | 2.466 | 6,599 | 0.9292 |
| $(Zr,W)B_2$ | 2.732 | -1,985 | 0.9949 |
| $(Zr,Ti)B_2$ | 2.217 | 16,170 | 0.9810 |
| $(Zr,Y)B_2$ | 3.031 | -20,490 | 0.9245 |
| $(Zr,Ta)B_2$ | 1.776 | 26,400 | 0.6035 |
| $(Zr,Mo)B_2$ | 2.936 | -4023 | 0.9618 |
| $(Zr,Re)B_2$ | 2.332 | 18,170 | 0.9469 |
| $(Zr,V)B_2$ | 2.657 | 3376 | 0.9816 |
| $(Zr,Cr)B_2$ | 3.507 | -5217 | 0.9789 |

The values for the Lorenz numbers vary widely based on the additive in solution. The linear regression for $(Zr,Ta)B_2$ does not have a very good linear regression. This is most likely due to the fact that the thermal conductivity of this composition did not change much with temperature. Additionally, some of the added terms have a negative value. This would indicate a negative phonon contribution to thermal conductivity and therefore, the Lorenz numbers determined for these compositions is most likely not valid.

Since the determined Lorenz values are related to the theoretical Lorenz number according to Equation 8, it is evident that certain transition metal additions have a larger influence on the mean free path for electrical conduction, while others have a larger effect on the mean free path for thermal conduction.

**A1.5 Reaction Hot-Pressed $ZrB_2$.** Dense $ZrB_2$ was fabricated by ball milling and hot-pressing $ZrH_2$ and B powders. The $ZrH_2$ powder was from Chemetall (Grade S) and Materion (99.7% pure, -325 mesh) and was utilized due to their lower hafnium contents, than the commercially available $ZrB_2$ powders that were used in Papers 1 and 2. These ceramics were used to compare the effect of Hf impurities on the electrical resistivity of $ZrB_2$. The electrical resistivity as a function of hafnium content is shown in Figure A4. A sharp increase in resistivity is noticed for very low Hf contents, <1 mol%. The increase in resistivity is similar to what would be expected according to Nordheim's rule for solid solutions. More compositions should be investigated to continue mapping out the effect of Hf concentration on the electrical resistivity of $ZrB_2$.

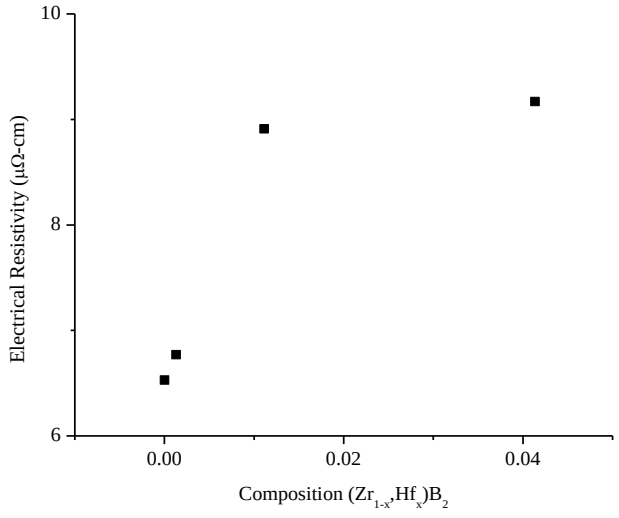


**Figure A4:** Measured electrical resistivity at 25°C as a function of Hf content in $ZrB_2$.

## REFERENCES

[1] E. Wuchina, E. Opila, M. Opeka, W. Fahrenholtz, and I. Talmy, "UHTCs: Ultra-High Temperature Ceramic Materials for Extreme Environment Applications," *Interface*, **16**[4] 30-36 (2007).

[2] B. Post, F. W. Glaser, and D. Moskowitz, "Transition metal diborides," *Acta Metallurgica*, **2**[1] 20-25 (1954).

[3] R. Telle, L. S. Sigl, and K. Takagi, "Boride-Based Hard Materials," pp. 802-945. in Handbook of Ceramic Hard Materials**, Vol. 2**, Edited by R. Riedel, Wiley-VCH Verlag GmbH, Weinheim, Germany 2008.

[4] H. J. Juretschke and R. Steinitz, "Hall effect and electrical conductivity of transition-metal diborides," *Journal of Physics and Chemistry of Solids*, **4**[1–2] 118-27 (1958).

[5] A. L. Chamberlain, W. G. Fahrenholtz, G. E. Hilmas, and D. T. Ellerby, "High-Strength Zirconium Diboride-Based Ceramics," *Journal of the American Ceramic Society*, **87**[6] 1170-72 (2004).

[6] Y. Murata, "Cutting tool tips and ceramics containing hafnium nitride and zirconium diboride." U.S. Patent, **3**, 487-594 (1970).

[7] W. G. Fahrenholtz, G. E. Hilmas, I. G. Talmy, and J. A. Zaykoski, "Refractory Diborides of Zirconium and Hafnium," *Journal of the American Ceramic Society*, **90**[5] 1347-64 (2007).

[8] B. E. Stucker, "Rapid prototyping of zirconium diboride/copper electrical discharge machining electrodes," pp. 205-05 p. in, **Vol. 9800816**. Texas A&M University, Ann Arbor, 1997.

[9] D. M. Van Wie, D. G. Drewry, Jr., D. E. King, and C. M. Hudson, "The hypersonic environment: Required operating conditions and design challenges," *J Mater Sci*, **39**[19] 5915-24 (2004).

[10] T. A. Jackson, D. R. Eklund, and A. J. Fink, "High speed propulsion: Performance advantage of advanced materials," *J Mater Sci,* **39**[19] 5905-13 (2004).

[11] D. Kalish and E. V. Clougherty, "Densification Mechanisms in High-pressure Hot-Pressing of $HfB_2$," *Journal of the American Ceramic Society,* **52**[1] 26-30 (1969).

[12] J. W. Zimmermann, G. E. Hilmas, W. G. Fahrenholtz, R. B. Dinwiddie, W. D. Porter, and H. Wang, "Thermophysical Properties of $ZrB_2$ and $ZrB_2$–SiC Ceramics," *Journal of the American Ceramic Society,* **91**[5] 1405-11 (2008).

[13] S. Guo, T. Nishimura, and Y. Kagawa, "Preparation of zirconium diboride ceramics by reactive spark plasma sintering of zirconium hydride–boron powders," *Scripta Materialia,* **65**[11] 1018-21 (2011).

[14] V. I. Matkovich, "Boron and Refractory Borides.″ Springer: Berlin, (1977).

[15] P. Vajeeston, P. Ravindran, C. Ravi, and R. Asokamani, "Electronic structure, bonding, and ground-state properties of $AlB_2$-type transition-metal diborides," *Physical Review B,* **63**[4] 045115 (2001).

[16] J. K. Burdett, E. Canadell, and G. J. Miller, "Electronic structure of transition-metal borides with the $AlB_2$ structure," *Journal of the American Chemical Society,* **108**[21] 6561-68 (1986).

[17] P. S. Gennady and L. I. Alexander, "The chemical bonding and electronic properties of metal borides," *Russian Chemical Reviews,* **63**[9] 711 (1994).

[18] G. V. Samsonov, Y. M. Goryachev, and B. A. Kovenskaya, "Electronic structure and chemical bonding in transition element borides," *Journal of the Less Common Metals,* **47**[0] 147-56 (1976).

[19] O. J. Żogał, Z. Fojud, P. Herzig, A. Pietraszko, A. B. Lyashchenko, S. Jurga, and V. N. Paderno, "Crystal structure, electric field gradient, and electronic charge densities in $ReB_2$: A single crystal x-ray, $B_{11}$ nuclear magnetic resonance, and first-principles study," *Journal of Applied Physics,* **106**[3] (2009).

[20] M. Frotscher, W. Klein, J. Bauer, C. M. Fang, J. F. Halet, A. Senyshyn, C. Baehtz, and B. Albert, "$M_2B_5$ or $M_2B_4$? A Reinvestigation of the Mo/B and W/B System," *Zeitschrift für anorganische und allgemeine Chemie,* **633**[15] 2626-30 (2007).

[21] R. Kiessling, "The Crystal Structures of Molybdenum and Tungsten Borides," *Acta Chemica Scandinavica,* **1** 893-916 (1947).

[22] M. Zhang, H. Wang, H. Wang, T. Cui, and Y. Ma, "Structural Modifications and Mechanical Properties of Molybdenum Borides from First Principles," *The Journal of Physical Chemistry C,* **114**[14] 6722-25 (2010).

[23] A. L. Ivanovskii, I. R. Shein, and N. I. Medvedeva, "Non-stoichiometric s-, p- and d-metal diborides: synthesis, properties and simulation," *Russian Chemical Reviews,* **77**[5] 467 (2008).

[24] D. W. Hahn "Heat Conduction." Wiley-Blackwell: Hoboken, N.J, (2012).

[25] G. Grimvall, "Thermophysical Properties of Materials." Elsevier: Amsterdam, Netherlands, (1999).

[26] T. M. Tritt, "Thermal Conductivity: Theory, Properties, and Applications." Kluwer Academic/Plenum Publishers: New York, (2004).

[27] ASTM Standard C177, 2013, "Steady-State Heat Flux Measurements and Thermal Transmission Properties by Means of the Guarded-Hot-Plate Apparatus." ASTM International, West Conshohocken, PA, 2013, DOI: 10.1520/C0177, www.astm.org.

[28] ASTM Standard C1113, 2009, "Thermal Conductivity of Refractories by Hot Wire." ASTM International, West Conshohocken, PA, 2009, DOI: 10.1520/C1113_1113M, www.astm.org.

[29] ASTM Standard E1225, 2013, "Thermal Conductivity of Solids Using the Guarded-Comparative-Longitudinal Heat Flow Technique." ASTM International, West Conshohocken, PA, 2013, DOI: 10.1520/E1225, www.astm.org.

[30] ASTM Standard E1461, 2013, "Standard Test Method for Thermal Diffusivity by the Flash Method." ASTM International, West Conshohocken, PA, 2013, DOI: 10.1520/E1461-13, www.astm.org.

[31] D. W. Lee and W. D. Kingery, "Radiation Energy Transfer and Thermal Conductivity of Ceramic Oxides," *Journal of the American Ceramic Society*, **43**[11] 594-607 (1960).

[32] D. Rasch, "Transport Theory in Low Dimensional Systems from Thermoelectric Effects in Luttinger Liquids to Hydrodynamic Expansion of Cold Atoms." in. Universität zu Köln, 2010.

[33] G. S. Kumar, G. Prasad, and R. O. Pohl, "Experimental determinations of the Lorenz number," *J Mater Sci*, **28**[16] 4261-72 (1993).

[34] P. J. Price, "The Lorenz Number," *IBM Journal of Research and Development*, **1**[2] 147-57 (1957).

[35] K. C. Lukas, W. S. Liu, G. Joshi, M. Zebarjadi, M. S. Dresselhaus, Z. F. Ren, G. Chen, and C. P. Opeil, "Experimental Determination of the Lorenz Number in $Cu_{0.01}Bi_2Te_{2.7}Se_{0.3}$ and $Bi_{0.88}Sb_{0.12}$," (2012).

[36] K. T. Tee and G. T. Meaden, "Thermal conductivity and Lorenz number of high-purity praseodymium," *J Low Temp Phys*, **9**[5-6] 447-56 (1972).

[37] Y. Zhang, N. P. Ong, Z. A. Xu, K. Krishana, R. Gagnon, and L. Taillefer, "Determining the Wiedemann-Franz ratio from the thermal hall conductivity: application to Cu and $YBa_2Cu_3O_{6.95}$," *Physical review letters*, **84**[10] 2219-22 (2000).

[38] R. G. Sharma, M. S. R. Chari, and D. K. Reddy, "The electronic Lorenz number in transition metals at high temperatures," *Journal of Physics F: Metal Physics*, **16**[5] 603-07 (1986).

[39] "Thermal Conductivity of Metals and Alloys: Introduction." ASM International, 1990.

[40] R. P. Tye and E. V. Clougherty, "THERMAL AND ELECTRICAL CONDUCTIVITIES OF SOME ELECTRICALLY CONDUCTING COMPOUNDS," pp 396-401 of Proceedings of the Fifth Symposium on Thermophysical Properties. /Bonilla, C. F. (ed.). New York American Society of Mechanical Engineers (1970).; Other Information: From 5. symposium on thermophysical properties; Boston, Mass. (Sep-Oct 1970). See CONF-700901. Orig. Receipt Date: 31-DEC-71 Medium: X (1970).

[41] L. Zhang, D. A. Pejaković, J. Marschall, and M. Gasch, "Thermal and Electrical Transport Properties of Spark Plasma-Sintered $HfB_2$ and $ZrB_2$ Ceramics," *Journal of the American Ceramic Society,* **94**[8] 2562-70 (2011).

[42] G. V. Samsonov, B. A. Kovenskaya, and T. I. Serebryakova, "Some physical characteristics of the diborides of transition metals of groups IV and V," *Soviet Physics Journal,* **14**[1] 11-14 (1971).

[43] T. M. Branscomb and J. O. Hunter, "Improved Thermal Diffusivity Method Applied to $TiB_2$, $ZrB_2$, and $HfB_2$ from 200°C-1300°C," *Journal of Applied Physics,* **42**[6] 2309-15 (1971).

[44] M. J. Thompson, "Densification and Thermal Properties of Zirconium Diboride Based Ceramics." Ph. D. Dissertaion, in. Missouri University of Science and Technology, 2012.

[45] M. J. Thompson, W. G. Fahrenholtz, and G. E. Hilmas, "Elevated Temperature Thermal Properties of $ZrB_2$ with Carbon Additions," *Journal of the American Ceramic Society,* **95**[3] 1077-85 (2012).

[46] B. K. Venkanna, "Fundamentals of Heat and Mass Transfer.″ PHI Learning Pvt. Ltd, (2010).

[47] M. Patrick and M. Saad, "Examination of thermal properties of carbon-carbon and graphatized carbon-carbon composites," *Frontiers in Heat and Mass Transfer,* **3**[4] (2012).

[48] W. J. Parker, R. J. Jenkins, C. P. Butler, and G. L. Abbott, "Flash Method of Determining Thermal Diffusivity, Heat Capacity, and Thermal Conductivity," *Journal of Applied Physics,* **32**[9] 1679-84 (1961).

[49] L. M. Clark III and R. E. Taylor, "Radiation loss in the flash method for thermal diffusivity," *Journal of Applied Physics,* **46**[2] 714-19 (1975).

[50] J. Xue, X. Liu, Y. Lian, and R. Taylor, "The effects of a finite pulse time in the flash thermal diffusivity method," *Int J Thermophys,* **14**[1] 123-33 (1993).

[51] M. Mallik, A. J. Kailath, K. K. Ray, and R. Mitra, "Electrical and thermophysical properties of $ZrB_2$ and $HfB_2$ based composites," *Journal of the European Ceramic Society,* **32**[10] 2545-55 (2012).

52. R. Loehman, E. Corral, H. P. Dumm, P. Kotula, and R. Tandon, "Ultrahigh-temperature ceramics for hypersonic vehicle applications," *Industrial Heating,* **71**[1] 36-38 (2004).

[53] D. R. Gaskell, "Introduction to the Thermodynamics of Materials," 5th ed. Taylor & Francis: New York, (2008).

[54] ASTM Standard D2766, 2009, "Specific Heat of Liquids and Solids." ASTM International, West Conshohocken, PA, 2009, DOI: 10.1520/D2766-95R09, www.astm.org.

[55] ASTM Standard E1269, 2011, "Determining Specific Heat Capacity by Differential Scanning Calorimetry." ASTM International, West Conshohocken, PA, 2011, DOI: 10.1520/E1269-11, www.astm.org.

[56] X. Zhang, X. Luo, J. Han, J. Li, and W. Han, "Electronic structure, elasticity and hardness of diborides of zirconium and hafnium: First principles calculations," *Computational Materials Science,* **44**[2] 411-21 (2008).

[57] E. Schreiber and O. L. Anderson, "Pressure Derivatives of the Sound Velocities of Polycrystalline Alumina," *Journal of the American Ceramic Society,* **49**[4] 184-90 (1966).

[58] D. W. Richerson, "Modern ceramic engineering: properties, processing, and use in design," **Vol. 1.** M. Dekker: New York, (1992).

[59] E. F. Westrum Jr and G. A. Clay, "Hypostoichiometric titanium diboride ($TiB_{1.964}$) and hyperstoichiometric tantalum diboride ($TaB_{2.11}$): the heat capacity and thermodynamic properties from 5 to 350 K," *The Journal of Chemical Thermodynamics,* **10**[7] 629-36 (1978).

[60] A. S. Bolgar, M. I. Serbova, T. I. Serebryakova, L. P. Isaeva, and V. V. Fesenko, "High-temperature enthalpy and heat capacity of borides of the niobium-boron system," *Powder Metall Met Ceram,* **22**[3] 207-11 (1983).

[61] ASTM Standard E228, 2011, "Linear Thermal Expansion of Solid Materials With a Push-Rod Dilatometer." ASTM International, West Conshohocken, PA, 2011, DOI: 10.1520/E0228-11, www.astm.org.

[62] Y. Touloukian, C. Ho and D. Dewitt, "Thermal Expansion: Nonmetallic Solids," pp. 784-89, **Vol. 13.** Edited by Touloukian. IFI/Plenum, New York, 1977.

[63] S. O. Kasap, "Principles of electrical engineering materials and devices.″ McGraw-Hill Higher Education, (2000).

[64] ASTM Standard F76, 2008, "Standard Test Methods for Measuring Resistivity and Hall Coefficient and Determining Hall Mobility in Single-Crystal Semiconductors." ASTM International, West Conshohocken, PA, 2008, DOI: 10.1520/F076-08, www.astm.org.

[65] R. Ward, "Electrical Engineering Science.″ McGraw-Hill: Maidenhead, (1971).

[66] D. Cvijović, "The Bloch-Gruneisen function of arbitrary order and its series representations," *Theor Math Phys,* **166**[1] 37-42 (2011).

[67] V. A. Gasparov, N. S. Sidorov, I. I. Zver'kova, and M. P. Kulakov, "Electron transport in diborides: Observation of superconductivity in $ZrB_2$," *Jetp Lett.,* **73**[10] 532-35 (2001).

[68] "Superconductivity at 39 K in magnesium diboride," *Nature,* **410**[6824] 63-64 (2001).

[69] D. S. McLachlan, M. Blaszkiewicz, and R. E. Newnham, "Electrical Resistivity of Composites," *Journal of the American Ceramic Society,* **73**[8] 2187-203 (1990).

[70] C. Y. Ho, M. W. Ackerman, K. Y. Wu, T. N. Havill, R. H. Bogaard, R. A. Matula, S. G. Oh, and H. M. James, "Electrical Resistivity of Ten Selected Binary Alloy Systems," *Journal of Physical and Chemical Reference Data,* **12**[2] 183 (1983).

[71] S. Zhu, W. G. Fahrenholtz, G. E. Hilmas, and S. C. Zhang, "Pressureless sintering of carbon-coated zirconium diboride powders," *Materials Science and Engineering: A,* **459**[1–2] 167-71 (2007).

[72] W. G. Fahrenholtz, G. E. Hilmas, S. C. Zhang, and S. Zhu, "Pressureless Sintering of Zirconium Diboride: Particle Size and Additive Effects," *Journal of the American Ceramic Society,* **91**[5] 1398-404 (2008).

[73] M. M. Opeka, I. G. Talmy, E. J. Wuchina, J. A. Zaykoski, and S. J. Causey, "Mechanical, Thermal, and Oxidation Properties of Refractory Hafnium and zirconium Compounds," *Journal of the European Ceramic Society,* **19**[13–14] 2405-14 (1999).

[74] S. C. Zhang, G. E. Hilmas, and W. G. Fahrenholtz, "Pressureless Densification of Zirconium Diboride with Boron Carbide Additions," *Journal of the American Ceramic Society,* **89**[5] 1544-50 (2006).

[75] L. Silvestroni, H. J. Kleebe, S. Lauterbach, M. Müller, and D. Sciti, "Transmission electron microscopy on Zr- and Hf-borides with $MoSi_2$ addition: Densification mechanisms," *Journal of Materials Research,* **25**[05] 828-34 (2010).

[76] D. Sciti, A. Balbo, and A. Bellosi, "Oxidation behaviour of a pressureless sintered $HfB_2$–$MoSi_2$ composite," *Journal of the European Ceramic Society,* **29**[9] 1809-15 (2009).

[77] W. G. Fahrenholtz, "Thermodynamic Analysis of $ZrB_2$–SiC Oxidation: Formation of a SiC-Depleted Region," *Journal of the American Ceramic Society,* **90**[1] 143-48 (2007).

[78] L. Silvestroni, D. Sciti, and A. Bellosi, "Microstructure and Properties of Pressureless Sintered $HfB_2$-Based Composites with Additions of $ZrB_2$ or HfC," *Advanced Engineering Materials,* **9**[10] 915-20 (2007).

[79] M. Gasch, S. Johnson, and J. Marschall, "Thermal Conductivity Characterization of Hafnium Diboride-Based Ultra-High-Temperature Ceramics," *Journal of the American Ceramic Society,* **91**[5] 1423-32 (2008).

[80] F. Peng, R. Erdman, G. Van Laningham, R. F. Speyer, and R. Campbell, "Thermal Conductivity of $ZrB_2$ SiC $B_4C$ from 25 to 2000 °C," *Advanced Engineering Materials,* **15**[6] 425-33 (2013).

[81] A. L. Chamberlain, W. G. Fahrenholtz, and G. E. Hilmas, "Pressureless Sintering of Zirconium Diboride," *Journal of the American Ceramic Society*, **89**[2] 450-56 (2006).

[82] M. W. Chase, National Institute of Science and Technology, "NIST-JANAF thermochemical tables,″ **Vol. no. 9.** American Chemical Society: Woodbury, N.Y, (1998).

[83] E. F. Westrum Jr. and G. A. Clay, "Zirconium diboride: heat capacity and thermodynamic properties from 5 to 350K," *J. Chem. Eng.,* **8** 2385 (1963).

[84] J. W. Lawson, M. S. Daw, and C. W. Bauschlicher, "Lattice thermal conductivity of ultra high temperature ceramics $ZrB_2$ and $HfB_2$ from atomistic simulations," *Journal of Applied Physics,* **110**[8] - (2011).

[85] S. Guicciardi, A. K. Swarnakar, O. Van der Biest, and D. Sciti, "Temperature dependence of the dynamic Young's modulus of $ZrB_2$–$MoSi_2$ ultra-refractory ceramic composites," *Scripta Materialia,* **62**[11] 831-34 (2010).

# VITA

Devon Lee McClane was born on October 31st, 1989 in Hamilton, OH. Devon moved to Round Rock, TX in 1992, Orlando, FL in 1997, and Fort Mill, SC in 1999. In August of 2008, Devon started his undergraduate degree in general engineering at Clemson University. The following year he decided to join the materials science and engineering department. During his undergraduate career, Devon joined several student groups, including: Material Advantage, the Student Alumni Association, FCA, and IPTAY, and was the vice-president of Material Advantage in 2011. Additionally, Devon spent time working as a shift manager at Wendy's, and as an undergraduate research assistant for Dr. John Ballato at the Clemson Center for Optical Materials Science and Engineering Technology. Devon co-authored several papers on photonic bandgap fibers and was awarded the Gilbert Robinson Research Award in 2012. Devon received his B.S. degree in Ceramic and Materials Engineering from Clemson University in May of 2012.

Devon began his graduate work as a Masters student for Dr. William Fahrenholtz and Dr. Greg Hilmas at Missouri University of Science and Technology in August of 2012. During his graduate career, Devon focused his research on the thermal properties of zirconium diboride – transition metal boride solid solutions. He also assisted with the characterization of materials lab, gave presentations at two different conferences, and published two papers. Devon received his M.S. degree in Materials Science and Engineering from Missouri University of Science and Technology in May of 2014.